



Swansea University
Prifysgol Abertawe

**Photovoltaic Emulation System and Maximum Power Point
Tracking Algorithm Under Partial Shading Conditions**

By

Yidong Wang

Submitted to Swansea University in fulfilment of the requirements for
the Degree of Doctor of Philosophy

Department of Electrical and Electronic Engineering, Swansea University

Copyright: The Author, Yidong Wang, 2023.

Distributed under the terms of a Creative Commons Attribution 4.0 License
(CC BY 4.0).

February 2023

Abstract

In this thesis, a novel photovoltaic (PV) emulator and the state-of-art learning-based real-time hybrid maximum power point tracking (MPPT) algorithms have been presented. Real-time research on PV systems is a challenging task because it requires a precise PV emulator that can faithfully reproduce the nonlinear properties of a PV array. The prime objective of the constructed emulator based on integration of unilluminated solar panels with external current sources is to overcome the constraints such as the need for wide surrounding space, high installation cost, and lack of control over the environmental conditions. In addition, the proposed PV emulator is able to simulate the electrical characteristics of the PV system under uniform irradiation as well as partially shading conditions (PSC). Moreover, the application of MPPT technology in PV systems under PSC conditions is challenging. Under complex environmental conditions, the power-voltage (P-V) characteristic curve of a PV system is likely to contain both local global maximum power points (LMPPs) and global maximum power points (GMPP). The MPPT algorithm applied to a PV system should have minimal steady-state oscillations to reduce power losses while accurately searching for the GMPP. The proposed MPPT algorithms resolved the drawbacks of the conventional MPPT method that have poor transient response, high continuous steady-state oscillation, and inefficient tracking performance of maximum power point voltage in the presence of partial shading. The intended algorithms have been verified using MATLAB/Simulink and the proposed PV emulator by applying comparative analysis with the traditional MPPT algorithms. In addition, the performance of the proposed MPPT algorithms and control scheme is validated experimentally with the implementation of MATLAB/Simulink/Stateflow on dSPACE Real-Time-Interface (RTI) 1007 processor board and DS2004 A/D and CP4002 Digital I/O boards. The results indicate that the algorithm is effective in reducing power losses and faster in tracking the speed of the maximum power point with less oscillation under partial shading conditions. In addition, excellent dynamic characteristics of the proposed emulator have been proven to be an ideal tool for testing PV inverters and various maximum power point tracking (MPPT) algorithms for commercial applications and university studies.

Declaration and statements

This work has not previously been accepted in substance for any degree and is not being concurrently submitted in candidature for any degree.

.....

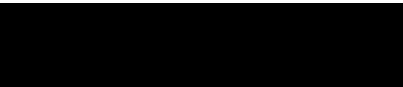
Date.....21/06/2023.....

This thesis is the result of my own investigations, except where otherwise stated. Other sources are acknowledged by footnotes giving explicit references. A bibliography is appended.

.....

Date..... 21/06/2023.....

I hereby give consent for my thesis, if accepted, to be available for electronic sharing

.....

Date..... 21/06/2023.....

The University's ethical procedures have been followed and, where appropriate, that ethical approval has been granted.

.....

Date..... 21/06/2023.....

List of publication

1. Y. Wang, C. Yanarates, and Z. Zhou, "External Current Source–Based Unilluminated PV Partial Shading Emulation System Verified Through the Hybrid Global Search Adaptive Perturb and Observe MPPT Algorithm," *Frontiers in Energy Research*, vol. 10, p. 1, 2022.
2. C. Yanarates, Y. Wang, and Z. Zhou, "Unity proportional gain resonant and gain scheduled proportional (PR-P) controller-based variable perturbation size real-time adaptive perturb and observe (P&O) MPPT algorithm for PV systems," *IEEE Access*, vol. 9, pp. 138468-138482, 2021.
3. Zhongfu Zhou, Yidong Wang and YANARATES Cagfer, "Current Source and Actual PV Module-based Photovoltaic (PV) Emulator for MPPT Testing," Conference on Industrial Electronics for Sustainable Energy Systems, 2023.
4. [In submission] Y. Wang and Z. Zhou, "A Hybrid Fast Global Maximum Power Point Tracking (MPPT) Algorithm Assisted Through a Fuzzy Logic Based Variable Step-size Perturb and Observe (P&O) Method for Photovoltaic System Under Partial Shading Conditions"

Content

Chapter 1. Introduction.....	1
1.1 Background	1
1.2 The operational principle of PV cells.....	1
1.3 PV cells modelling	3
1.4 Introduction of PV emulator.....	6
1.4.1 Construction of PV emulator	6
1.4.2 Classification of PV emulators	7
1.5 Partial shading conditions in PV system	10
1.6 Introduction of maximum power point tracking technique.....	12
1.6.1 Conventional MPPT algorithms	13
1.6.2 Advanced MPPT algorithms.....	18
1.6.3 Comparison study of existing MPPT methods	25
1.7 Summary	26
1.8 Objectives of the thesis.....	27
1.9 Thesis synopsis.....	28
Chapter 2. External current source-based unilluminated PV emulation system	29
2.1 Introduction	29
2.2 Single solar panel emulator system.....	29
2.3 Partial shading emulation of PV array using the proposed PV source emulator....	35
2.4 Series-connected solar panels emulator system	36
2.4.1 Emulated electrical characteristics under uniform solar irradiation	37
2.4.2 Emulated electrical characteristics under partial shading.....	38
2.5 Parallel-connected solar panels emulator system.....	40
2.5.1 Emulated electrical characteristics under uniform solar irradiation	41
2.5.2 Emulated electrical characteristics under partial shading.....	45
2.6 Summary	48
Chapter 3. MPPT algorithms under partial shading conditions.....	49
3.1 Introduction	49
3.2 Hybrid Global search adaptive perturb and observe MPPT algorithm	49
3.3 Hybrid fast global maximum power point tracking algorithm assisted through fuzzy logic based variable step-size perturb and observe method.....	54
3.3.1 Proposed MPPT through fast global tracking (FGT) method.....	54
3.3.2 Fuzzy logic P&O MPPT method	56
3.3.3 Description of FGT-fuzzy logic P&O algorithm	61
3.4 Summary	63
Chapter 4. Simulation results of the proposed MPPT algorithms	64
4.1 Introduction	64
4.2 Boost DC-DC converter	64
4.3 Simulation results of hybrid global search adaptive perturb and observe MPPT algorithm.....	69
4.4 Simulation results of FGT-fuzzy logic P&O algorithm	72
4.4.1 Simulation results of FGT algorithm	72

4.4.2	Simulation results of FGT-Fuzzy P&O algorithm	83
4.5	Summary	89
Chapter 5.	Experimental verification of the proposed MPPT methods.....	90
5.1	Introduction	90
5.2	dSPACE system.....	91
5.2.1	Composition of dSPACE system	92
5.3	Boost DC-DC converter components selection.....	93
5.4	Experimental system setup	94
5.5	Experiment results of proposed hybrid global search adaptive perturb and observe MPPT algorithm.....	95
5.6	Experiment results of proposed hybrid FGT MPPT algorithm assisted through fuzzy logic based variable step-size perturb and observe method.....	98
5.7	Summary	105
Chapter 6.	Conclusions.....	106
Chapter 7.	Future work.....	108
REFERENCES	110
APPENDIX A.	DATASHHET FOR POWER MOSFET IRFS4321	116
APPENDIX B.	DATASHHET FOR DIODE IDH12S60C.....	117
APPENDIX C.	DATASHHET FOR DIODE IDH08S120	118
APPENDIX D.	DATASHHET FOR DIODE IDH12SG60CXKSA2.....	119
APPENDIX E.	DATASHHET FOR DRIVER IR4426	120
APPENDIX F.	DATASHHET SOLAR PANEL SUNTECH STP175S-24/Ac	122
APPENDIX G.	TEST DATA FOR CONSTRUCTED PV EMULATOR.....	124
APPENDIX H.	SIMULINK BLOCK DIAGRAM OF ADAPTIVE P&O.....	130
APPENDIX I.	SIMULINK BLOCK DIAGRAM OF FL CONTROLLER	131
APPENDIX J.	PROPOSED GLOBAL SEARCH METHOD.....	132
APPENDIX K.	PROPOSED FAST GLOBAL TRACKING METHOD	134

Acknowledgements

First of all, I would like to express my deep gratitude to Dr. Zhongfu Zhou for his guidance and inspiration over the past four years. I would also like to thank him for his continued support, understanding and trust in me. Not only for his expertise in electrochemistry, but also for his hard work, kindness and sense of humor that will always encourage me.

The second thank you must go to my parents. I was unable to spend more time with them because of the epidemic and I am very grateful for their concern and support. Without their help and support, I would not have been able to complete my studies overseas. I am who I am because they give everything to me.

I am very grateful to Chris Wang because she supported me during my doctoral studies. She always inspires me to work hard, gives me strength when I encounter difficulties, and gives me advice when I am confused.

To the other extraordinary people I met in Swansea, thanks also to my friend Jixiang Tan, and for his kind help in work and life. I would also like to thank Dr. Cagfer Yanarates for all the advice and help you have given me in my studies and for sharing your life experiences. Thanks to all the people I have met, I know I will never be alone.

Finally, I would also like to express my sincere thanks to the School of Engineering at Swansea University for providing me with a great learning environment and resources to help me complete my project. The time I spent at Swansea University is one of the best memories of my life.

List of Figures

Figure 1.1 Schematic diagram of Electron-hole generation in solar cell	2
Figure 1.2 A p-n junction PV cell.....	2
Figure 1.3 The equivalent circuit of a solar cell (a) SEM model (b) DEM model	3
Figure 1.4 I-V characteristic of the PV module	5
Figure 1.5 The schematic of the PV emulator	7
Figure 1.6 Boost converter-based and buck converter-based PV emulator	8
Figure 1.7 Commercial PV emulator system.....	10
Figure 1.8 Hot spot phenomenon in a PV array.....	11
Figure 1.9 Schematic of typical PV array	12
Figure 1.10 Power characteristic curves of a PV panel under (a) constant temperature (b) constant irradiation.....	13
Figure 1.11 Schematic diagram of P&O MPPT algorithm	14
Figure 1.12 Schematic diagram of the P&O MPPT algorithm drift problem.....	15
Figure 1.13 Flow chart of the P&O algorithm.....	16
Figure 1.14 Schematic diagram of INC method	17
Figure 1.15 Flow chart of the INC method.....	18
Figure 1.16 Fuzzy logic controller block diagram.....	19
Figure 1.17 Triangular Membership function of FLC	19
Figure 1.18 Movement of a particle in PSO algorithm.....	21
Figure 1.19 The flow chart of PSO method	23
Figure 1.20 The schematic diagram of the ACO algorithm.....	24
Figure 2.1 Equivalent circuit of the emulated PV source	29
Figure 2.2 The equivalent circuit of a single diode solar panel	30
Figure 2.3 Equivalent circuit of the emulated PV source	32
Figure 2.4. Measured electrical characteristics of the constructed PV source based on a single solar panel at different current source currents	33
Figure 2.5 Laboratory set up for proposed unilluminated emulated PV system.....	34
Figure 2.6 Equivalent circuit of proposed emulated PV system.....	36
Figure 2.7 Measured and datasheet given electrical characteristics of the emulated PV arrays based on two series solar panels	38
Figure 2.8 Measured and datasheet given electrical characteristics of the emulated PV arrays under two different partial shading operation conditions	39
Figure 2.9 The proposed PV array partial shading emulation system with two parallel-connected unilluminated solar panels	40
Figure 2.10 Measured and datasheet given electrical characteristics of the emulated PV arrays based on two parallel solar panels	42
Figure 2.11 Measured output currents of emulated solar panels with two identical blocking diodes	44
Figure 2.12 Measured output currents of emulated solar panels with two different blocking diodes	45
Figure 2.13 Measured and datasheet given electrical characteristics of the emulated PV arrays	

under two different partial shading operation conditions	46
Figure 2.14 Measured output currents of emulated solar panels with two different blocking diodes	47
Figure 3.1 The schematic diagram of slope-based adaptive perturbation step size.....	52
Figure 3.2 The flow chart of the proposed MPPT algorithm.....	53
Figure 3.3 The relationship between particle convergence speed and number of iterations of the algorithm	56
Figure 3.4 The membership function of proposed fuzzy logic controller (a) change of power; (b) PV curve slope $S(k)$	58
Figure 3.5 The membership function of proposed fuzzy logic controller for variable perturbation step.....	59
Figure 3.6 Viewer surface plot of the FLC	60
Figure 3.7 The flow chart of fuzzy logic P&O algorithm.....	61
Figure 3.8 Flow chart of the proposed MPPT algorithm	62
Figure 4.1 Topology of boost converter.....	64
Figure 4.2 Boost converter on state equivalent circuit	65
Figure 4.3 Boost converter off state equivalent circuit.....	65
Figure 4.4 Relationship between input and output voltages of an ideal boost converter at different duty cycles.....	67
Figure 4.5 Relationship between V_{out}/V_{in} and duty cycle for a non-ideal boost converter....	68
Figure 4.6 Equivalent circuit of simulation set up for global search adaptive P&O algorithm	70
Figure 4.7 Case 1 and case 2 P-V curves from datasheet	70
Figure 4.8 Voltage comparison of conventional P&O MPPT and the proposed adaptive variable step size P&O MPPT	71
Figure 4.9 Power comparison of conventional P&O MPPT and the proposed adaptive variable step size P&O MPPT	72
Figure 4.10 Equivalent circuit of simulation set up for FGT-fuzzy logic P&O algorithm	72
Figure 4.11 Simulation results for five times iterations of FGT MPPT algorithm	74
Figure 4.12 Simulation results for ten times iterations of FGT MPPT algorithm	75
Figure 4.13 Simulation results for fifteen iterations of FGT MPPT algorithm	76
Figure 4.14 Schematic of pattern 3 and pattern 4 irradiation conditions	79
Figure 4.15 Simulation results of FGT MPPT algorithm under complex partial shading conditions.....	79
Figure 4.16 Simulation results of five-particle FGT MPPT algorithm.....	81
Figure 4.17 Simulation results of nine-particle FGT MPPT algorithm	82
Figure 4.18 Simulation results for FGT-fuzzy logic-based P&O (a) output power and (b) output voltage under pattern 1 and pattern 2	84
Figure 4.19 Simulation results for FGT-fuzzy logic-based P&O (a) output power and (b) output voltage under pattern 5 and pattern 1	85
Figure 4.20 Simulation results for FGT-fuzzy logic-based P&O (a) output power and (b) output voltage under pattern 5 and pattern 1	86
Figure 4.21 Simulation results of output power for PSO algorithm (a) pattern 1 and (b) pattern 2	88

Figure 5.1 The block diagram of experiment PV system set up	90
Figure 5.2 Brief block diagram of dSPACE implement	91
Figure 5.3 dSPACE accessories	92
Figure 5.4 Experimental system set up	95
Figure 5.5 Conventional and proposed MPPT PV voltage and current measured results for partial shading under case 1 and case 2 irradiation.....	97
Figure 5.6 Measured and datasheet given P-V characteristics of the emulated PV arrays under pattern 1 and pattern 2.....	99
Figure 5.7 Experimental results of the proposed FGT method with different iteration settings for varying irradiation from pattern 2 to pattern 1	101
Figure 5.8 Experimental results of the FGT method with different particle number settings	103
Figure 5.9 Experiment results of FGT-Fuzzy P&O method for varying irradiation from pattern 2 to pattern 1	104
Figure 5.10 Experiment results of FGT-Fuzzy P&O method for varying irradiation from pattern 1 to pattern 2	105
Figure 7.1 Microcontroller-based experimental system topology	109

List of tables

Table 1.1 Impact of components on the diode model PV emulator.....	8
Table 1.2 Advantages and disadvantages of different FL input	20
Table 1.3 Characteristics of mentioned MPPT methods	26
Table 2.1 The parameters of solar panel STP175S-24/Ac.....	32
Table 3.1 Fuzzy Logic Rules	60
Table 4.1 Performance comparison of different iteration setting	77
Table 4.2 Performance comparison of different particle setting.....	83
Table 4.3 Parameter of PSO algorithm	87
Table 4.4 Performance comparison of different MPPT methods.....	88
Table 5.1 List of boost converter components	94
Table 5.2 Boost DC-DC converter parameters	95
Table 5.3 Boost DC-DC converter parameters	98

Abbreviations

ACO: Ant colony optimization

AI: Artificial intelligence

CV: Constant voltage

DC: Direct current

DC-DC: Direct current to direct current

DEM: Double exponential model

FGT: Fast global tracking

FL: Fuzzy logic

FLC: Fuzzy logic controller

GMPP: Global maximum power point

GS: Global search

IGBT: Insulated-gate bipolar transistor

INC: Incremental Conductance

I-V: Current-voltage

I_{SC}: Short circuit current

LMPPs: Local maximum power points

MPP: Maximum power point

MPPT: Maximum power point tracking

MOSFET: Metal-Oxide-Semiconductor Field-Effect Transistor

P&O: Perturb and observe

PSO: Particle swarm optimization

P-V: Power-voltage

RTI: Real time interface

SEM: Single exponential model

STC: Standard testing condition (1000W/m² and 25°C)

V_{OC}: Open circuit voltage

Chapter 1. Introduction

1.1 Background

Widespread research of renewable energy source to eliminate global warming emissions has categorically found that such sources are a sustainable, environmentally friendly option to solve the challenge of depleting fossils fuels and energy dependency [1]. When considering the lifecycle of emissions from cleaner energy sources; specifically, from each stage in a technology's lifespan (from manufacturing to decommissioning), global warming emissions from sustainable energy sources, are almost non-existent [2]. Among the sources of clean energy, solar energy is becoming increasingly important. Solar energy provides the advantage of environment-friendly power generation, low maintenance cost and great development potential in energy conversion efficiency [3]. As a pioneer in the field of energy transition, the UK is gradually shifting the focus of its energy development to solar energy. Total installed photovoltaic capacity in the UK increased by 160% over the five years from 2014 to 2019, from 5,230 MW to 13,616 MW [4]. In order to extract the maximum amount of energy from solar energy, research on maximum power point tracking (MPPT) is becoming increasingly popular. The MPPT technique is one of the PV energy generation system's components. The MPPT makes sure the maximum power is taken from the PV module for a given irradiation condition [5]. However, tracking to the maximum power point of a PV system in complex environmental conditions is still a challenge. In addition, experiments on PV systems (including verification of MPPT algorithms) are subject to many limitations, such as need for wide surrounding space, high equipment and installation cost, uncontrollable experimental environments, etc. As an alternative, therefore, PV simulators are beginning to attract the attention of researchers. The PV emulator provides controlled environmental conditions indoors for faster and more efficient testing of experiments related to solar power systems [5, 6].

1.2 The operational principle of PV cells

Solar cells are mainly based on silicon-based semiconductor materials and work on the principle that solar cells absorb radiation energy and then undergo a photovoltaic effect. When the

absorbed energy is greater than the band gap of its semiconductor, electrons in the semiconductor are ejected, resulting in an electron-hole pair which can be seen in Figure 1.1 [7].

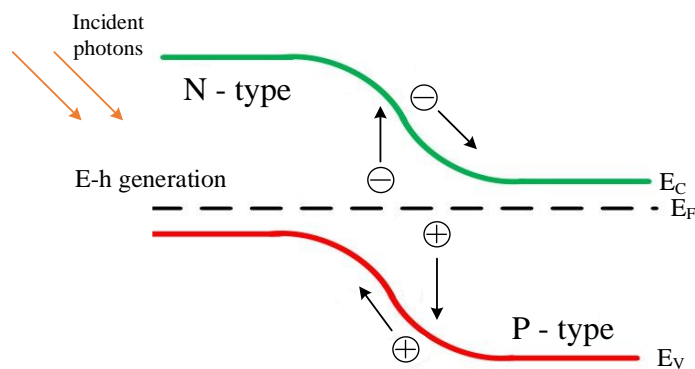


Figure 1.1 Schematic diagram of Electron-hole generation in solar cell

Where E_C indicates conduction band, E_F is the fermi energy level, E_V represents valence band and E-h is the electron-hole pair generation. The diagram of PV cell structure is shown in the Figure 1.2.

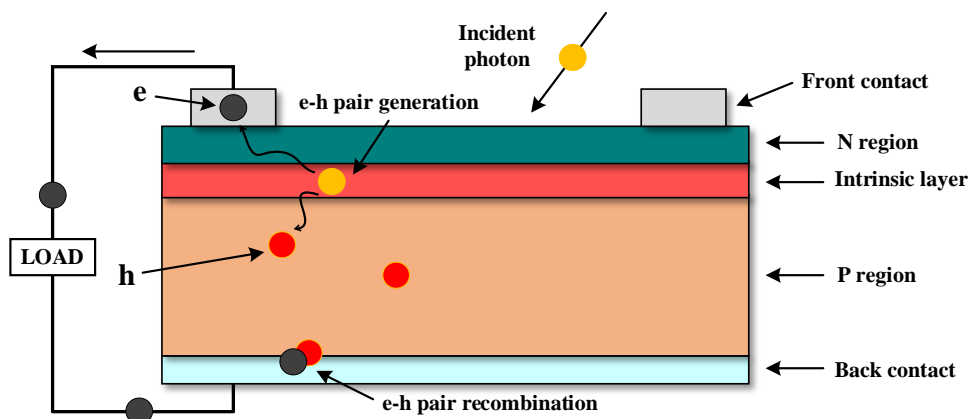


Figure 1.2 A p-n junction PV cell

As solar cells work on the basis of the photovoltaic effect, the photovoltaic effect can be divided into three main processes [8-10]. Firstly, when the absorbed photon energy is higher than the gap energy of the doped semiconductor material, its energy is used to excite an electron from the valence band to the conduction band and leave a hole (vacancy) in the valence level. Thus, a p-n junction semiconductor produces an electron-hole pair after absorbing a sufficiently high photon energy. The separation of the charge carriers occurs next. In an external solar circuit, holes can

flow away from the junction through the p-region, while electrons flow away through the n-region and through the circuit then recombine with the holes. Finally, an electric circuit can be driven using the split electrons. The electrons will unite with the holes once they have completed the circuit. It is worth noting that in order to generate current efficiently, the n-type must be designed to be thinner than the p-type because the electrons can pass through the circuit in a short time and generate current before recombining with the holes.

1.3 PV cells modelling

Photovoltaic solar panels consist of photovoltaic cells connected in series or in parallel. PV cells are essentially p-n junction diodes that convert solar energy into electrical energy and an ideal PV cell can be equated to an ideal current source. In practice, the PV cell is modelled by an electrical circuit model according to Kirchhoff's current law [11]. The Single Exponential Model (SEM) and the Double Exponential Model (DEM) are often used to represent the equivalent circuit of a non-ideal solar cell, as shown in Figure 1.3.

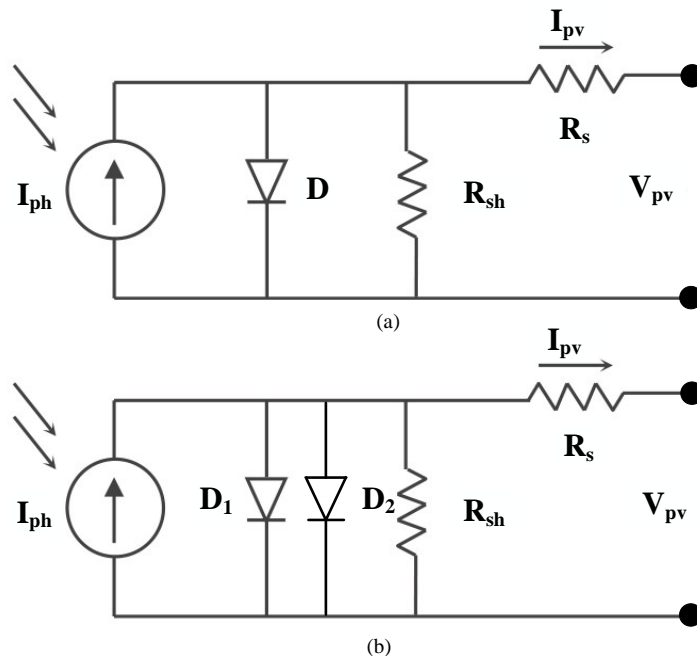


Figure 1.3 The equivalent circuit of a solar cell (a) SEM model (b) DEM model

where I_{ph} is the photo-generated current, I_{pv} represents PV module current, V_{pv} is PV module voltage; R_s represents the PV module series resistance, R_{sh} is the PV module parallel resistance. Compared to the SEM model (also known as single diode model), the dual diode model (also known as double diode model) increases the model parameters and provides superior performance and a more accurate simulation of the electrical characteristics of the solar cell. However, the single diode model is simple and easy to implement [12]. As this research does not consider the effects of complex environmental factors such as air pollutants, dust, etc., the single diode model will be explored. Equation 1.1 gives the output current of the solar cell.

$$I_{pv} = I_{ph} - I_D - I_{sh} \quad (1.1)$$

where I_D is the diode current and can be expressed as follows:

$$I_D = I_s \left(e^{\frac{V_D}{V_t}} - 1 \right) \quad (1.2)$$

where I_s represents dark saturation current. The diode equivalent voltage V_D is given by:

$$V_D = V_{pv} + I_{pv} \cdot R_s \quad (1.3)$$

The junction thermal voltage of the diode V_t , is given by:

$$V_t = \frac{K_b \cdot T \cdot A}{q} \quad (1.4)$$

where K_b is Boltzmann constant (1.38×10^{-23} J/K), T represents temperature in Kelvin, q is charge of the electron (1.6×10^{-19} C) and A is the ideal factor. For the monocrystalline silicon solar cell, A is chosen as 1.2 [13].

The leakage current I_{sh} is expressed in Equation 1.5:

$$I_{sh} = \frac{V_{pv} + I_{pv} \cdot R_S}{R_{sh}} \quad (1.5)$$

Substituting the above equation into Equation 1.1, the electrical characteristic of single diode PV module is given by:

$$I_{pv} = I_{ph} - I_s \left(e^{\frac{V_{pv} + I_{pv} R_S}{V_t}} - 1 \right) - \frac{V_{pv} + I_{pv} R_S}{R_{sh}} \quad (1.6)$$

Figure 1.4 shows the I-V characteristic of the solar module.

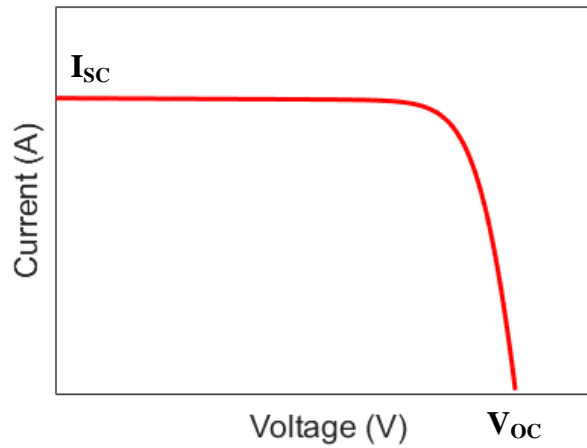


Figure 1.4 I-V characteristic of the PV module

The maximum voltage obtained from the PV module is defined as the open circuit voltage (V_{oc}) while the maximum current obtained from the PV module is short circuit current (I_{sc}). The equation of V_{oc} is expressed as follows [14]:

$$V_{oc} = \frac{nkT}{q} \ln \left(\frac{I_{ph}}{I_s} + 1 \right) \quad (1.7)$$

The short-circuit current is given by [15]:

$$I_{SC} = qG(L_n + L_p) \quad (1.8)$$

where G is the generation rate, L_n and L_p are the diffusion lengths of electrons and holes, respectively.

1.4 Introduction of PV emulator

During the development of photovoltaic-related power electronics systems, researchers frequently need to carry out hardware experiments on actual solar modules under outdoor sunlight to access their designs. However, the electrical characteristics of PV solar panels are mainly influenced by irradiation and temperature [16, 17]. Real PV module outdoor experiments are uncontrolled and extremely dependent on the weather because irradiation and temperature are continually changing in outdoor environment. It is preferable to carry out PV module experiments under controlled conditions inside of laboratory. For this reason, numerous hardware devices known as PV module emulators or simulators that mimic a PV module's electrical properties have been proposed [6, 18, 19].

1.4.1 Construction of PV emulator

A PV emulator's primary aim is to accurately reproduce the electrical characteristic of a real PV panel. The emulator should be designed to properly represent the actual I-V and P-V curves in an environment that is not only under uniformly irradiation but also under partially shading conditions. In addition, the simulator must be easy to interact with external interfaces to perform various power electronics experiments. Therefore, a reliable PV emulator has the following characteristics:

1. Ability to interact with external power electronics converters
2. Ability to accurately simulate electrical characteristic under different irradiation conditions
3. Ability to flexibly simulate the maximum power point of different photovoltaic solar panels

The PV emulator consists of three main parts, the PV model, the control strategy and the power

stage [6]. The schematic of the general PV emulator is shown in the Figure 1.5.

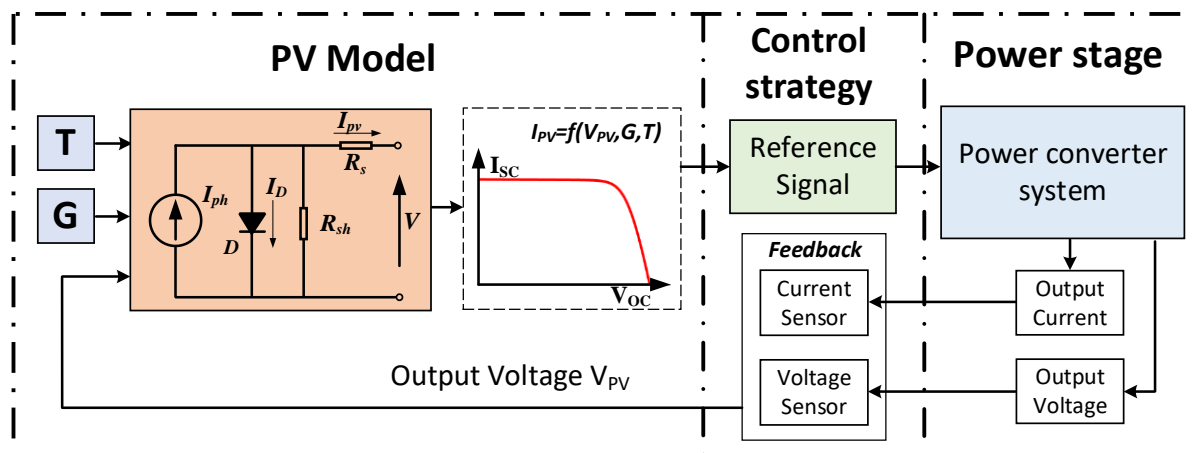


Figure 1.5 The schematic of the PV emulator [6]

The first part of PV emulator is PV model. The aim of PV model is to create the electrical characteristic of the signal from a PV module. Real-time calculations of the PV model are necessary for the PV emulator to function successfully. Since accuracy of the I-V characteristics produced must not be compromised, the PV model employed in the PV emulator programme must stay simple. The control strategy is the second component of the PV emulator system. The control strategy is the bridge between the PV model and the power stage. It is to control the power converter to implement the PV emulator functions. The power converter is the third component of the PV emulator system. The electrical characteristic signal of PV model is converted by the power converter into an electrical characteristic that can transmit power.

1.4.2 Classification of PV emulators

One of the most commonly used techniques for the construction of emulators is the diode model approximation. Researchers have used the diode-based approximation method to simulate solar PV characteristics because PV panels display non-linear behaviour [20-22]. An operational amplifier-based analogue circuit is used to implement the design of the solar PV emulator based on the single diode approximation model in order to precisely duplicate the change in irradiation [23, 24]. The output current of diode model is given in Equation 1.6. It can be seen that the parameter settings of I_{sh} , I_{ph} , R_s and R_{sh} determine the value of the output current. Table

1.1 displays the importance of each element in diode modelling [18].

Table 1.1 Impact of components on the diode model PV emulator

<i>Component</i>	<i>Representation</i>	<i>Replacement PV Characteristic</i>
Current source I_{ph}	Irradiation losses	Current characteristic
Diode D	Recombination losses	Effect of temperature
Resistance $R_S R_{sh}$	Ohmic losses	Effect of load

DC-DC converters are already widely used in solar PV emulators. In addition, to achieve impedance matching, DC-DC converters are typically utilised as an interface between the PV panel and the load [25]. For a converter-based PV emulator, it can be designed with a DC source coupled to the load via power electronic interface. Meanwhile, in order to obtain the expected electrical characteristics of solar panels, the researcher usually programs the controller according to the data sheet of the actual solar panel. For example, the structure of a boost converter-based and buck converter-based PV emulator is shown in Figure 1.6 [26, 27].

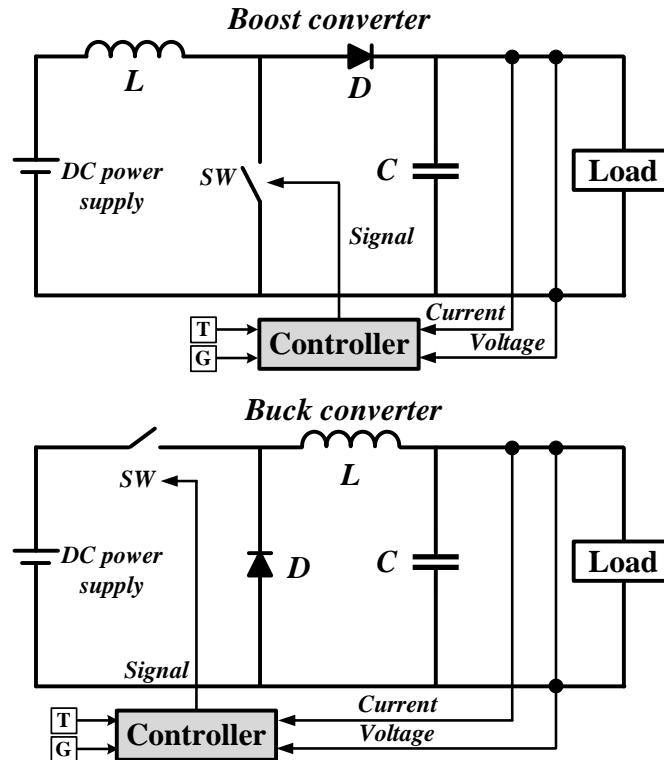


Figure 1.6 Boost converter-based and buck converter-based PV emulators

However, conventional PV simulators are generally designed for simple external experimental conditions such as uniform irradiation or constant ambient temperature. Nowadays, the performance of MPPT algorithms under partially shading conditions is of increasing interest. Therefore, in order to test and validate advanced MPPT algorithms, PV simulators are required to simulate electrical characteristics in complex environmental condition. More and more commercial and digital-controlled PV emulators are being used in the field of photovoltaic system research. It is worth noting that high-end commercial emulators can almost simulate the electrical characteristics of actual solar panels. These emulators are completely independent of external environmental conditions and can simulate the P-V and I-V characteristic curves of solar panels under various complex conditions. In addition, commercial emulators can simulate the electrical characteristics of different solar panels depending on the actual situation, with the flexibility to obtain operating points [19, 28]. The electrical characteristics of the commercial emulator output are obtained by computer simulation based on the key parameters provided (e.g. open circuit voltage, short circuit current, local maximum power point voltage and global maximum power point voltage). However, the key data required may rely on advance outdoor measurements or data provided by solar panel manufacturer. The expected solar panel characteristics must be subjected to complex computer simulations. In addition, the high cost of commercial simulators must also be considered. The main commercial PV simulators available on the market include single panel simulators (output power less than 300W) and PV array simulators (output power greater than 300W). However, this type of PV simulator is expensive, ranging from a few thousand pounds to tens of thousands of pounds [29-31]. As a result, a great deal of research has been carried out on PV simulators to reduce the overall cost of PV simulators while effectively simulating the electrical characteristics of PV systems under various environmental conditions. A diagram of the commercial emulator system is shown in the Figure 1.7 [18, 32].

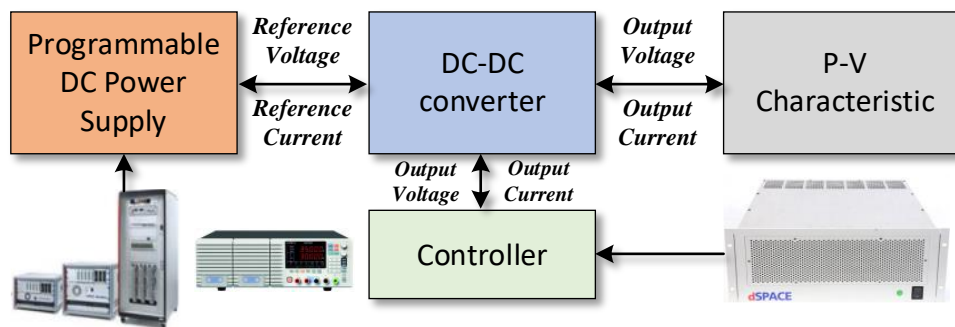


Figure 1.7 Commercial PV emulator system

1.5 Partial shading conditions in PV system

For a photovoltaic system, power generation relies not only on a single solar panel, but on photovoltaic modules connected in series or parallel to form a photovoltaic array to meet the demand for voltage and current [33]. However, the power generation of a PV array is always lower than the sum of the power generation of the individual solar panels. This is mainly due to the fact that in practice the PV array does not operate at a uniform irradiance owing to weather changes or shading by buildings or dust covered on the solar panel surface [34]. Taking PV arrays connected in series as an example, even when some PV cells under the shading produce less photon current, all the cells in a series array are compelled to carry the same amount of current. When some cells provide less current than others, these cells will act as a load, operating in reverse bias mode and consuming the power generated by the normally operating cells. In this case, under partially shading conditions, hot spot reliability problems (high local solar cell temperatures) may occur if the PV array is not properly protected. Not only will the power generated by the PV array drop, but in extreme cases PV arrays may be irreversibly damaged [35]. Figure 1.8 shows the hot spot phenomenon in a PV array [36].

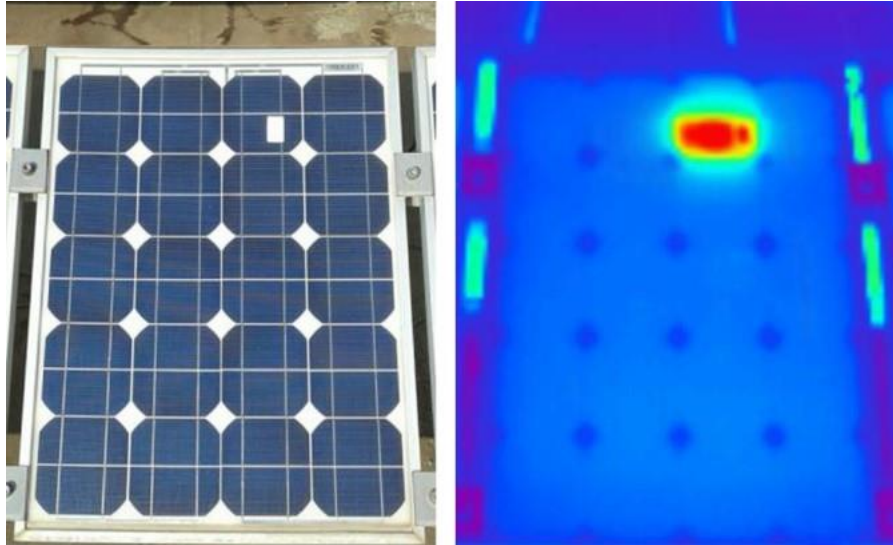


Figure 1.8 Hot spot phenomenon in a PV array

When reverse bias occurs in some solar cells, whether it is detrimental to the PV array depends primarily on the reverse current-voltage characteristics of the PV cell's p-n junction [37]. The reverse I-V characteristic is mainly influenced by two parameters: breakdown voltage V_B and shunt resistance R_{sh} , where breakdown voltage V_B is the maximum reverse voltage allowed to be applied to the p-n junction, R_{sh} is the parallel resistance (also known as shunt resistance) of the PV cell. Due to the shading problem, a small part of the current generated by the PV cell flows to the shunt resistor R_{sh} . This part of the current does not generate power and thus does not lead to a short circuit in the solar cell. However, it will cause the cell to heat up [38]. The bypass diode is added to the PV panel in order to deal with the hazards posed by the hotspot problem [39]. A typical PV panel with bypass diode is shown in Figure 1.9.

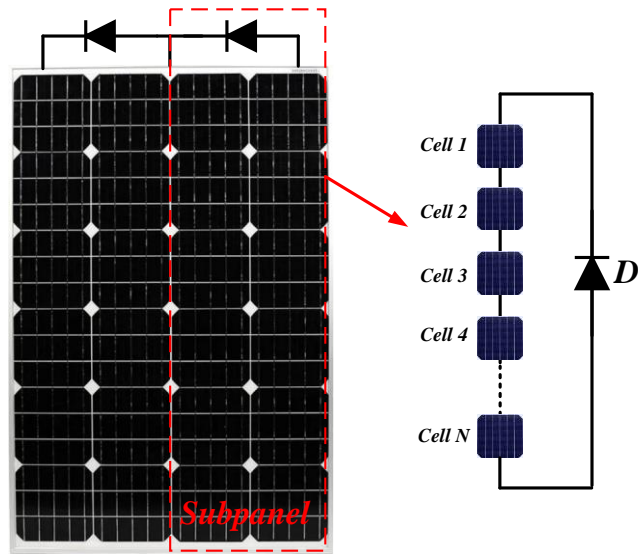


Figure 1.9 Schematic of typical PV array

Each sub-module is connected to a diode connected in reverse parallel. When an area of the PV array is under partial shading, the bypass diode is used to provide a new flow path for the current generated by the normally operating cell to cross over to the faulty cell, thus avoiding hot spots and ensuring continuity of power generation.

1.6 Introduction of maximum power point tracking technique

Since solar energy is abundant and clean, energy generation from photovoltaic arrays will become the most important renewable energy source by 2040 [40]. Despite the many advantages of power generating through PV array, the efficiency of energy conversion is currently low. Factors including solar irradiation, PV cell temperature and surface dirtiness all have a significant impact on power generation of a solar panel [41]. Under uniform solar irradiation conditions, PV panels exhibit a non-linear PV power characteristic curve which are shown in Figure 1.10.

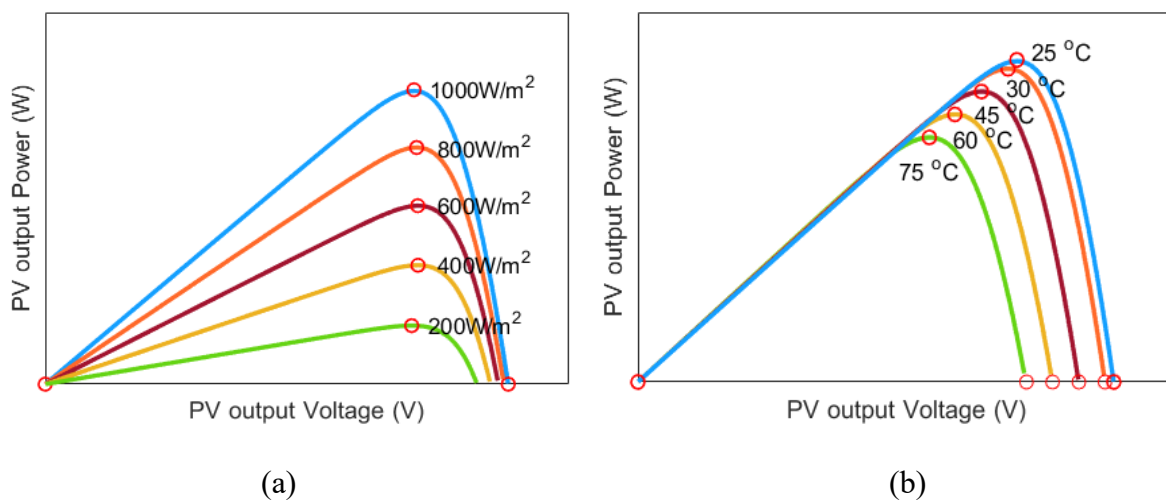


Figure 1.10 Power characteristic curves of a PV panel under (a) constant temperature and variable irradiation (b) constant irradiation and variable temperature

Therefore, in order to maximize the output of solar panels, the MPPT algorithm is applied to PV systems. The main goal of MPPT technology is to obtain the maximum output power from the PV system without being affected by the external environmental conditions (temperature and solar irradiation) [42]. There are two main types of MPPT control algorithms, conventional methods such as perturb and observe, and advanced methods such as fuzzy logic that will be mentioned in the next section. In order to select the appropriate algorithm for a PV system, several aspects should be evaluated, such as the required tracking accuracy, tracking speed, complexity of the PV system, cost, etc [43].

1.6.1 Conventional MPPT algorithms

Conventional MPPT methods are simple, cost effective and easy to implement in PV control systems. Some of these methods are based on fixed-step methods; therefore, they can lead to considerable power losses due to oscillations that occur when the PV system is operating at the maximum power point [43]. In addition, under complex irradiation conditions, the conventional MPPT algorithm may lead to tracking failure of the PV system [5].

1.6.1.1 Perturb and observe (P&O) MPPT algorithm

The P&O algorithm is widely used for maximum power point tracking in PV systems because of its low cost and simple operation [44]. The basic working principle of P&O is to detect the maximum output power by continuously varying the system operating voltage. First, the actual output power is obtained by continuously detecting the output current of the solar panel and the operating voltage of the solar panel. By constantly changing the reference voltage, the output power of the current cycle is compared with the output power of the previous cycle. If the power change is positive, continue to perturb the system operating voltage and measure the next output power. If the change in power is negative, the reference voltage is reduced. By constantly perturbing the voltage, the operating voltage of the PV system will eventually oscillate around the maximum power point voltage. A schematic of the P&O method is shown in Figure 1.11.

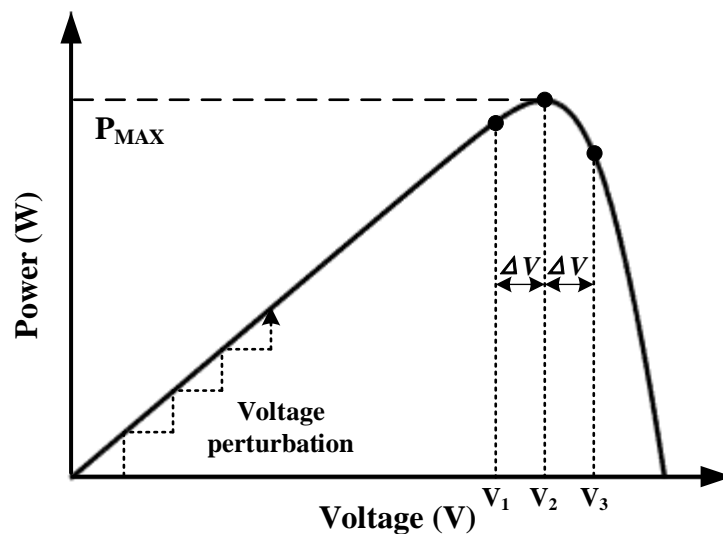


Figure 1.11 Schematic diagram of P&O MPPT algorithm

However, the drawback of this algorithm is the possibility of drift problems when the irradiation to which the PV system is exposed changes suddenly. The drift problem is due to the lack of identification of whether the increase in output power is due to voltage perturbation or to an increase in irradiation. Drift problems occur for increasing irradiation, and can be severe for rapid increases in irradiation that usually occur on cloudy days [45]. For example,

as shown in Figure 1.12, under stage 1, the PV system voltage operates at V_{MPP1} and the output power is P_{MAX1} . If the system is subjected to an increase in irradiance stage 2, the output power will increase and the system operation voltage will tend to move to the V_{MPP2} to track the maximum output power. It is clear that V_{MPP2} is less than and to the left of V_{MPP1} . However, the increase in irradiation level may cause the direction of perturbation to proceed to the right side, which is contrary to the new V_{MPP2} being to the left of V_{MPP1} . This will result in a loss of power until the algorithm corrects the direction of the perturbation. Besides, since the traditional P&O algorithm is based on fixed steps, the operating voltage of the PV system will oscillate at the peak of the PV curve, so that the system will lose a certain amount of output power. The setting of the perturbation step will also affect the tracking speed and accuracy of the P&O algorithm. The tracking time at the maximum power point is always in conflict with the tracking accuracy. A large perturbation step ensures that the system tracks the MPP faster, but the losses caused by power oscillations also increase. A small step size reduces the system power loss, but is less efficient. The following Figure 1.13 shows the flow chart of the P&O algorithm

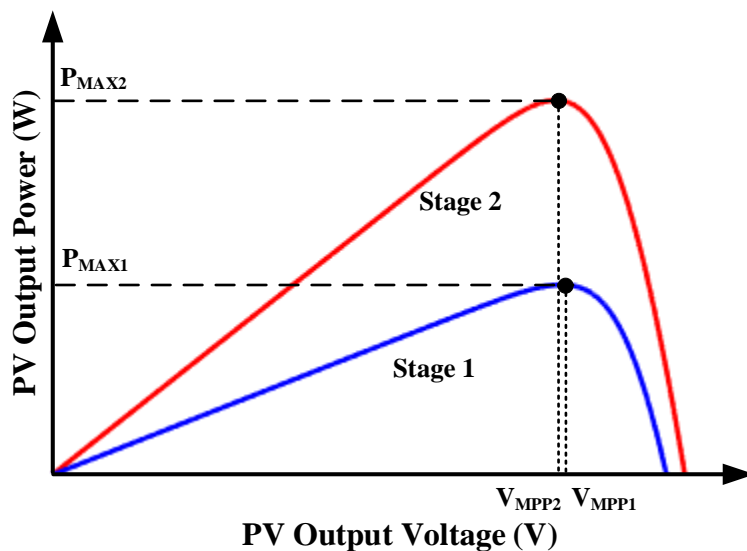


Figure 1.12 Schematic diagram of the P&O MPPT algorithm drift problem

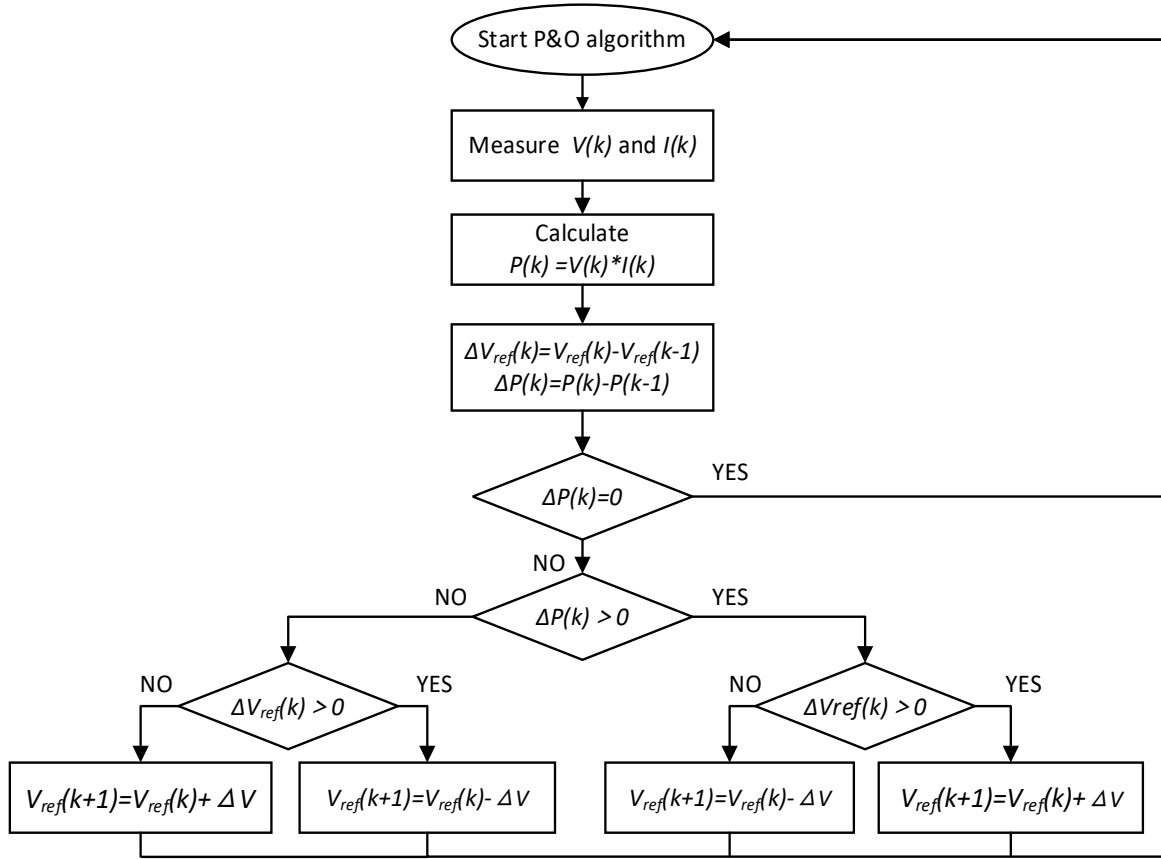


Figure 1.13 Flow chart of the P&O algorithm

1.6.1.2 Incremental conductance (INC) MPPT algorithm

The basic principle of the INC MPPT method is based on slope of P-V characteristic curves of PV array [44]. Output The output current and voltage are measured at each step to obtain the instantaneous conductance (I_{PV}/V_{PV}) and the incremental conductance (dI/dV). Using Watt's law and deriving the PV system output power P with respect to the operating voltage V, it is obtained:

$$\frac{dP}{dV} = \frac{d(V \times I)}{dV} = I + V \frac{dI}{dV} \quad (1.9)$$

$$\frac{1}{V} \frac{dP}{dV} = \frac{1}{V} + \frac{dI}{dV} \quad (1.10)$$

The schematic diagram of slope-based INC method shown in Figure 1.14.

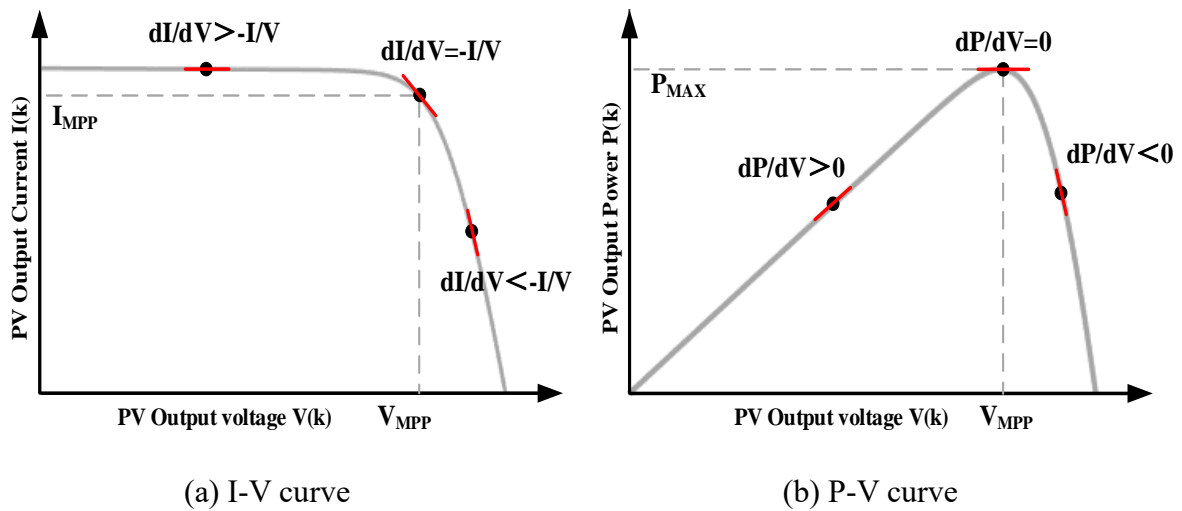


Figure 1.14 Schematic diagram of INC method

According to the schematic, when the PV system is operating at the maximum power point, there is $dP/dV=0$ and $dI/dV=-I/V$. When the tracking algorithm operates on the left side of the MPP, $dP/dV > 0$ and $dI/dV > -I/V$. When the system is working on the right side of the MPP point, $dP/dV < 0$ and $dI/dV < -I/V$. By continuously measuring the output voltage and current and comparing the results with those measured in the previous cycle, the voltage reference is continuously iterated to make the system work at MPP. The advantage of the INC method is that the oscillations are smaller when tracking the maximum power point. However, this algorithm is more complex compared to the P&O method and the accuracy of the measurements per cycle affects the performance of the algorithm. In addition, the INC method requires high system hardware performance [46, 47]. The flow chart of INC method is given in Figure 1.15.

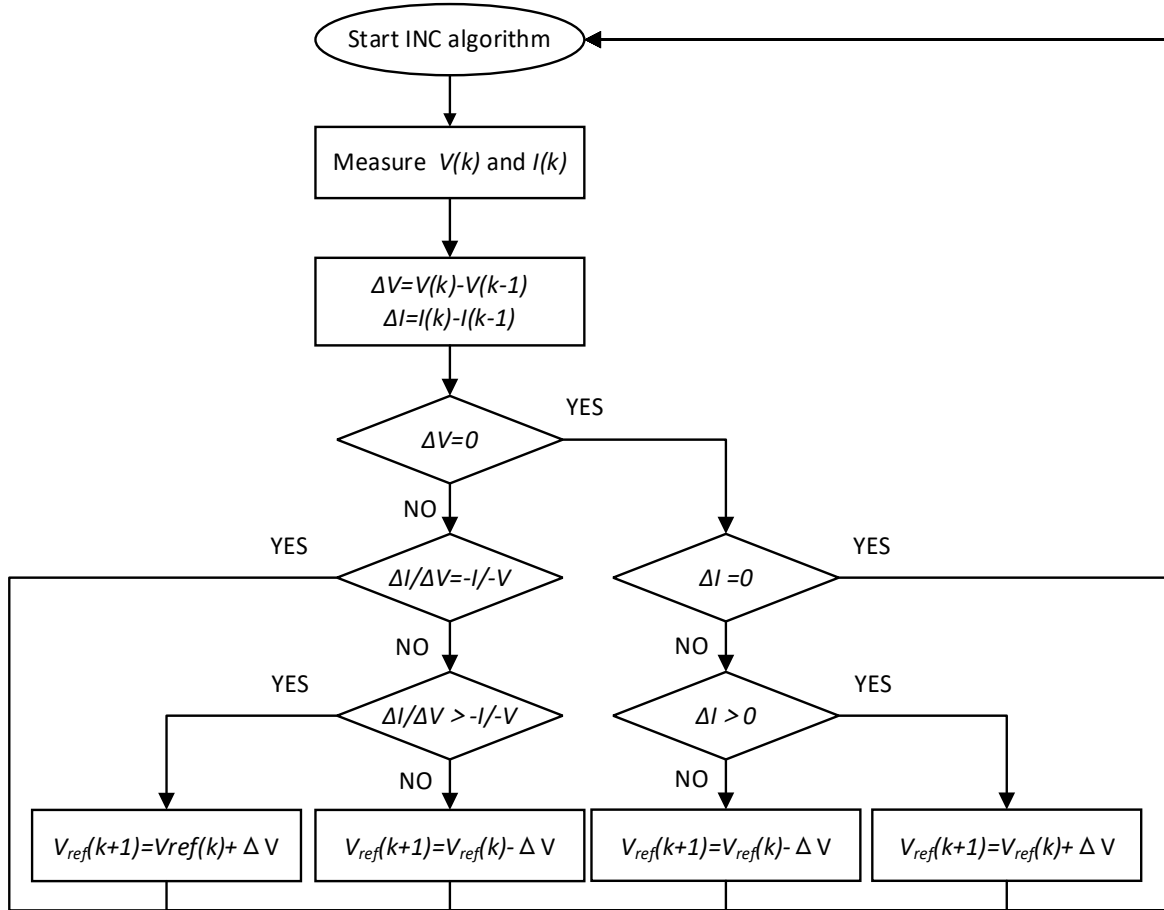


Figure 1.15 Flow chart of the INC method

1.6.2 Advanced MPPT algorithms

Conventional tracking methods may be failures when the PV arrays are exposed to different radiation levels. In addition, high tracking time and high steady-state oscillations are not negligible problems [48]. To resolve the conflict between tracking time and output power of conventional methods, more and more advanced algorithms with variable step size are proposed. Besides, the implementation of artificial intelligence (AI) algorithms can effectively solve the problem of tracking failure in PV systems under complex environmental conditions [43].

1.6.2.1 Fuzzy logic (FL) method

Since fuzzy logic techniques accurately predict the optimal voltage, current and power of PV systems without the need for precise mathematical models or exact inputs, it is considered an

intelligent method and is widely used in MPPT applications [49]. The fuzzy logic controller consists of four basic elements known as the fuzzification, the rules, the inference engine and the defuzzification which can be seen in Figure 1.16.

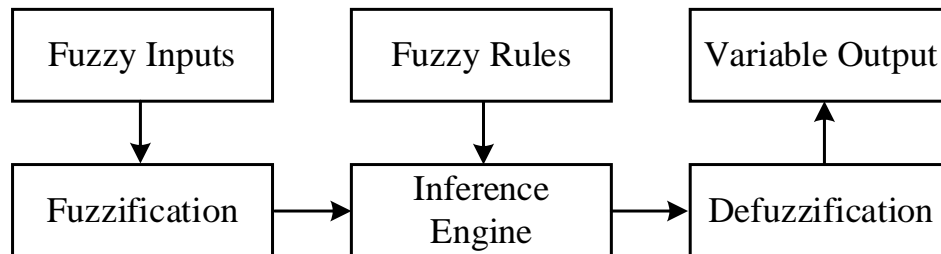


Figure 1.16 Fuzzy logic controller block diagram

The fuzzification step involves obtaining clear inputs, such as changes in PV system operating voltage or changes in system output power, and combining them with stored affiliation functions to produce fuzzy inputs. Input values are transformed into fuzzy variables by using triangular or trapezoidal membership functions. In general, the number of functions affects the system more than the type of function. Systems have higher accuracy but longer processing time when they have more membership functions. Systems with fewer membership functions exhibit better time response, but has a greater likelihood of bias [50]. A triangle membership function using negative large (NB), negative small (NS), zero (Z), positive small (PS), and positive large (PB) as linguistic variables is shown in the diagram 1.17.

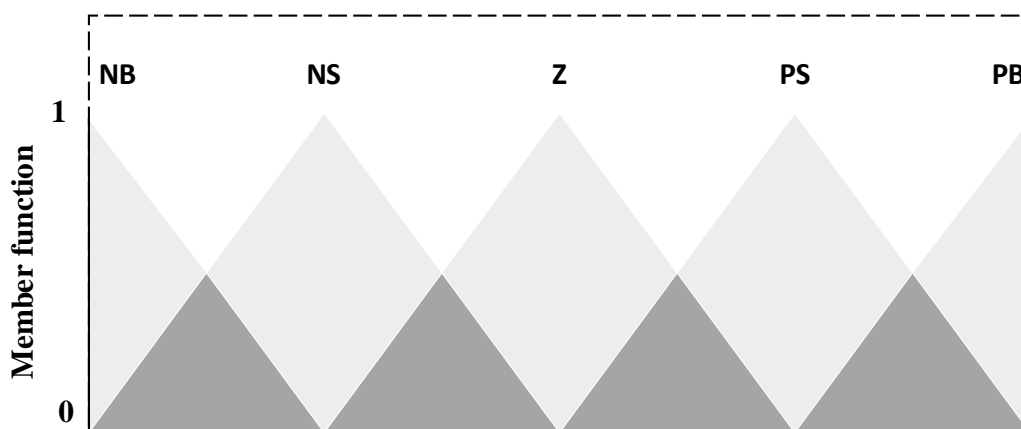


Figure 1.17 Triangular Membership function of FLC

The second step in fuzzy logic control is rule evaluation. The fuzzy input will be sent to the inference engine to be evaluated by rules. The fuzzy processor uses pre-set rules to determine what control actions should occur in response to a given set of input values, producing the corresponding outputs. When the output of the inference method is generated, a defuzzification process should be implemented to convert the fuzzy variables into real values [50]. The output of the defuzzification phase depends on the output required by the designed system. For example, for MPPT algorithms, the output of the defuzzification can be either a duty cycle or a variable perturbation step. The success of the fuzzy logic MPPT method depends on the appropriate choice of fuzzy input variables and fuzzy rules. The advantages and disadvantages of some different fuzzy inputs are summarized in Table 1.2 [51]. It is clear that the input of fuzzy logic has a significant impact on MPPT performance. The focus of the MPPT algorithm should be taken into account when designing the FLC. For example, when the PV system operates near the maximum power point, MPP misjudgments do not occur, so the P-V slope and change of output power ΔP_{PV} can be selected as input to the FLC to improve tracking efficiency.

Table 1.2 Advantages and disadvantages of different FL input

Input variable	Advantages	Disadvantages
Rate of change of PV system output power (P-V slope) and changes of slope	The change in slope makes it easy to determine the location of the system operating voltage.	<ol style="list-style-type: none"> 1. Output errors and fluctuations may occur near the maximum power point. 2. Poor tracking accuracy at low irradiance
Rate of change of PV system output power (P-V slope) and changes of output power ΔP_{PV}	<ol style="list-style-type: none"> 1. It is easy to determine if the system voltage is operating at the maximum power point. 2. ΔP_{PV} ensures tracking accuracy under low irradiation levels. 	Slope-based input could lead to misjudgments, which could result in power fluctuations
Changes of PV system output power ΔP_{PV} and	A very straightforward and simple approach.	<ol style="list-style-type: none"> 1. Slow response when irradiation changes

changes of PV system output voltage ΔV_{PV}		2. Inability to identify the maximum power point
		3. Low tracking speed
Changes of PV system output voltage ΔV_{PV} and changes of PV system output current ΔI_{PV}	1. Suitable for tracking MPP under increasing irradiation or constant irradiation	1. Slow response when irradiation changes
	2. A very straightforward and simple approach.	2. Inability to identify the maximum power point
		3. The tracking accuracy of MPPT is not too high at low irradiance.

1.6.2.2 Particle swarm optimization (PSO) MPPT method

In 1995 Eberhart and Kennedy proposed the particle swarm theory. The principle of this algorithm is derived from the foraging behavior of birds and fish groups. The core idea of the method is to use the information sharing among individuals in the group to find the optimal solution for the whole group. The advantage of PSO is that it is simple and easy to implement and does not have many parameters to adjust [52, 53]. The basic principle diagram of the particle swarm method is shown in the Figure 1.18.

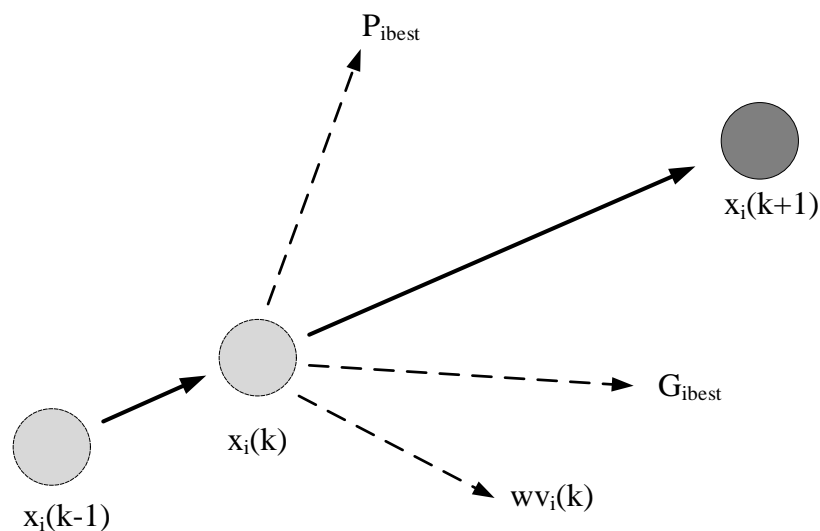


Figure 1.18 Movement of a particle in PSO algorithm

The standard formulation of the particle swarm algorithm is shown below:

$$v_i^{k+1} = \omega v_i^k + c_1 r_1 (P_{ibest} - x_i^k) + c_2 r_2 (G_{ibest} - x_i^k) \quad (1.11)$$

$$x_i^{k+1} = x_i^k + v_i^{k+1} \quad (1.12)$$

Where v_i and x_i are the velocity and position of particle; ω is inertia weight; r_1, r_2 are random variables between 0 and 1; c_1 and c_2 are positive constants represent the acceleration coefficients; P_{best} is the individual best position of a particle and G_{best} is the best position of all particles [53]. The working steps of the PSO algorithm are explained as follows while the flow chart is given in Figure 1.19 [54].

Step 1: Particle initialization. Particles are randomly and uniformly distributed in the search space

Step 2: Fitness evaluation. By providing the potential solution to the objective function, fitness is evaluated.

Step 3: Update individual and global best position.

Step 4: Update velocity and position of each particle. The velocity and position of each particle in the particle swarm will be updated according to Equations 1.11 and 1.12.

step 5: Determination of iteration termination. Check if the iteration is terminated. If the conditions for termination are met, then the optimization search can be terminated. Otherwise, the search will continue.

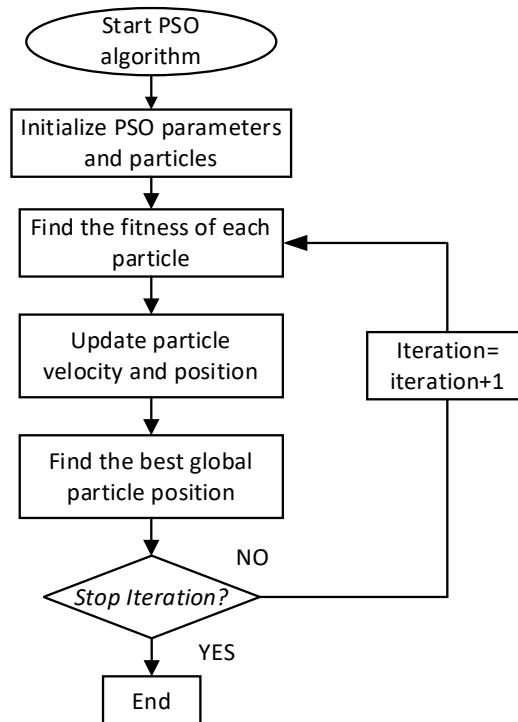


Figure 1.19 The flow chart of PSO method

PSO algorithms have been widely used in PV systems, and they can be divided into three main categories: standard PSO method, modified PSO method and hybrid PSO method. The advantages of the standard methods over the traditional MPPT methods are good performance under partial shading conditions, simplicity of implementation and high accuracy under constant weather conditions [47]. However, the tracking process of this method requires constant scanning of the PV curves and updating, and thus may lead to long tracking time and large computational effort for the PV system, which results in large power loss. Modified PSO methods typically improve the search speed and reduce the output power oscillation based on standard PSO methods. However, it may be more complex and place greater demands on the system performance. The hybrid PSO MPPT method has better tracking time and accuracy than the traditional PSO method, and is a very promising MPPT method [55].

1.6.2.3 Ant colony optimization (ACO) MPPT method

The ACO method was first proposed by Dorigo and has recently been successfully used in a number of applications in the MPPT field. Ant colony optimization method mimics the behavior of an ant colony and is an algorithm to find the optimal solution based on the behavior

of ants searching for food [56].

Ants search for food randomly in a certain area and they leave a pheromone trail behind them as they move. Ants within a colony have the ability to sense pheromones and they will walk along paths with higher pheromone concentrations. In the process of searching, ants with shorter paths release more pheromones. Therefore, the accumulated pheromone concentration on the shorter paths gradually increases, and the number of ants choosing that path also increases. In this way, the ants always pursue the shorter path to the food source during the optimizing process [57]. The schematic diagram of the ACO algorithm is shown in Figure 1.20.

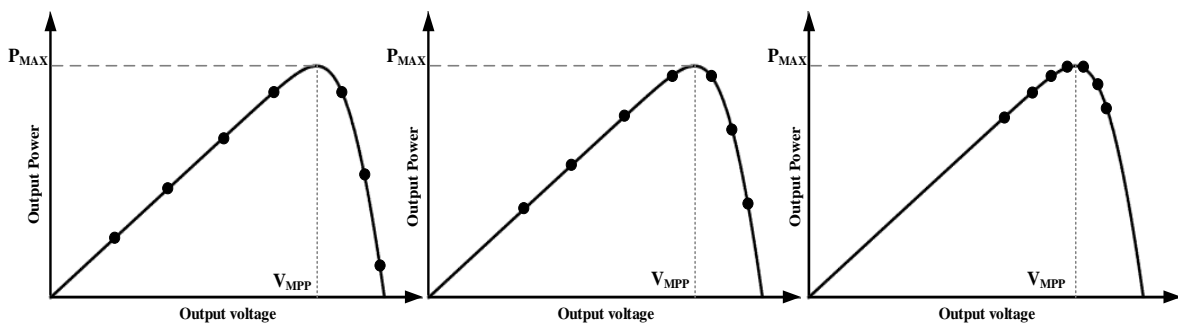


Figure 1.20 The schematic diagram of the ACO algorithm

The steps of the ACO-based MPPT algorithm are as follows [57, 58].

Initialize ant locations. A certain number of ants are deployed at random locations within the range interval in which the MPP is likely to occur. In the MPPT technique, the ant locations correspond to the duty cycle of the DC-DC converter. The PV system output power corresponding to the duty cycle is considered as the pheromone concentration. For each ant position, the ACO algorithm will calculate the corresponding output power of the PV system. In this step, the ant with the highest pheromone concentration will stay in its original position, while the rest of the ants will adjust their position to move closer to the ant with the highest pheromone concentration. When all ants have completed their movement, one iteration is considered complete. Repeat the above steps until all ants have converged to MPP.

The ACO algorithm has many advantages which provides parallel computing and has a strong global search ability. However, in the early search stage, the convergence of the ACO search can be very slow due to the low amount of information available because of low concentration of pheromones [59].

1.6.2.4 Hybrid MPPT method

Although conventional algorithms are low cost and easy to be applied, they have the potential to make the system fail in tracking under complex environmental conditions; or lead to large power losses in the PV system due to the limitations of fixed step size. Besides, the difficulty involved in advanced MPPT algorithm strategies and the increasing system computing requirements make the implementation cost of these techniques a must to be taken into account [60]. To overcome the limitations of traditional fixed step voltage disturbances, advanced and conventional techniques are often combined to improve the conflict between the MPPT algorithm transient response and MPP power fluctuations [61].

Some common applications are the use of fuzzy logic as a variable step generator in combination with traditional MPPT methods. Fuzzy logic controllers are combined with P&O, INC algorithms respectively, to improve MPPT performance of MPPT algorithm [62, 63]. On the other hand, advanced and traditional methods are combined to simplify the complexity of MPPT algorithms. For example, the combination of PSO and P&O algorithm ensures that the MPPT algorithm does not suffer from output power loss due to tracking failure under complex environmental conditions [64].

1.6.3 Comparison study of existing MPPT methods

Due to the nonlinear curve of the PV system output voltage and current, MPPT techniques have been developed to maximize power generation. The overall characteristics of the mentioned MPPT technique are summarized by Table 1.3 [41, 46, 47, 65]. It is worth to mention that the efficiency of MPPT methods can be calculated by comparing the actual power generation of the PV system with the theoretical maximum output power of the PV system. The efficiency can be calculated using the following formula:

$$\eta = \frac{\text{actual power generation}}{\text{theoretical maximum power generation}} \times 100\% \quad (1.13)$$

Table 1.3 Characteristics of mentioned MPPT methods

<i>Characteristic</i>	<i>P&O</i>	<i>INC</i>	<i>FL-P&O</i>	<i>PSO</i>	<i>ACO</i>
<i>Stability</i>	High	High	High	High	High
<i>Convergence speed</i>	High	High	Very high	Very high	Very high
<i>Complexity</i>	Low	Low	Moderate	High	High
<i>Implementation</i>	Easy	Easy	Moderate	Moderate	Moderate
<i>Efficiency</i>	Over 97%	Over 97%	Over 98%	Over 98%	Over 98%

The main advantages of traditional MPPT algorithms, such as P&O and INC, are their low cost and ease of application. However, they have long tracking time and considerable oscillations around the MPP. In addition, it is possible that the MPP cannot be tracked accurately under complex irradiation conditions. On the other hand, advanced MPPT methods, such as fuzzy logic, PSO, and ACO, effectively improve the performance of the MPPT and reduce the search time of the system as well as the oscillations at steady state. However, they are more complex and more expensive to implement than traditional MPPT methods. Therefore, on the basis of ensuring that the PV system can accurately track the MPP under complex irradiation conditions, traditional MPPT algorithm and advanced MPPT algorithm are combined to build the hybrid MPPT algorithms to achieve superior performance.

1.7 Summary

The PV emulator is an important application for power electronics experiments on photovoltaic systems. It not only provides the researcher with controlled external conditions, but also allows for a repeatable experimental environment. In addition, the PV emulator should be easy to interact with power electronics. At the same time, the limitations of the actual PV system should be taken into account, such as hot spot issue, simulating partially shading conditions, etc. Due

to the non-linear curves obtained by the PV system, MPPT methods are developed to extract maximum power generation. The main advantages of conventional MPPT methods are their low cost and ease of application. However, they suffer from high stabilization times and large power losses when tracking. Advanced MPPT methods, on the other hand, reduce the rise time and the oscillations in the steady state, but the complexity of the system is higher. Therefore, in order to reduce the complexity of the advanced techniques and improve the performance of the conventional MPPT, hybrid MPPT methods are proposed in this thesis.

1.8 Objectives of the thesis

1. The objective of this thesis is to propose a novel partial shading emulation system of a PV array which was constructed by using unirradiated solar panels and external current sources in a laboratory environment in which each external current source (DC power supply) is connected in parallel with a solar panel. The constructed PV array partial shading emulation system has the same dynamic characteristics as that of the PV array under actual sunlight. By regulating the output currents of the parallel-connected current sources, the proposed PV array emulation system can emulate the electrical characteristics of various connected PV array under various solar irradiance and partial shading conditions. The proposed PV simulator can be used for power electronics experiments on PV systems, providing researchers with a PV experimental system with controlled and reproducible external environmental conditions.

2. Two MPPT algorithms for partial shading conditions were developed and verified using the proposed PV emulator. The hybrid global search and adaptive P&O algorithm performs a global search in the area of the PV system where the maximum power point is likely to occur and is therefore unlikely to miss the global maximum power point. After the location of the maximum power point has been determined the algorithm switches to a local adaptive P&O algorithm to reduce the power loss during tracking. The proposed fast global tracking (FGT)-fuzzy logic P&O algorithm searches the voltage locations of only seven possible maximum power points of the PV system per iteration at the early stage and narrows the search area with each iteration. This has the advantage of significantly reducing the computation of the algorithm and reducing the requirement for system computing power. After obtaining an approximate maximum power point for the PV system the algorithm moves to a local fuzzy

logic P&O algorithm to continue tracking in order to reduce the power loss in the tracking process. The performance verification of the designed algorithms has been validated using proposed emulation system, boost converter and dSPACE Real Time Interface (RTI) hardware. The proposed MPPT algorithms can track the MPP of the PV system under partial shading conditions. In addition, the proposed MPPT methods combines the advantages of both conventional and advanced methods to provide faster tracking speed and higher efficiency at steady state compared to existing MPPT algorithms.

1.9 Thesis synopsis

Chapter 1: Gives an over review of the topic, providing general information of PV emulator system and maximum power point tracking algorithm as well as contributions.

Chapter 2: In this segment, the proposed PV emulator system is presented. The operational principle as well as test results are shown. The experimental results show that the proposed PV emulator can simulate the electrical characteristics of real PV system under uniform irradiation and partial shading conditions.

Chapter 3: On this chapter, it is covered the proposed MPPT algorithm under partial shading conditions. The design methods and principles of the two MPPT methods are presented.

Chapter 4: The overall topology of PV emulator system and simulation results of the proposed MPPT algorithms are presented in this section. Simulation results show the superior tracking performance of the two proposed MPPT methods.

Chapter 5: The experimental verification results obtained from dSPACE system are presented in this chapter. The experimental results are consistent with the simulation results, again demonstrating the feasibility of the proposed algorithm.

Chapter 6: Presents the conclusions of proposed PV emulator and MPPT algorithms under partial shading conditions.

Chapter 7: In this chapter, presents the future improvement direction of proposed PV emulator and MPPT algorithms. The microcontroller will be used as an alternative to the dSPACE control system to re-validate the proposed MPPT method.

Chapter 2. External current source-based unilluminated PV emulation system

2.1 Introduction

In this section, a PV emulator is constructed by using a real PV panel and a DC power supply. By regulating the output currents of the parallel-connected current sources, the proposed PV array emulation system can emulate the electrical characteristics of various connected PV array under various solar irradiance conditions. The math model and electrical characteristic of the PV emulator were discussed and analyzed, explaining the reasons for the differences between the PV simulator and the actual solar system. In addition, the proposed PV emulator simulates the I-V, P-V characteristics of a PV system under uniform and partially shading irradiation conditions.

2.2 Single solar panel emulator system

The operational principle of the proposed PV source emulating system is by connecting an external current source in parallel with a solar panel [66]. The equivalent circuit of the emulated PV source is shown in Figure 2.1.

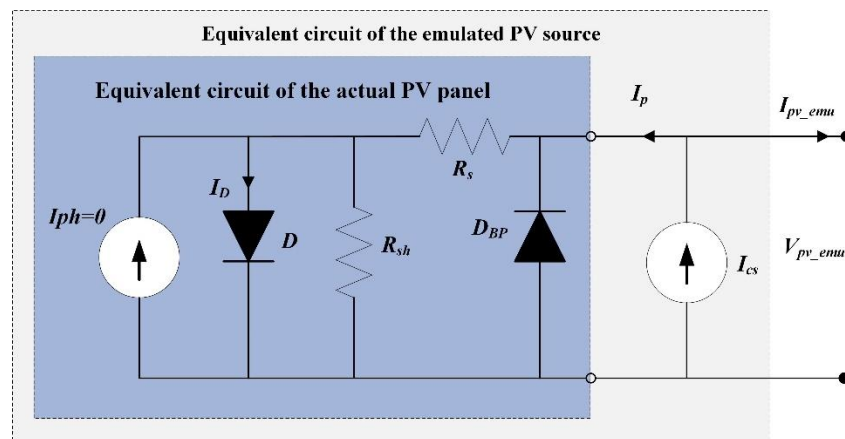


Figure 2.1 Equivalent circuit of the emulated PV source

Due to the low irradiation in an indoor environment, there is no photo-current from a solar panel can be generated. Therefore, an external current source is employed and connected in parallel with the solar panel. The photo-current generated by actual sunlight is represented by the current source current. Variation of the external current source current represents different

irradiance levels of solar irradiance received by the solar panel and it will be easy to emulate the variation of solar irradiance by regulating the current source current. D_{BP} in Figure 2.1 represents the bypass diode integrated with the PV panel. The role the bypass diode is to avoid hot spots formed when some solar cells in a PV panel or some PV panels in a PV array receive less solar irradiance than others during partial shading [67]. To simplify the description of the operational principle and characteristics of the emulated PV source, the single-diode model was used to represent the equivalent circuit of the emulated PV source. The equivalent circuit of a single diode solar panel is shown in Figure 2.2.

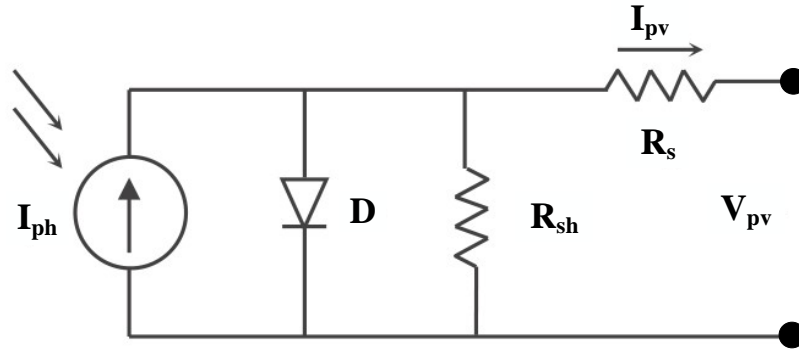


Figure 2.2 The equivalent circuit of a single diode solar panel

The general I-V characteristic is given by:

$$I_{pv} = I_{ph} - I_s \left(e^{\frac{V_{pv} + I_{pv}R_s}{N_s V_t}} - 1 \right) - \frac{V_{pv} + I_{pv}R_s}{R_{sh}} \quad (2.1)$$

where V_t is the junction thermal voltage, I_s represents dark saturation current, R_s is panel series resistance, R_{sh} represents the panel parallel resistance, N_s is the number of cells connected in series [68].

The photo-generated current, I_{ph} , is mainly influenced by irradiation and is proportional to the solar radiance falling on the solar panel. Since the dark saturation current I_s is very small, the output current of the solar panel is mainly dominated by the I_{ph} . For an emulated PV panel, the

generated current is supplied by an external current source and is injected into the PV panel through R_S . The voltage across the diode can be seen in Equation 2.2:

$$V_{D_emu} = V_{pv} - I_p \cdot R_S \quad (2.2)$$

In indoor conditions, assume the photo-current generated by indoor light is zero. The electrical characteristics of the emulated PV simulator can be expressed by Equation 2.3:

$$I_{pv_emu} = I_{CS} - I_S \left(e^{\frac{V_{pv_emu} - I_p R_S}{n N_s V_t}} - 1 \right) - I_{sh} \quad (2.3)$$

$$V_{pv_emu} = I_p R_S + V_t R_S \cdot \ln \frac{I_p - I_{sh} + I_S}{I_S} \quad (2.4)$$

$$I_{sh} = \frac{V_{pv} - I_p R_S}{R_{sh}} \quad (2.5)$$

Where I_{pv_emu} and V_{pv_emu} are the terminal current and voltage of the emulated PV source, I_{CS} represents the external current source current, I_p represents the current injected into the PV panel, I_S represents the dark saturation current, R_S and R_{sh} are the series and shunt resistances of the solar panel, n is the diode quality factor, N_s is the number of series-connected PV cells in the PV panel, V_t is the solar cell thermal voltage, where k is Boltzmann's constant ($1.38 \times 10^{-23} J/K$), q is the elementary charge ($1.6 \times 10^{-19} C$), and T is $p-n$ junction temperature in Kelvin [69]. For a given DC source current I_{CS} , the current injected into the real solar panel is:

$$I_p = I_{CS} - I_{pv_emu} \quad (2.6)$$

Nevertheless, it is important to note that temperature also influences the performance of the solar panel in addition to solar irradiance. The Equation for the excitation current I_{CS} is shown below [66]:

$$I_{cs} = [I_{CS_{STC}} + C_T(T - T_{ref})] \frac{S}{S_{ref}} \quad (2.7)$$

where C_T represents the temperature coefficient of photo-current which is 1.7×10^{-3} (A/K), T is actual cell temperature, S_{ref} represents reference irradiation 1000 W/m^2 .

To evaluate the proposed PV source emulation system, a test system was set up as shown in Figure 2.3, where a SUNTEC 175 W solar panel STP175S-24/Ac was employed and connected with an external source (TENMA 72-2940 Programmable Bench Power Supply) in parallel. The parameters of a single PV panel under standard test conditions (STC) (i.e. irradiance 1000 W/m^2 , module temperature 25°C) can be seen in Table 2.1.

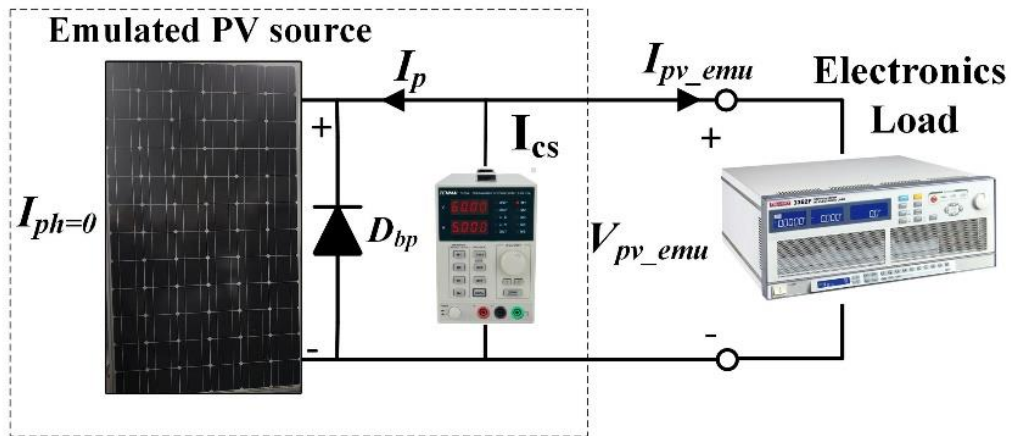
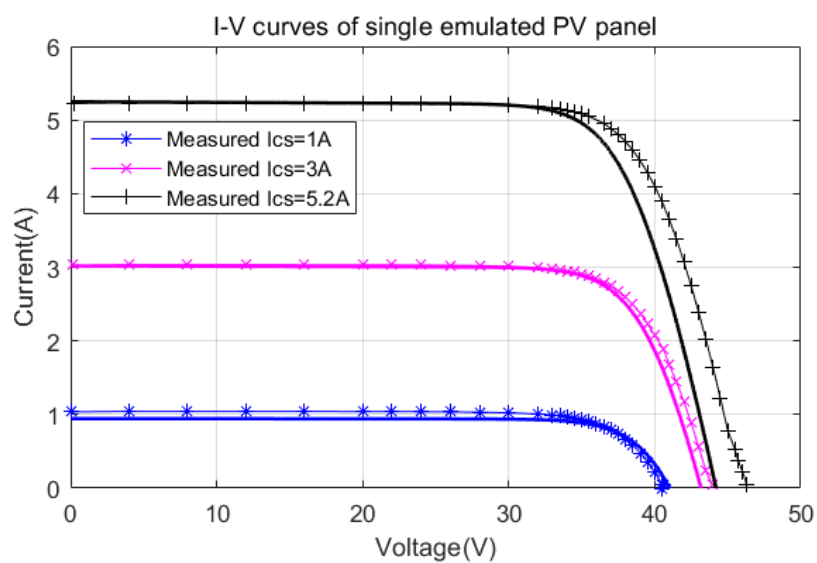


Figure 2.3 Equivalent circuit of the emulated PV source

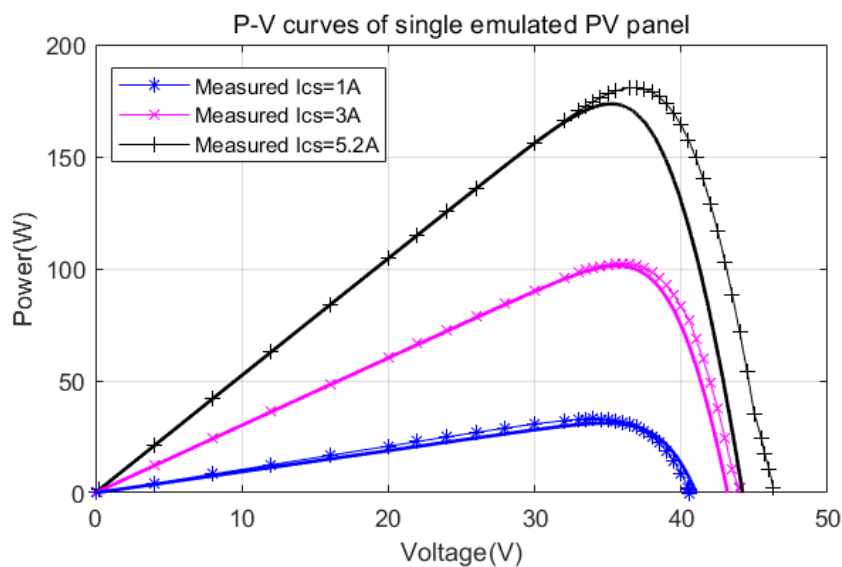
Table 2.1 The parameters of solar panel STP175S-24/Ac

<i>Parameter and components</i>	<i>Value</i>
<i>Maximum output power</i>	174.24 W
<i>Short-circuit current I_{SC}</i>	5.2 A
<i>Open-circuit voltage V_{OC}</i>	44.2 V
<i>Current at MPP I_{MPP}</i>	4.95 A
<i>Voltage at MPP V_{MPP}</i>	35.2 V
<i>Cells per Module</i>	72

A PRODOGIT 3362F DC load was employed for measuring the I-V and P-V characteristics of the emulated PV source. The DC Load operated in its constant voltage (CV) mode and the voltage was swept from 0 to 44.2 V (open-circuit voltage of the solar panel) with a step of 0.5 V. Figure 2.4 shows the measured and datasheet given I-V and P-V curves of the proposed PV source emulator with three different solar irradiance levels emulated by setting three different external current source current levels and the given characteristic from datasheet (thick solid line). The three different current levels of the external current source current was set as $I_{CS} = 1.0\text{ A}$, $I_{CS} = 3.0\text{ A}$, $I_{CS} = 5.2\text{ A}$, respectively.



(a) I-V curves



(b) P-V curves

Figure 2.4. Measured electrical characteristics of the constructed PV source based on a single solar panel at different current source currents

It can be observed that the emulated I-V and P-V curves are quite close in nature to those produced by the real PV panel, despite the fact that there is a minor error between the measured I-V curve from the emulated PV panel and that provided by the datasheet of the actual PV panel. The error occurs mainly when the system operating voltage crosses the maximum power point voltage. According to the Equation 2.6, the current supplied by the DC power source remains constant and as the voltage increases, the output current of the solar panel will decrease, resulting in an increase in the current injected into the solar panel. The product of the series resistance and the current injected into the solar panel from the external current source results in the difference between the simulator I-V characteristic curve and the actual solar panel datasheet, as shown in Equation 2.8 [27]:

$$\Delta V = R_s \cdot I_p \quad (2.8)$$

According to the I-V characteristic curves, it is known that when the PV system is operating at the open circuit voltage of the solar panel, all the current supplied by the DC voltage source will be injected into the solar panel. When the current flowing through R_s increases, the equivalent voltage of R_s also increases, which leads to a maximum voltage error of ΔV_{MAX} . Based on the difference of open circuit voltage between measured emulated PV panel values and datasheet given values, the series resistance of the PV panel can be estimated by:

$$R_{S_estimated} = \frac{V_{pv_emu_open} - V_{pv_datasheet_open}}{I_{CS}} \quad (2.9)$$

When the emulated PV system is under $1000\text{W}/\text{m}^2$ irradiation conditions ($I_{CS}=5.2\text{ A}$), the open voltage of the PV emulator is 46.3V and the datasheet given open circuit voltage is 44.2V . Therefore, the estimated series resistance is about 0.4 ohms . It is important to note that, in addition to the I_{CS} , the temperature also has an impact on electrical characteristic of PV array. The effect of temperature variation on MPP values has not been considered in this thesis due to the small temperature variations in room and the temperature cannot easily be controlled at a constant level. The electrical characteristics provided by the simulator are almost identical to

those of an irradiation illuminated PV module. In contrast to actual outdoor PV panels or other emulator solutions, the PV emulator presented requires only simple laboratory equipment to implement.

2.3 Partial shading emulation of PV array using the proposed PV source emulator

I-V and P-V characteristic curves above show that by applying an external current source, the solar panel can be effectively simulated under various irradiation conditions. Therefore, a new emulation system consisting of two PV emulators connected in series can be used for emulating partial shading performance of a PV array. When the partial shading occurs, the PV array is operating under uniform insolation as results of partial shading, the photocurrent of shaded PV cells reduces while the unshaded cells remain higher photo-current. In this case, the shaded cells will operate in reverse bias region and consume power due to reverse voltage polarity and resulting in a hot spot and potential cell breakdown. With commercial PV panels, an anti-parallel bypass diode is usually connected to the PV panel to limits the reverse voltage and reduce the power loss in the shaded panel [70]. This partial shading and the additional bypass diode result in complicated shape of the P-V curves characterized by multiple peaks including several local maximum power points (LMPPs) and a global maximum power point (GMPP). These multiple peaks might result in conventional maximum power point tracking (MPPT) trapped around an LMPP and therefore reduce the actual power output significantly [71]. When the PV emulator is connected in parallel, the simulated PV system is not partially shading because in a parallel circuit each solar panel has an independent current path. The output voltage of each solar panel connected in parallel is the same, which means that even if one of the solar panels is partially shading, the other solar panels can still continue to output current without being affected. Based on the idea presented in previous section, this section will present a novel PV array emulator that can emulate partial shading performance of PV array with both series and parallel connections of PV panels. The laboratory set up is shown in Figure 2.5.

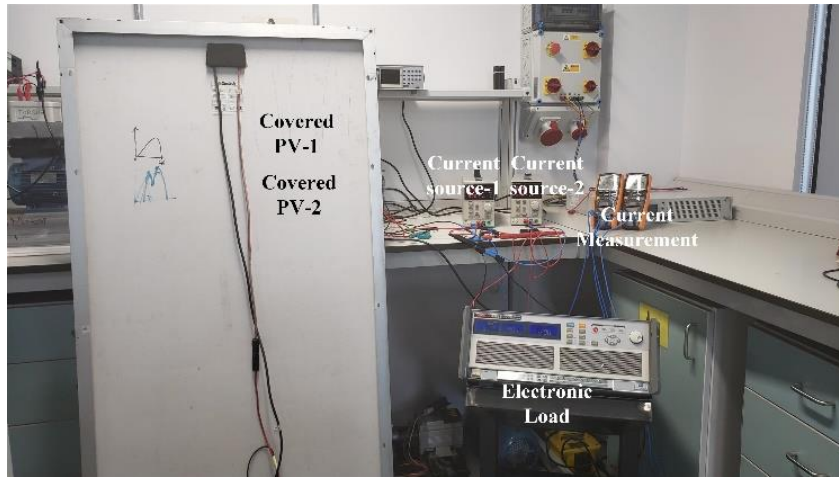


Figure 2.5 Laboratory set up for proposed unilluminated emulated PV system

2.4 Series-connected solar panels emulator system

Based on the idea presented in section 2.2, a partial shading emulation system using two series-connected solar panels and two external current sources was proposed and constructed. The equivalent circuit of the partial shading emulation system and experiment setup are shown in Figure 2.6.

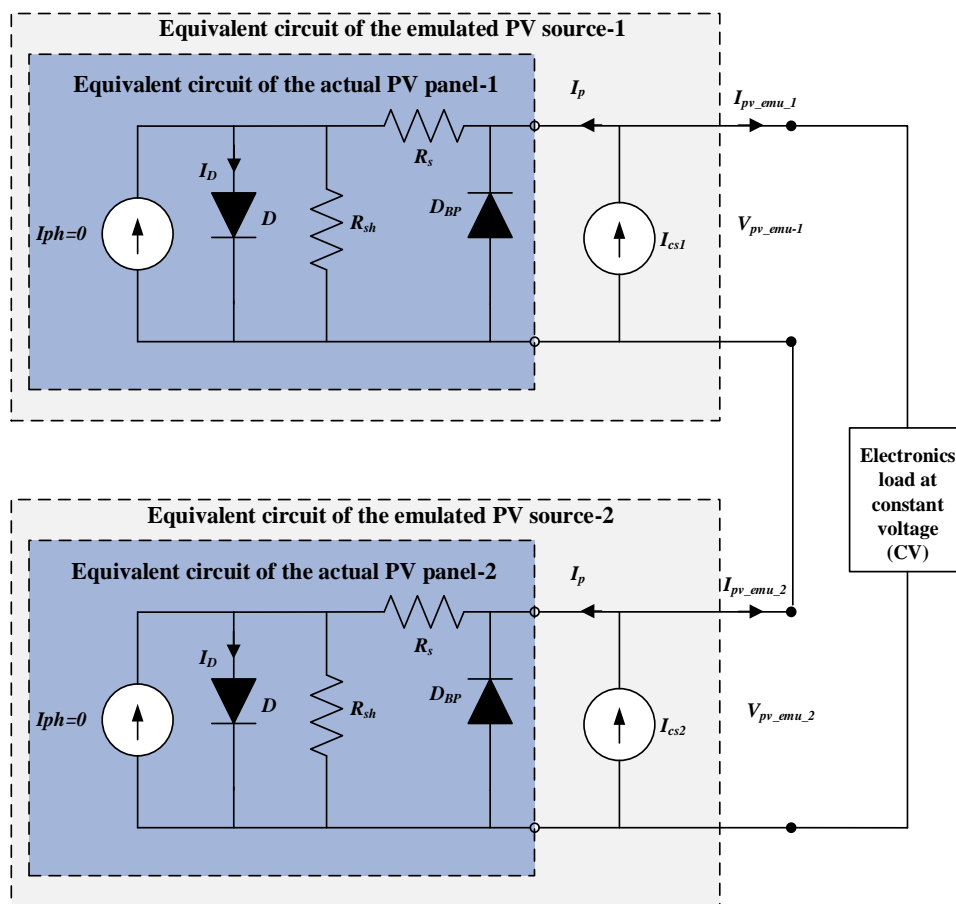


Figure 2.6 Equivalent circuit of proposed emulated PV system

Two SUNTEC 175 W solar panels (STP175S-24/Ac) were employed and connected in series. As the solar panel located inside the laboratory with very weak solar insolation, there is almost no photo-current generated from indoor solar panels, i.e. $i_{ph} \cong 0$. The photo-currents of the two solar panels were emulated by output of the two TENMA 72-2940 Programmable Bench current sources, respectively. Assumes that two solar panels are identical with the same leakage current, dark saturation current, as well as the same external current source current I_{CS} , the output current and output voltage of the emulated PV system were derived as 2.10 and 2.11:

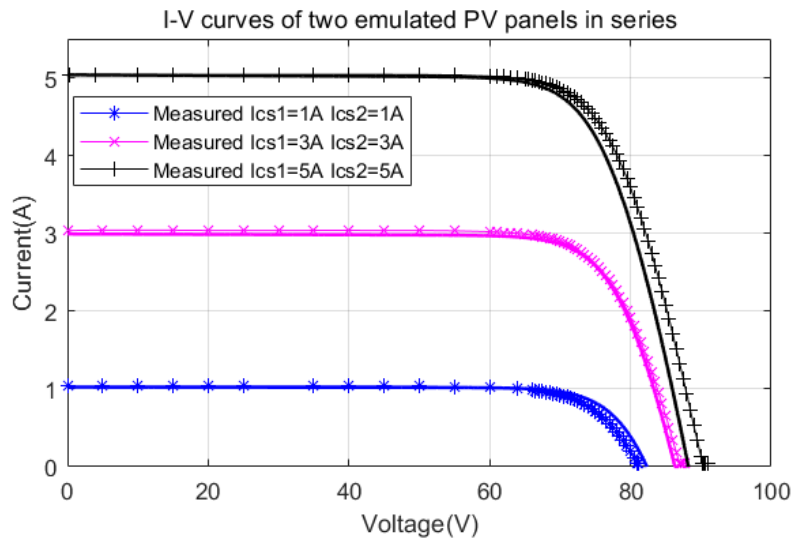
$$I_{pv_emu} = I_{CS} - I_s \left(e^{\frac{V_{pv_emu} - I_p \cdot m \cdot R_s}{V_t \cdot m \cdot N_s}} - 1 \right) - I_{sh} \quad (2.10)$$

$$V_{pv_emu} = I_p(mR_s) + V_t(mR_s) \cdot \ln \frac{I_p - I_{sh} + I_s}{I_s} \quad (2.11)$$

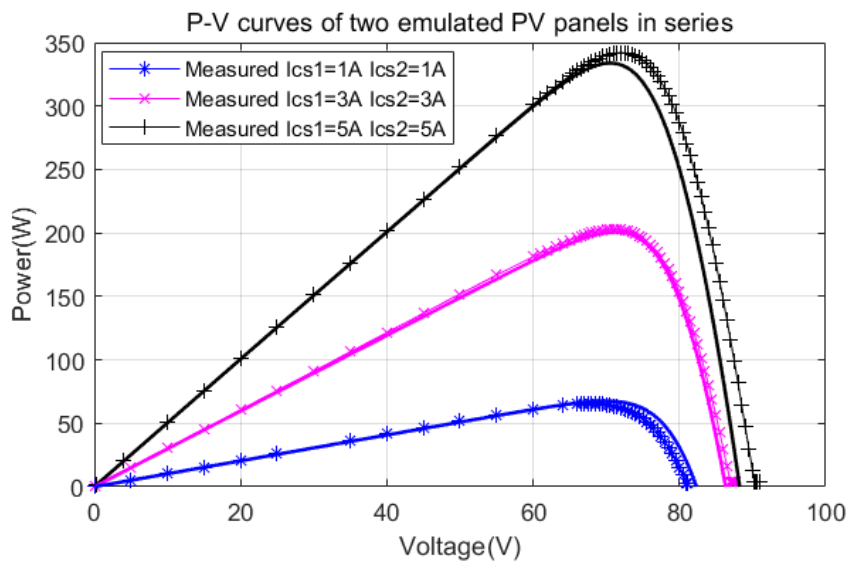
where $m=2$ represents the number of solar panels connected in series [27].

2.4.1 Emulated electrical characteristics under uniform solar irradiation

Figure 2.7 shows the measured and datasheet given (thick solid lines) electrical characteristics of the emulated PV array based on two series solar panels with different solar irradiance, the different solar irradiance level was emulated by setting both external current source current as 1A/3A/5A (corresponding to the actual I-V and P-V curves under 200W/m², 600W/m² and 1000W/m² solar irradiance).



(a) I-V curves



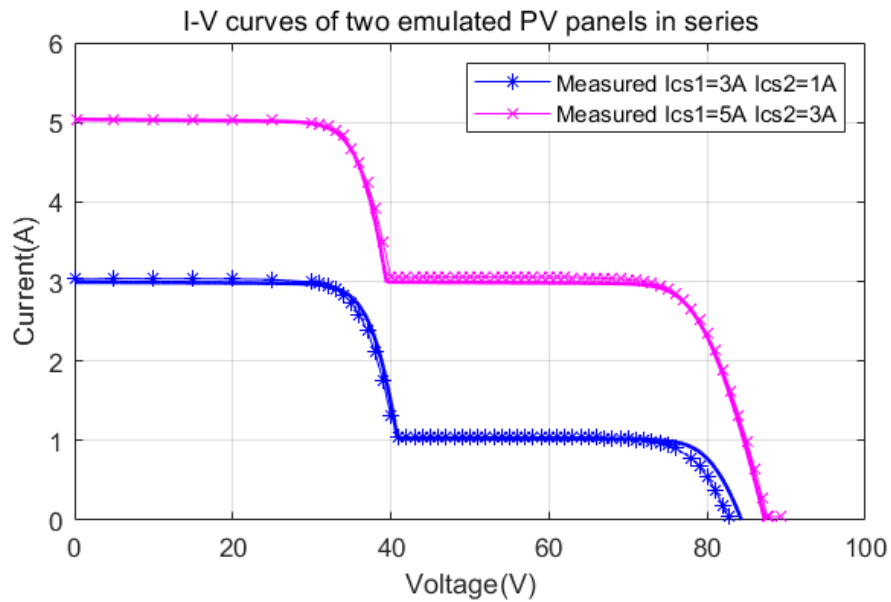
(b) P-V curves

Figure 2.7 Measured and datasheet given electrical characteristics of the emulated PV arrays based on two series solar panels

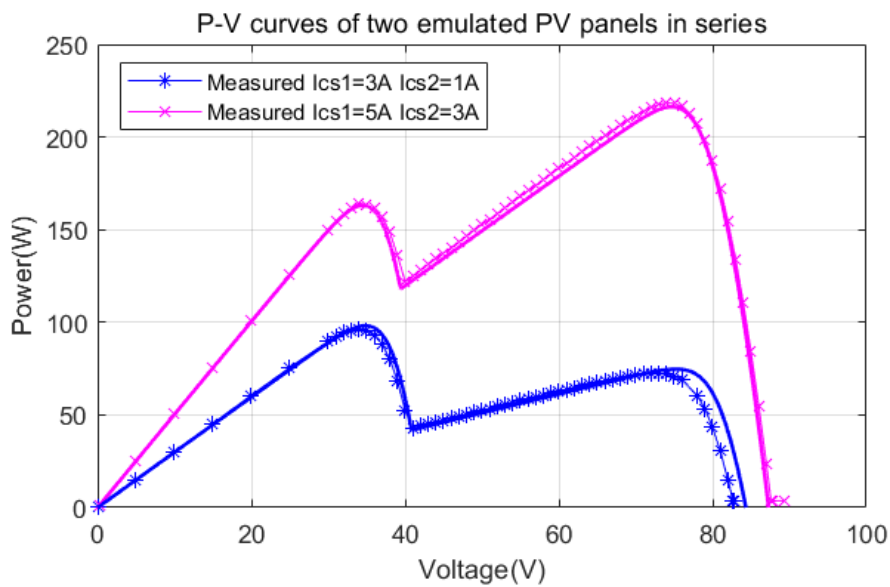
2.4.2 Emulated electrical characteristics under partial shading

By varying the current source currents, various solar irradiance received by each solar panel can be emulated. Figure 2.8 shows the I-V and P-V curves at two current source setting. In the first partial shading condition, the two current sources were set as $I_{CS1}=3A$, $I_{CS2}=1A$, respectively. In the second case, the two current source currents were set as $I_{CS1}=5A$ $I_{CS2}=3A$, respectively. Since the anti-parallel connected bypass diodes integrated with the solar panels provide an alternate current path, the solar panels no longer carry the same current when partial

shaded. In this case, there are multiple maximum power points developed in the P-V curve as shown in Figure 2.8. The emulated P-V curves, therefore, can be used to test advanced MPPT algorithms to find the actual global maximum power point (GMPP) for partial shading conditions.



(a) I-V curves



(b) P-V curves

Figure 2.8 Measured and datasheet given electrical characteristics of the emulated PV arrays under two different partial shading operation conditions

Figures above show that two solar panels connected in series work under partial shading, and the I-V and P-V curves are different from the PV system operating under uniform irradiation, with two peaks, which are similar to the given datasheet and simulation results.

2.5 Parallel-connected solar panels emulator system

Figure 2.9 shows an equivalent circuit partial shading emulation circuit based two parallel-connected solar panels and two external current sources.

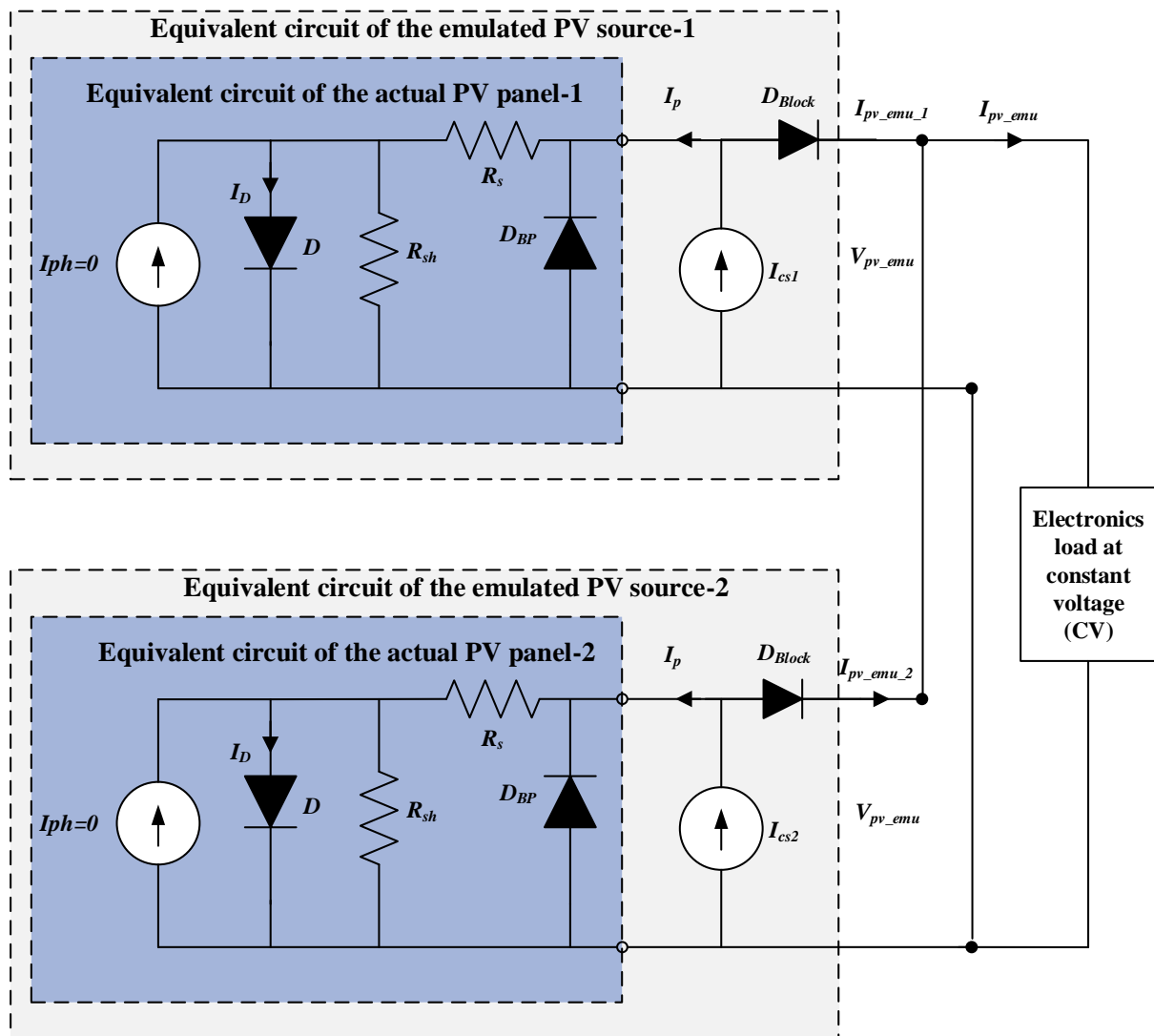


Figure 2.9 The proposed PV array partial shading emulation system with two parallel-connected unilluminated solar panels

For each emulated PV panel, one blocking diode is connected in series between the external

current source and output terminal for blocking the current injecting into the PV panel from other current sources when emulate partial shading operation of the PV array. Assumes that two unilluminated solar panels are identical with the same leakage current, dark saturation current, as well as the same external current source current I_{CS} , the output current and output voltage of the PV emulation system, were derived as Equation 2.12 and 2.13:

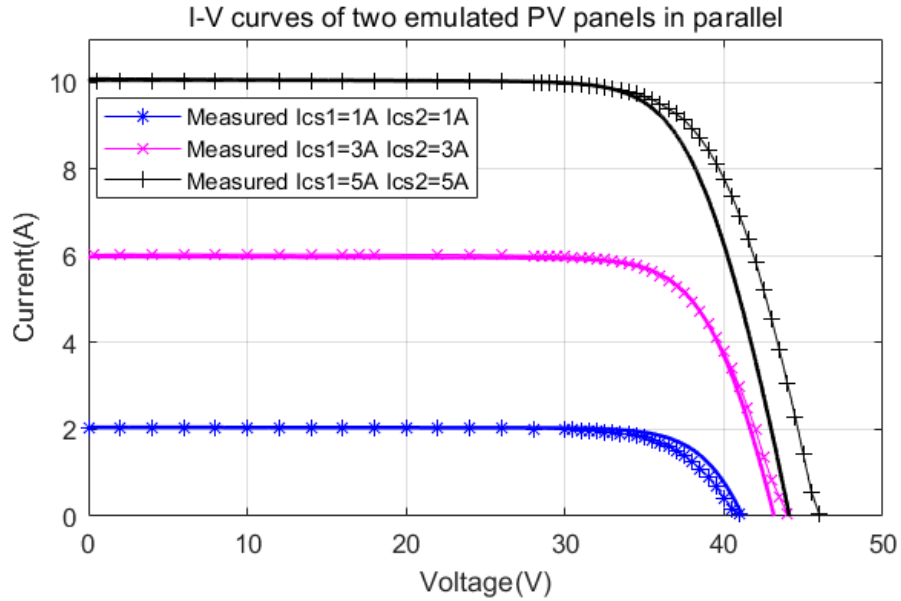
$$I_{pv_emu} = mI_{CS} - mI_s \left(e^{\frac{V_{pv_emu} - I_p \cdot R_s}{V_t \cdot N_s}} - 1 \right) - mI_{sh} \quad (2.12)$$

$$V_{pv_emu} = I_p(R_s) + V_t(R_s) \cdot \ln \frac{I_p - I_{sh} + I_s}{I_s} \quad (2.13)$$

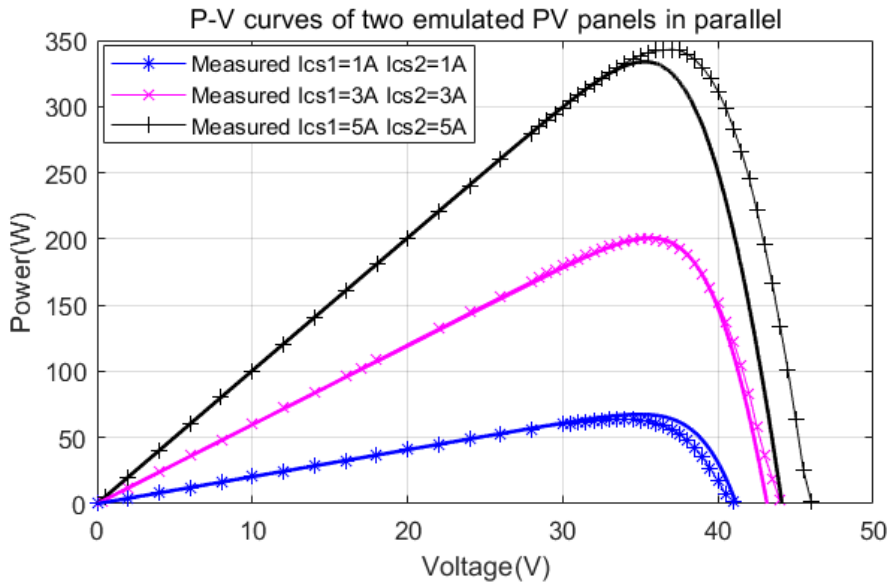
where $m=2$ represents the number of solar panels connected in parallel [27].

2.5.1 Emulated electrical characteristics under uniform solar irradiation

Figure 2.10 shows the measured and datasheet (thick solid lines) electrical characteristics of the emulated PV array with on two parallel-connected unilluminated solar panels at three different emulated solar irradiances. The curve 1 (blue lines), curve 2 (red lines) and curve 3 (black lines) represent the I-V and P-V curves emulated by setting both current source currents I_{cs1} and I_{cs2} as 1A/3A/5A, respectively (corresponding to the actual I-V and P-V curves under $200W/m^2$, $600W/m^2$ and $1000W/m^2$ solar irradiance).



(a) I-V curves

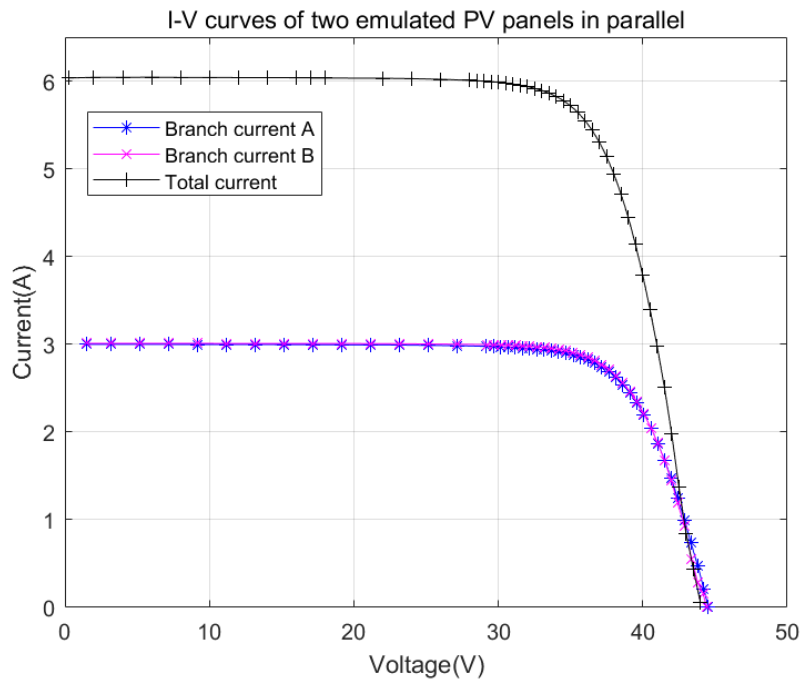


(b) P-V curves

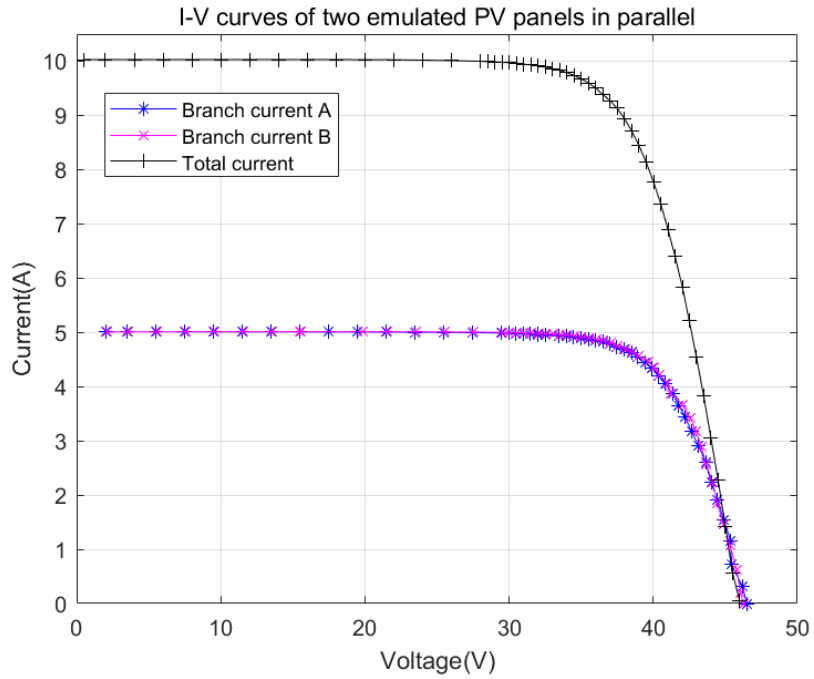
Figure 2.10 Measured and datasheet given electrical characteristics of the emulated PV arrays based on two parallel solar panels

In the case of two different blocking diodes (one is Infineon D08S120, one is D12S60C) the conduction resistances of two blocking diodes are different. For D08S120, at 25°C, when the current through the diode is 7.5A, the voltage is 1.65V. Therefore, the on-resistance of the diode is about 0.22Ω. At the same temperature, when D12S60C passes 12A current, the diode voltage is 1.5V, and the on-resistance is around 0.083Ω. The datasheets of D08S120 and D12S60C are shown in [72] and [73]. The difference of the conduction resistance results in unbalanced

currents between the two output currents of two emulated PV panels in parallel, as shown in Figure 2.11 and Figure 2.12. In Figure 2.12 (a) both two current source currents were set as 3A, however as the different of the conduction resistance of the two diodes the short circuit current of the first emulated PV panel is about 3.5 A, and the second is about 2.5 A, the two output currents are unbalanced significantly. Figure 2.12 (b) shows the measured output currents of emulated solar panels with two different blocking diodes, in this case, both the two current source currents were set as 5 A. However, as the different of the conduction resistance of the two diodes the short circuit current of the first emulated PV panel is about 6.2 A, and the second is about 4.8 A, the two output currents are unbalanced significantly.

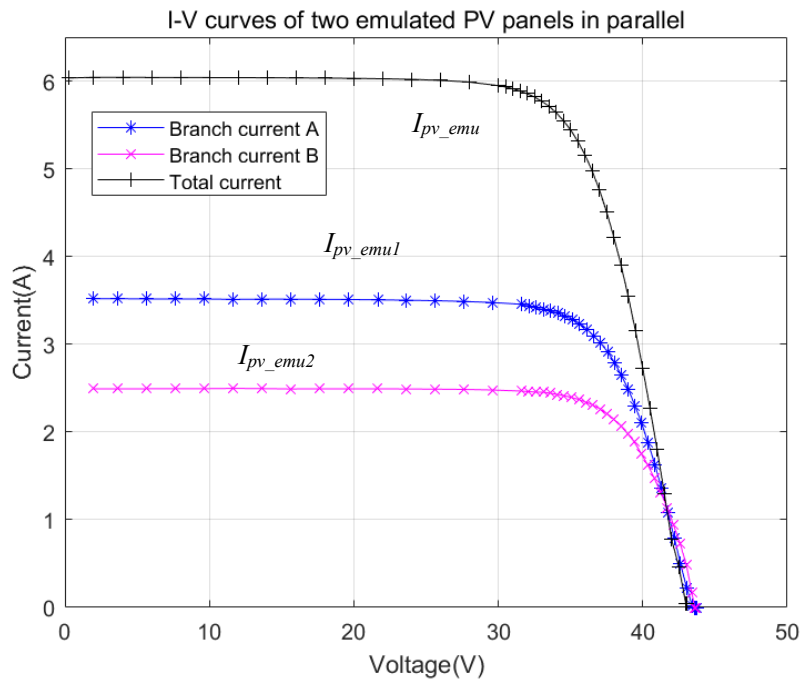


(a) $I_{cs1}=3$ A, $I_{cs2}=3$ A

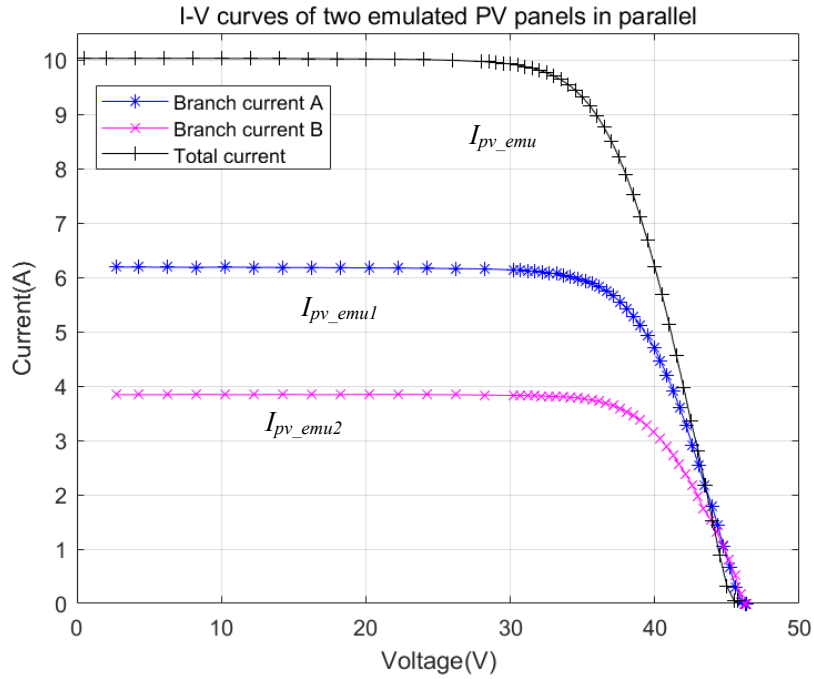


(b) $I_{cs1}=5\text{ A}$, $I_{cs2}=5\text{ A}$

Figure 2.11 Measured output currents of emulated solar panels with two identical blocking diodes



(a) $I_{cs1}=3\text{ A}$, $I_{cs2}=3\text{ A}$

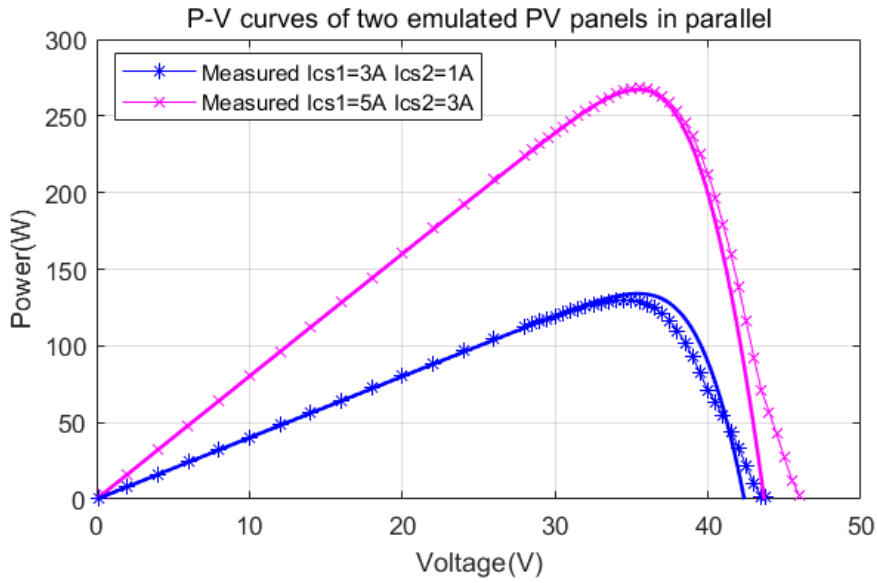


(b) $I_{cs1}=5A, I_{cs2}=5A$

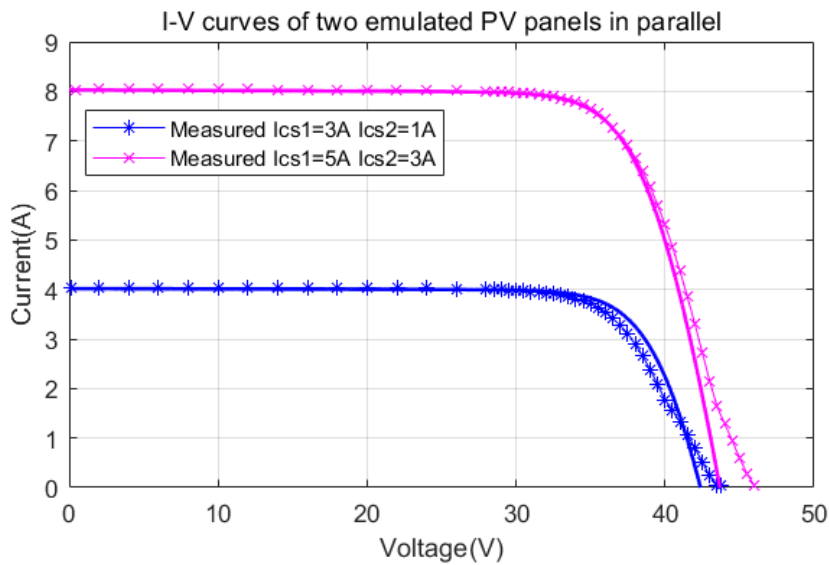
Figure 2.12 Measured output currents of emulated solar panels with two different blocking diodes

2.5.2 Emulated electrical characteristics under partial shading

By setting the two current source currents I_{cs1} and I_{cs2} differently, various I-V and P-V curve of PV array with parallel-connected solar panels under partial shading conditions can be emulated. Figure 2.13 shows electrical characteristics under two different partial shading conditions. The blue curves represent emulated I-V and P-V curves with $I_{CS1}=3A, I_{CS2}=1A$, which corresponds to the electrical characteristics of two PV panel under $600W/m^2$ and $200 W/m^2$ solar irradiance respectively. The red lines represent emulated I-V and P-V curves with $I_{CS1}=5A, I_{CS2}=3A$, which corresponds to the electrical characteristics of two PV panel under $1000W/m^2$ and $600 W/m^2$ solar irradiance respectively. It is observed with the exist of blocking diode there is no multiple peaks in the power-voltage curves of the PV array. The output current of the PV array emulation system equals the sum of the output current of two solar panels. It is worth mentioning that it is easy to regulate emulated photo-current of each panel by simply regulating the current of the current source connected. Therefore, the proposed system can emulate both static and dynamic current easily.



(a) I-V curves

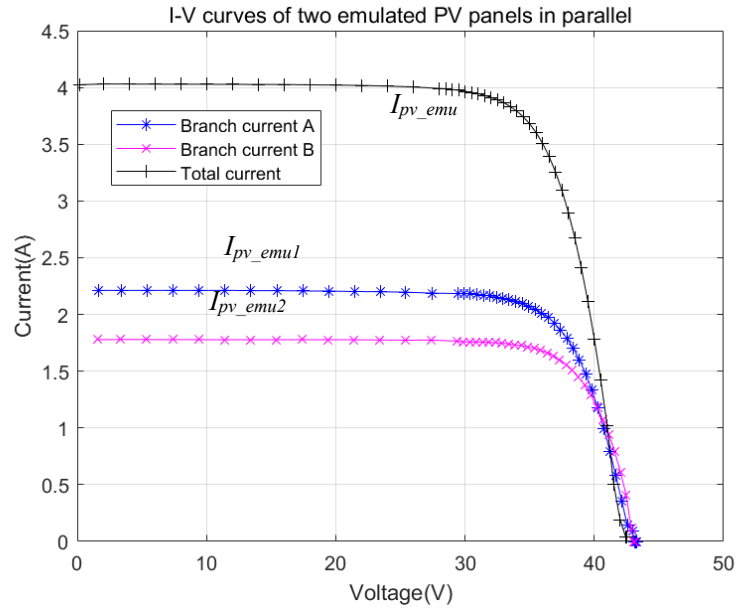


(b) P-V curves

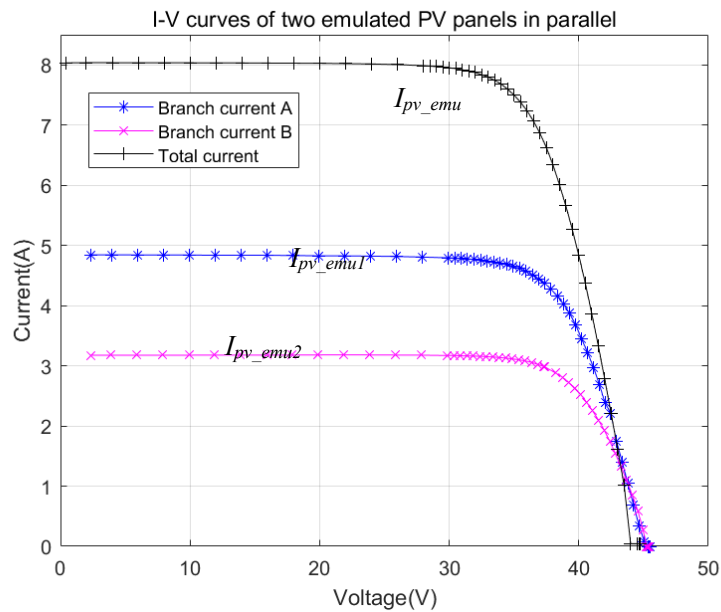
Figure 2.13 Measured and datasheet given electrical characteristics of the emulated PV arrays under two different partial shading operation conditions

The experimental results of the emulation PV system using two different blocking diodes (Infineon D08S120, one is D12S60C) under partial shading conditions were measured, as shown in Figure 2.14 below. In Figure 2.14 (a) two current source currents were set as $I_{CS1}=3A$, $I_{CS2}=1A$, however as the different of the conduction resistance of the two diodes, the short circuit current of the first emulated PV panel is around 2.2 A, and the other one is around 2.5

A. When two external current sources were set as $I_{CS1}=5A$, $I_{CS2}=3A$, Figure 2.14 (b), the short circuit current of the first emulated panel is about 4.8 A while the other one is 3.2 A, which are not equal to the injection current. The results verified the use of different blocking diodes leads to output current imbalances.



(a) $I_{CS1}=3A$ $I_{CS2}=1A$



(b) $I_{CS1}=5A$ $I_{CS2}=3A$

Figure 2.14 Measured output currents of emulated solar panels with two different blocking diodes

2.6 Summary

The emulation results show the constructed PV emulator can effectively simulate the operation of PV systems under general and partial shading conditions. Detailed circuit connection and operational principle were discussed. Various partial shading characteristics of PV array both with series-connected PV panels and parallel-connected PV panel were emulated using the proposed PV array emulation system. With the proposed system, the partial shading level can be emulated easily by regulating the external current source current so that the system can provide repeatable test conditions which are an essential function for testing power electronics converters and MPPT algorithms effectively. It is worth noting that the proposed PV emulator will experience an output voltage shift compared to the actual PV system. The open circuit voltage shift is greatest when the emulator is operating under high irradiation conditions. At lower irradiation levels, the electrical characteristics of the PV emulator almost match the electrical characteristics of the actual PV system. In addition, the choice of blocking diode will also affect the performance of the PV emulator. The application of blocking diodes with different internal resistances can result in a branch current bias at the output of a parallel PV emulator. To ensure proper operation of the PV emulator, blocking diodes of the same size should be used.

Chapter 3. MPPT algorithms under partial shading conditions

3.1 Introduction

It is important to extract the maximum available power from a PV system without being affected by changes in external irradiance. However, due to the occurrence of partial shading conditions, the power output of the PV array is drastically reduced and therefore the efficiency decreases. When the PV system is in a uniform irradiance situation, the characteristic curve of the PV array has only one maximum power point, and conventional MPPT algorithms can easily track to a single maximum power point. However, PV systems are not always under uniform irradiation. In partially shading conditions, the conventional MPPT technique may fail because it is not possible to distinguish between the local and global maximum power points. As a result, research into tracking the maximum power point of PV systems under partial shading conditions is becoming increasingly popular. The P&O method is widely used in the MPPT technique. However, as the conventional P&O method is based on a fixed perturbation step, it has limitations in terms of tracking speed and tracking efficiency. Variable perturbation step is an effective means to improve the performance of P&O methods and has received much attention from researchers. It is worth noting that the P&O algorithm lacks global search capability and tracking failures may occur under partial shading conditions. In addition, MPPT technique with global search capability may be deficient in local search capability. A cascading strategy that combines global search with P&O methods is a promising development and will be explored in this chapter. These hybrid methods are able to accurately search for global maximum power point under partial shading conditions, but also has good local search capabilities, thus improving the speed and efficiency of the MPPT technique for MPPT tracking.

3.2 Hybrid Global search adaptive perturb and observe MPPT algorithm

This thesis proposes a global search method based on the working principle of the P&O method to overcome the shortcomings of the traditional P&O method which lacks global search capability. In the proposed algorithm, the global search method searches for the maximum possible power point of the PV system by constantly perturbing the system operating voltage.

Some researchers have concluded that the global peak of PV solar panels never exceeds $0.9 V_{oc}$ [74, 75], where V_{oc} is the open circuit voltage of PV array under standard test condition (STC). According to the datasheet of emulated PV panels, the upper search boundary is set as 80V. The global search process is as follows:

Step 1. Initialize the parameters of the algorithm, at which point the mark flag of the algorithm is 0. Set the duty cycle range and the initial duty cycle. As the maximum power point of a PV system does not normally exceed 0.9 times the open circuit voltage, the reference voltage V_{ref} is set to 80V.

Step 2. Detect the operating voltage of the PV system V_{pv} . If the current voltage V_{pv} is less than the set reference voltage V_{ref} , it means that the global search has not yet been completed. Therefore, change the duty cycle of the boost converter to obtain the new voltage.

Step 3. After obtaining the new PV system operating voltage, multiply the measured PV system output current I_{pv} , to obtain the PV system output power P_{pv} .

Step 4. The algorithm will compare the difference between the current PV system output power and the output power of the previous iteration, retaining the maximum power detected by the system during the global search process.

Step 5. When the global search is completed, the output voltage corresponding to the detected maximum power output of the system will become the new reference voltage. Mark flag changes from 0 to 1.

When flag changes to 1, the maximum power point voltage V_{mpp} recorded by the algorithm during the global search will become the new reference voltage V_{ref_mpp} . The algorithm returns to step 2 to restart the iteration until the PV system is operating at the new reference voltage. Once the search is complete to obtain the voltage V_{mpp} for the maximum power, the algorithm continuously checks for sudden changes in power. If the output power of the PV

system varies too much, it means that the voltage at the maximum power point of the PV system may change significantly. In this case, the algorithm will go back to step 1 and initialize all parameters and restart the global search.

A noteworthy issue is that sudden changes in irradiation do not necessarily result in a change in the global peak of the P-V curve but in a shift in V_{mpp} . Therefore, if the inappropriate choice of the global search restart condition can lead to a loss of power during the search. To avoid power loss due to invalid restart conditions, the proposed algorithm introduces an adaptive perturbation observation method. The adaptive perturbation observation method performs a local optimisation after searching for the global MPP. This avoids the problem of power loss due to small changes in irradiation.

As the traditional P&O method is based on fixed-step perturbations, there is a conflict between reducing oscillations in the PV array output power near the maximum power point and tracking speed. Larger perturbation steps ensure a faster dynamic response of the algorithm but can lead to excessive oscillation of the PV array output power around the MPP. Conversely, a small perturbation step reduces the power loss around the MPP but slows the dynamic response to changes in irradiation.

The proposed adaptive P&O algorithm based on the slope of the P-V curve automatically adjusts the perturbation step during the tracking of the MPP in order to overcome the limitations of the traditional P&O algorithm. The schematic is shown in Figure 3.1. At a constant irradiance (stage 1), when the operating voltage is far from the MPP, the increasing V_{pv} leads to a continuous increase in the output power of the PV system every cycle. For example, as the operating voltage moves from V_1 to V_2 , the slopes K_1 and K_2 have similar values. As the operating voltage moves closer to the MPP, the slope of the P-V curve slowly decreases with each perturbation cycle until it equals to zero. This means that large perturbation steps are applied to the P&O algorithm when the PV system is operating at voltages away from the MPP, which can effectively increase the tracking speed. As the operating voltage of the PV system approaches MPP, the slope of the P-V curve becomes smaller. At this point small steps are

applied to the P&O method to reduce the oscillations of the operating voltage near the MPP, thus reducing power losses and improving tracking efficiency. As the irradiation level changes from stage 1 to stage 2, it produces a considerable change in output power. From the Figure 3.1 it can be seen that the slope around K_4 is greater than the slope around K_3 , so the proposed algorithm will track to the new maximum power point at a faster speed. The discretized I_{pv} and V_{pv} are used as input signals to the algorithm and the slope of the P-V curve is calculated by comparing the power change to the voltage change. As the operating voltage may be on either side of the MPP the absolute value of the slope is taken. If the slope of the P-V curve is greater than 1 then a fixed perturbation step of 0.5V is chosen, otherwise the slope is multiplied by a scaling factor as a perturbation step to reduce system oscillations around the MPP.

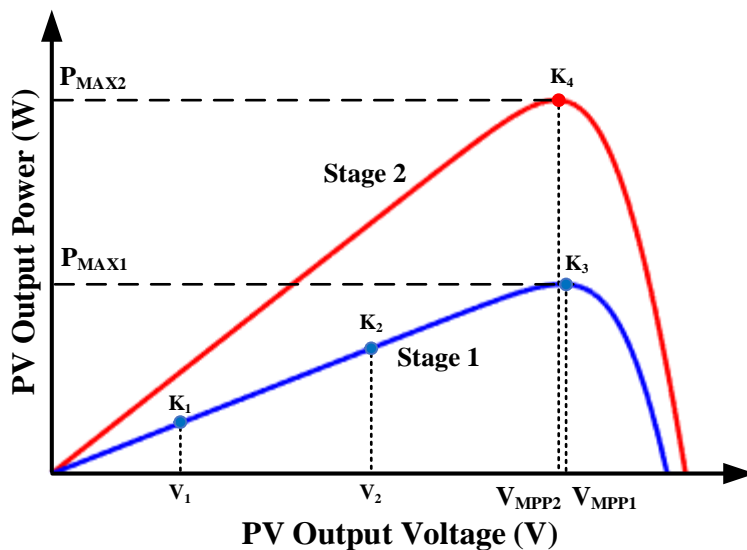


Figure 3.1 The schematic diagram of slope-based adaptive perturbation step size

The flow chart of the proposed hybrid global search adaptive P&O algorithm is shown in Figure 3.2. The algorithm takes advantage of the global search algorithm's merit-seeking capabilities and scans the entire search space, so it is unlikely to miss the global maximum power point. The proposed MPPT method continuously perturbs the system operating voltage and records the output power of the current cycle. The output power of each cycle is compared to determine the maximum power point voltage of the PV system. After the GMPP is tracked, adaptive P&O replaces the global search to begin local optimisation. As the PV system is already operating

near the maximum power point voltage, the adaptive P&O algorithm oscillates around the MPP in small steps. When the irradiation level changes slightly, the adaptive P&O method changes the perturbation step to track the new MPP more quickly. If the irradiation level changes significantly, the maximum power point of the PV system is likely to be far away from the previous maximum power point. Therefore, the global search stage is restarted to ensure that the PV system is operating at the global maximum power point.

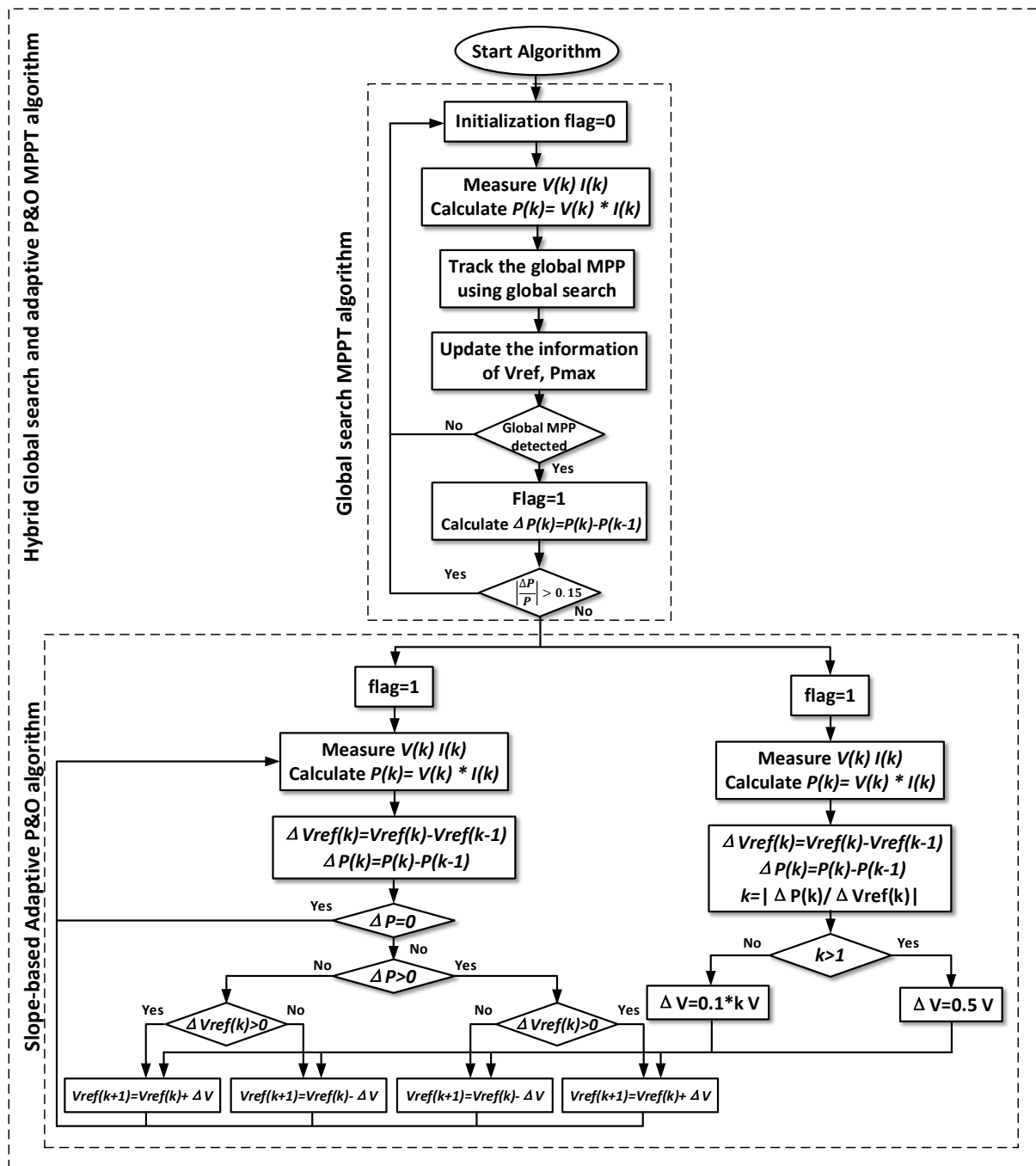


Figure 3.2 The flow chart of the proposed MPPT algorithm

3.3 Hybrid fast global maximum power point tracking algorithm assisted through fuzzy logic based variable step-size perturb and observe method

3.3.1 Proposed MPPT through fast global tracking (FGT) method

This thesis proposes a novel global search algorithm to address the shortcomings of current algorithms with global search capabilities, such as the ACO method, which are slow to track in the early stages of the search. The proposed FGT algorithm increases the speed as the search progresses to improve the tracking efficiency. FGT algorithm is implemented as follows:

Step 1. Initialization. For the fast global tracking MPPT algorithm, seven duty cycle particles namely $p(1)$ to $p(7)$ are applied. The positions of these particles are held in memory and are called continuously in each iteration. The setting of the number of iterations affects the efficiency and accuracy of the algorithm. If the number of iterations is too big, the final search results will be closer to the real maximum power point but will take longer time. Before the start of the iteration, these particles are positioned uniformly in the searching space corresponding to the voltage. It is worth to mention that this method of initializing duty ratio ensures convergence to global maximum power point. V_{start} and V_{end} indicate the lowest and highest point in the search space [76]. The upper bound of the search space is set as $0.9 \cdot V_{oc}$ while V_{oc} is the open-circuit voltage of the series PV panels. As a result, the probable searching space falls between 0V and 80V.

Step 2. The boost converter is engaged and power generation is computed according to the duty ratio obtained from step 1. The algorithm will record the seven output power values generated by each iteration.

Step 3. In this step, the duty ratio with the highest power with becomes reference position (p_{best}) and remains at its position. One iteration is completed when all duty cycle particles have updated their locations. All others six particles adjust their position by the equation below:

$$p = p(i) + (p_{best} - p(i)) \times \left(\frac{iteration(i)}{Number\ of\ iterations} \right)^2 \times rand() \quad (3.1)$$

Where, $p(i)$ is the position of a particle and the velocity coefficient of the particle is $\sqrt{iteration(i)/number\ of\ iterations}$. P_{best} is the best location for global particles. $Rand()$ represents a random value between 0 and 1. When the global particle optimum position P_{best} is greater than the current particle position $p(i)$, the difference between P_{best} and $p(i)$ is greater than zero. Therefore, according to the particle update equation, the duty cycle corresponding to the updated particle position will become larger, moving towards the global optimum position P_{best} . The velocity of a particle moving during a global search will be limited by the velocity coefficient. As can be seen from the equation, the speed of convergence of a particle is related to the number of iterations. A fast search speed makes the PV system fall into a local optimum easily while a slower search speed can improve the accuracy of the system, but not conducive to transient response. In the early stage of tracking, slower search speeds of the algorithm are deployed to ensure accurate GMPP finding. As the iteration proceeds, the search area becomes smaller, therefore speed up the tracking to reach the MPP. The relationship between particle convergence speed and number of iterations of the algorithm is shown in Figure 3.3. It is obvious that the particles move faster as the iterations progress. Furthermore, the larger the number of iterations set to terminate, the slower the particles move, although more accurate tracking may be guaranteed. In addition, during the global search, particles moving too fast may cause the algorithm to miss GMPP and fall into a local optimum solution. Too slow a convergence speed will increase the search time and thus lead to a loss of power generation. In this case, the velocity coefficient will be multiplied by a random value between 0 and 1 to ensure the randomness of the particles during the global search. In this way, the accuracy and efficiency of the algorithm is ensured, with good transient response performance and less chance of missing the global maximum power point tracking.

Step 4. Repeat step 2 and step 3 until the iteration is completed and all particles approach to the GMPP.

Step 5. Detect power drops. Changes in output power of the PV system imply a change in

external conditions, which leads to a possible varies in the MPP of the system. The algorithm will re-initialise and move back to step 1 if the output power has changed.

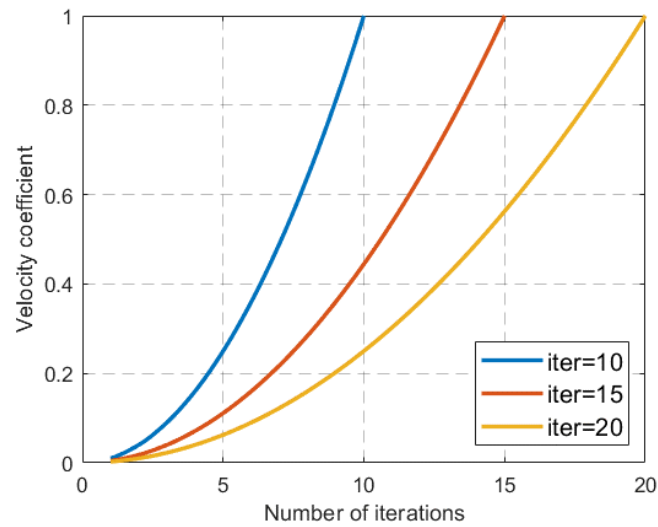


Figure 3.3 The relationship between particle convergence speed and number of iterations of the algorithm

By constantly narrowing the search area and by speeding up the particle movement, the efficiency of the MPPT method can be improved while ensuring that the global maximum power point is tracked.

3.3.2 Fuzzy logic P&O MPPT method

Due to its simplicity and low-cost, Perturb and observe (P&O) approach has been widely used in PV systems for tracking maximum power point [45]. The traditional P&O method works as shown on the left side of Figure 3.7, where the output voltage and output current of the PV system are detected at each sampling cycle and the output power is calculated. The algorithm continuously perturbs the system operating voltage, comparing the power change $\Delta P(k)$ and voltage change $\Delta V_{ref}(k)$ between cycles to determine whether the PV system is currently operating to the left or right of the maximum power point, so that the operating voltage can be increased or decreased in the next cycle. However, the traditional P&O fails to track the GMPP when solar systems are affected by PSC which leads to power extraction limitation. Hence, the conventional MPPT is often combined with advance fuzzy logic controller to overcome the

tracking difficulties under complex irradiation conditions. In addition, the downsides of this method include inadequate tracking, which may occur when irradiation varies suddenly, as well as slow tracking of rising time towards MPP. In steady-state situations, this approach also ends in continual oscillations of power generation around the MPP. There is always a conflict between tracking convergence of rising time and small power oscillation in steady-state. In order to minimise settling times and reduce power oscillations around the maximum power point, a variable step size MPPT method was investigated using fuzzy logic techniques. The variable step size MPPT method was developed using fuzzy logic techniques to create a constantly changing perturbation step size as an input to the traditional P&O algorithm. The fuzzy logic controller has two inputs: the first is the variation of power between current and previous cycle $\Delta P(k)$ and the second input is the instantaneous slope of P-V curve $S(k)$, where $S(k)=\Delta P(k)/\Delta V_{pv}(k)$, $\Delta V_{pv}(k)$ is the difference between the output voltage of the current cycle and the previous cycle. The choice of these two inputs makes it easy to identify if the operational point is on the MPP's left or right side. Additionally, it facilitates tracking speed at low irradiation conditions [51]. The algorithm converts from the continuous time domain to discrete PV panel voltages and currents and calculates the inputs $\Delta P(k)$ and $S(k)$ to the fuzzy logic controller. Based on these two inputs, the proposed method generates a variable perturbation step in each processing cycle. This variable perturbation step will be applied to the traditional P&O method to replace the fixed perturbation step.

In order to fuzzify the specific values entered into the fuzzy logic controller; triangular membership functions membership functions are often applied. The defined membership functions are implemented through the MANDANI fuzzy inference system. Assuming that the PV system is suddenly exposed to uniform irradiation, the P-V characteristic curve has only one maximum power point. Taking the P&O algorithm as an example, the MPPT algorithm continuously perturbs the PV system in certain steps and determines whether the maximum power point is tracked by comparing the power difference between the current cycle of the PV system and the previous cycle. In the early stages of the perturbation, as the PV system operating voltage point is to the left of the MPP point, this means that every change in the

reference voltage causes an increase in output power. Given the characteristics of the P-V curve, $\Delta P(k)$ is always a constant large value until the MPPT algorithm tracks to the maximum power point. As the system operating voltage approaches MPP, the variation in output power decreases. When the system is operating at the MPP point, $\Delta P(k)$ equals 0. Due to the inertia of the PV system and the P&O algorithm, the system operating voltage can overshoot. In this case, the operating voltage will shift to the right of the MPP with a negative value of $\Delta P(k)$. The P&O algorithm will correct the direction of the perturbation so that the system operating voltage will oscillate around the MPP. Considering the small power variation near the MPP, the range of $\Delta P(k)$ for the input of fuzzy logic controller is defined as $[-3,3]$. In addition, the principle of setting the range of $S(k)$ is similar to that of $\Delta P(k)$. When the system operating voltage is far from the MPP, the corresponding slope of the P-V curve is large. Assuming that the operating voltage is to the left of the MPP, $S(k)$ is a positive value. As the operating voltage approaches the MPP, the value of $S(k)$ decreases. When the PV system is operating at the MPP point, $S(k)$ is 0. If the system operating voltage is overshoot, $S(k)$ is negative. If the system operating voltage is to the right of the MPP and away from the MPP point, the value of $S(k)$ becomes smaller. The range of $\Delta P(k)$ and $S(k)$ for the input of fuzzy logic controller is shown in Figure 3.4.

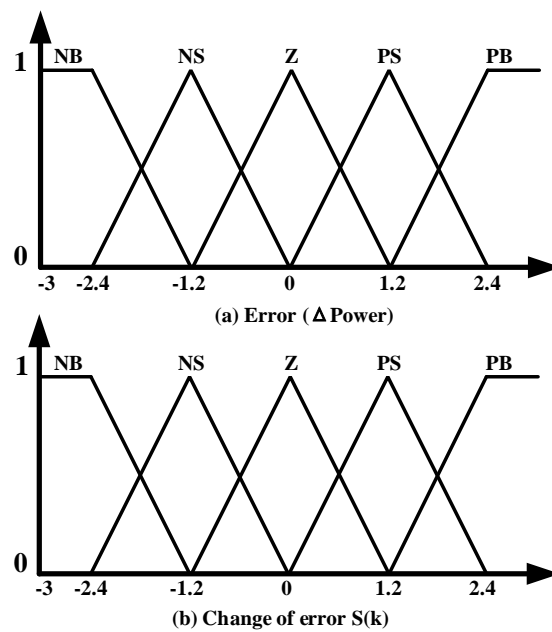


Figure 3.4 The membership function of proposed fuzzy logic controller (a) change of power;
(b) PV curve slope $S(k)$

In the proposed MPPT algorithm, the fuzzy logic controller is used as an auxiliary system to improve the performance of the traditional P&O MPPT method, therefore the output of the fuzzy logic controller is chosen to be a variable perturbation step (ΔV). The expectation is that the fuzzy logic controller gives the P&O algorithm a large perturbation step when the PV system is operating at a voltage away from the MPP to reduce the early search time. As the operating voltage of the system approaches the MPP, the step size of the perturbation becomes smaller to reduce the oscillations of the PV system around the MPP and thus reduce power losses. ΔV range for the output of fuzzy logic controller is shown in Figure 3.5.

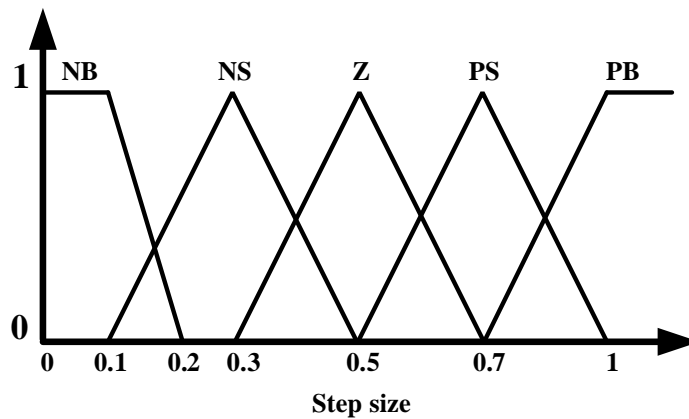


Figure 3.5 The membership function of proposed fuzzy logic controller for variable perturbation step

The fuzzification block analyses the variation of power and the measured slope of the P-V curve and inference is based on the set of fuzzy rules. In order to fuzzify the values of the input fuzzy controller and establish the relationship between the input and output, the values of the input and output are defined as negative big (NB), negative small (NS), zero (Z), positive small (PS), positive big (PB). The 25 IF THEN rules are given in Table 3.1.

Table 3.1 Fuzzy Logic Rules

ΔP dP	NB	NS	Z	PS	PB
NB	PB	PB	NB	PB	NB
NS	PB	PS	NB	PS	NB
Z	NB	NB	NB	NB	NB
PS	NB	NS	NB	PS	PB
PB	NB	NB	NB	PB	PB

Figure 3.6 depicts the viewer surface of fuzzy logic controller link between fluctuation of power, measured slope of P-V curve, and variable step-size output.

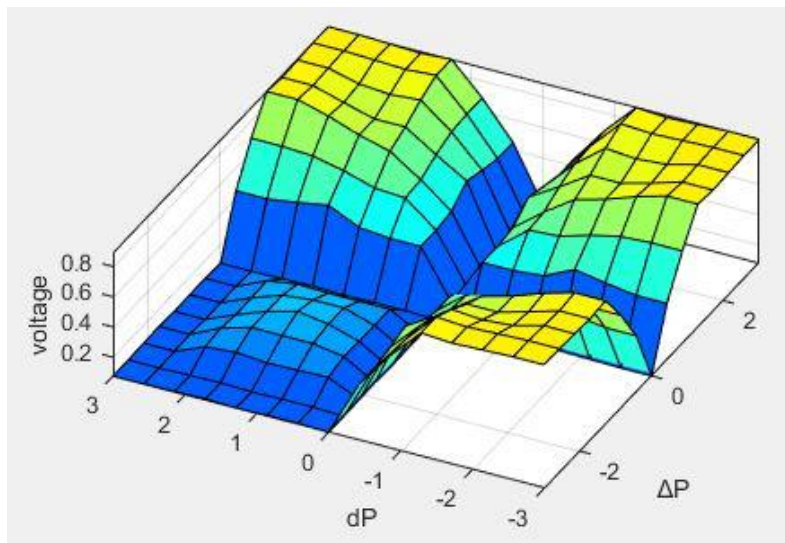


Figure 3.6 Viewer surface plot of the FLC

The flow chart of fuzzy logic P&O algorithm is given in Figure 3.7.

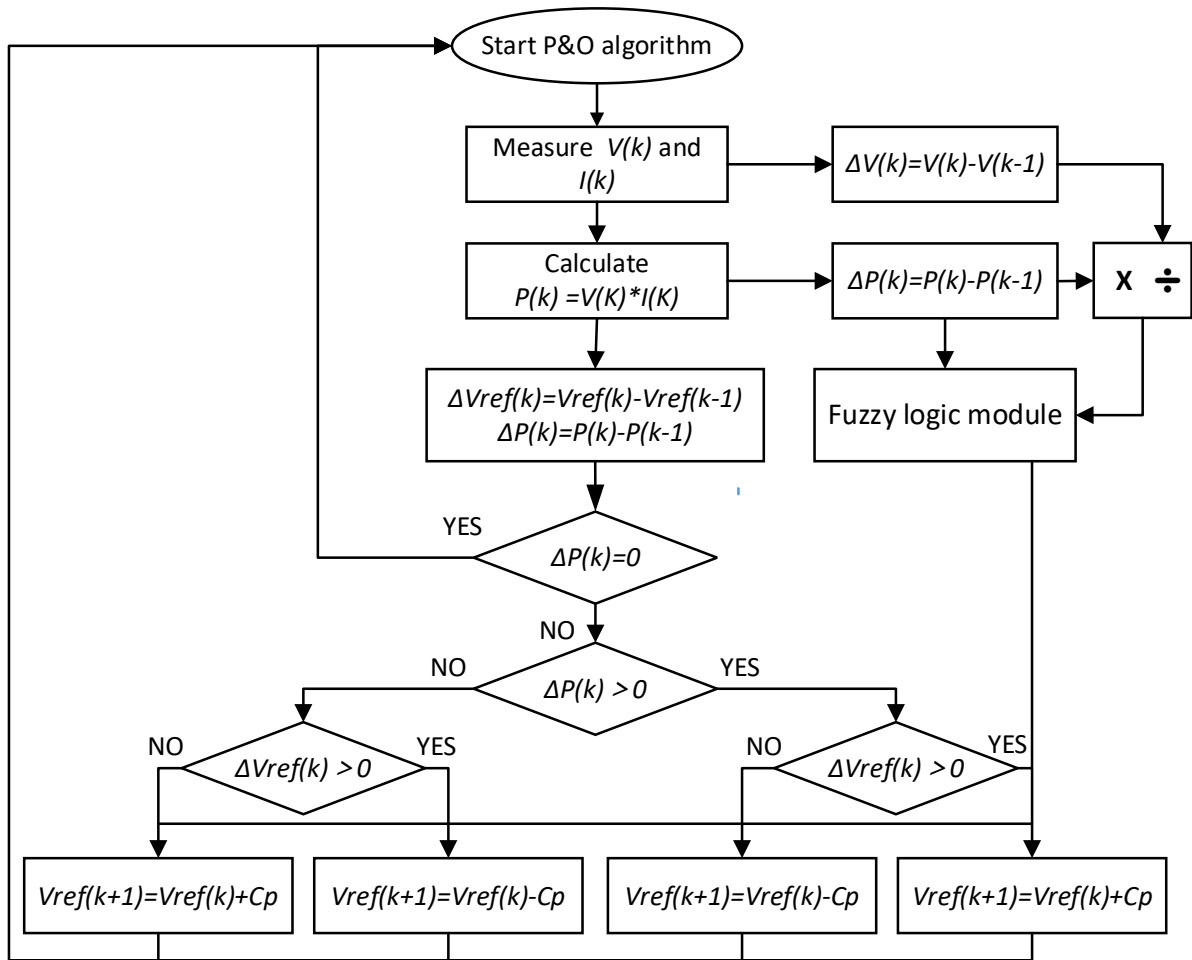


Figure 3.7 The flow chart of fuzzy logic P&O algorithm

3.3.3 Description of FGT-fuzzy logic P&O algorithm

The flow chart of the proposed algorithm is shown in Figure 3.8. Fast global tracking (FGT) method execute a global search in the early stage of scanning. A certain number of particles are evenly distributed over the duty cycle corresponding to the voltage at which the MPP may occur. The output power corresponding to each particle is detected and the particle corresponding to the maximum output power is used as the reference particle. Using the reference particle as a reference, the position of each particle is updated by means of a position update formula. The above steps are repeated until the iteration termination condition is met. The fuzzy logic-based P&O algorithm intervenes in the tracking when the global search is over. The P&O method will track the maximum power point more accurately around the global maximum power point. With the variable step size provided by the FL controller, only small oscillations in the operating voltage of the PV system occur, thus effectively reducing the power

loss of the PV system.

This cascaded strategy integrates the benefits of the FGT algorithm and P&O method to speed up the search while ensuring that the GMPP is accurately tracked. The simulation results of the proposed MPPT algorithm can be seen in next section.

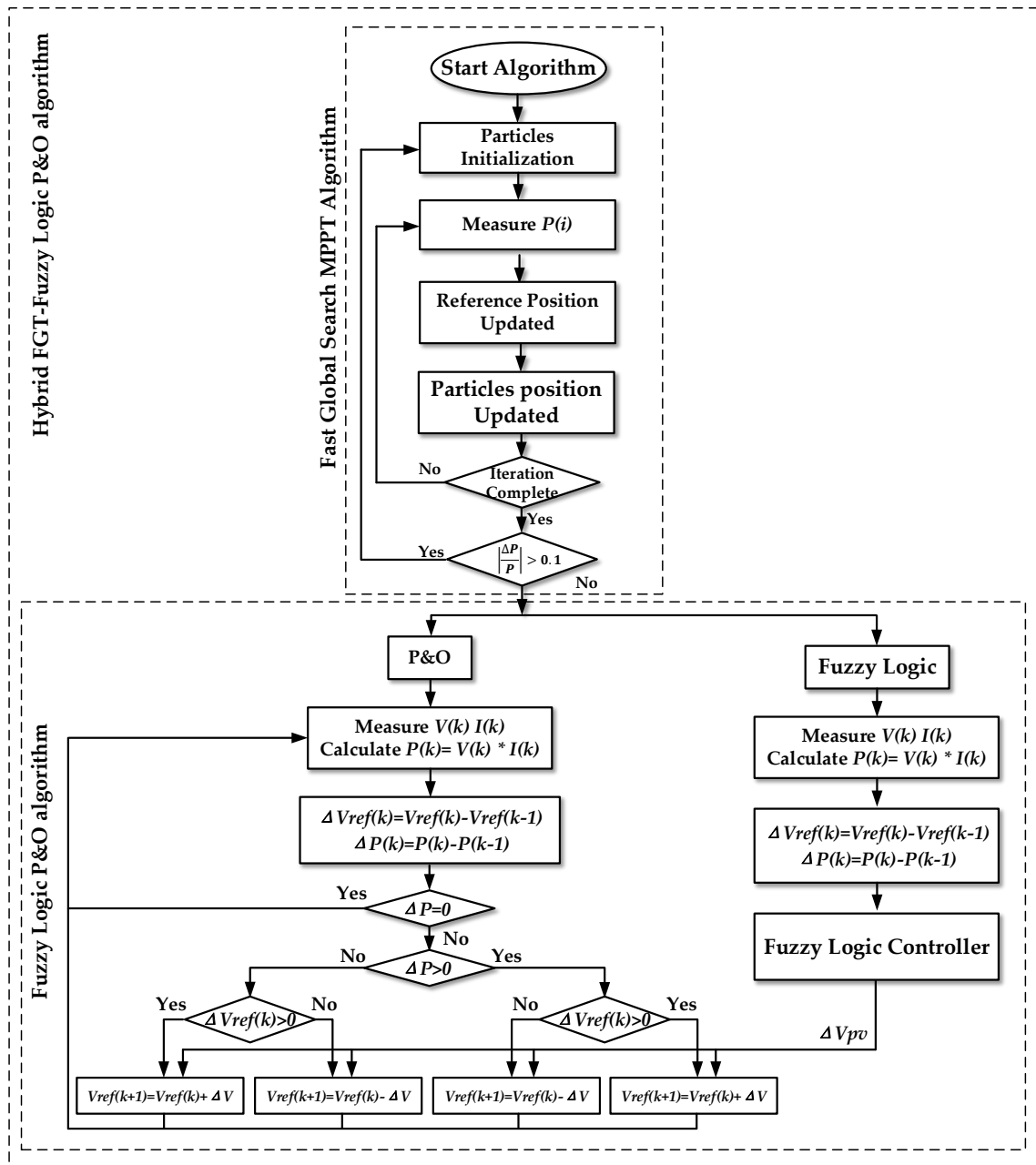


Figure 3.8 Flow chart of the proposed MPPT algorithm

3.4 Summary

This chapter presents two cascading strategies for MPPT methods, both of which can track to the maximum power point under partial shading conditions. The intervention of the cascade strategy facilitates the MPPT local search. When the PV system is subjected to small changes in irradiation, the maximum power point is likely to shift only slightly. At this point if the global search method is restarted, this will result in more power loss. Therefore, the P&O method can be applied to locally search for the maximum power point of the PV system, reducing the power loss caused by restarting the global search. It is worth mentioning that the proposed global search adaptive P&O method is simple to apply, searching the area where the MPP is likely to occur only once in the early global search stage. This has the advantage that the search is fast, but if irradiation changes occur during the search stage, the global MPP tracked may be inaccurate. For the proposed FGT-fuzzy logic P&O method, the early stage of the global search is based on the continuous reduction of the search area. This increases the complexity of the algorithm, but provides greater assurance of the accuracy of the global MPP tracked. In general, the MPPT method applied depends on the complexity of the PV system and the variability of the external irradiation.

Chapter 4. Simulation results of the proposed MPPT algorithms

4.1 Introduction

The two proposed MPPT methods will be verified in this chapter by means of simulation procedures. The results of the simulations are based on MATLAB/Simulink 2020a and take into account the parameters designed to simulate and test the system. The MPPT methods will be combined with the proposed PV emulator as well as a boost DC-DC circuit to test the performance of the MPPT methods under different irradiation conditions. Simulation circuits and simulation results are explained in detail in the following sections.

4.2 Boost DC-DC converter

DC-DC converters are widely implemented as a switch-mode converter to control an unregulated input voltage to obtain steady and constant output voltage. Due to variations in irradiation and temperature, the unregulated input of DC-DC converters, which is obtained from PV array will fluctuate. Although the input voltage varies in these converters, the average DC output voltage needs to be managed to equal the required value [77]. Hence, DC-DC converters are widely used in electric system of renewable energy. The boost converter was chosen as the appropriate topology for the thesis simulation and experiment because the electronic load must should function at higher voltage level than the ones supplied by PV array. The boost converter consists of a boost inductor, a controlled switch, a diode and a capacitor. The topology of boost converter is illustrated in Figure 4.1.

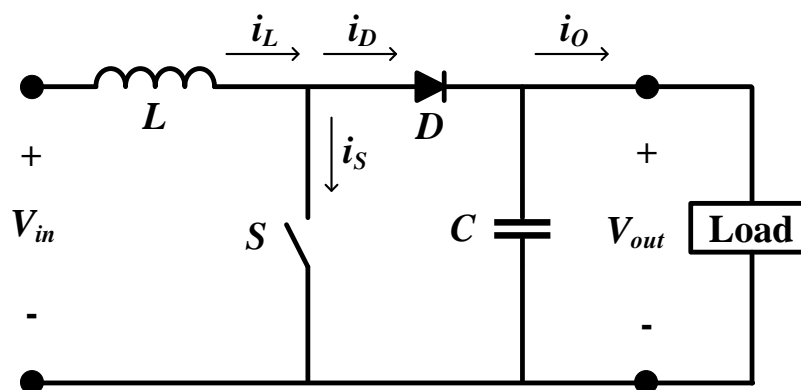


Figure 4.1 Topology of boost converter

In continuous conduction mode, the boost converter has two stages in each switching cycle, on and off state. Under on-state mode, switch S is connected, the energy of the inductor is increased by the current flowing through it from the power source, and diode D prevents the negative current to circulate from the load to the input source. Under off-state mode, switch S is disconnected, the stored energy is transferred from the inductor to the load. As a result, the output voltage is increased on accordance with the switch duty cycle. Besides, the capacitor connected in parallel with the load is to keep the output voltage stable and to reduce the ripple of the output voltage [78]. The working mode of boost DC-DC converter in one cycle is shown in Figure 4.2 and 4.3.

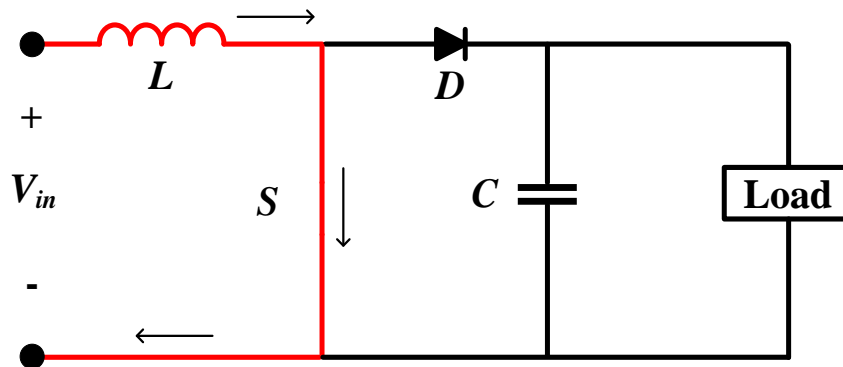


Figure 4.2 Boost converter on state equivalent circuit

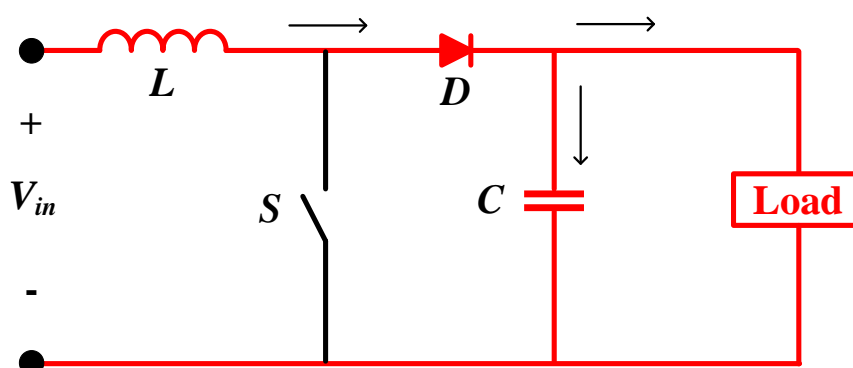


Figure 4.3 Boost converter off state equivalent circuit

Assuming that the time of switch conduction is T_{ON} , we have $T_{ON} = D \times T_S$, where D is duty cycle and T_S is one complete switching cycle. T_{OFF} is the duration of off state so that $T_{OFF} = (1-D) \times T_S$. According to Figure 4.1, the drain-to-source resistance R_{DS} will lead to a small

voltage drop of V_{DS} . Additionally, a minor voltage drop across the inductor is equal to $I_L \times R_L$. During on state, the voltage across the inductor is equal to $V_{IN} - (V_{DS} + I_L \times R_L)$, where V_{IN} is the input voltage of boost converter. Since the applied input voltage is constant, the inductor current also increases linearly. The increase of inductor current during the on-state condition can be expressed by the following relationship:

$$V_L = L \times \frac{di_L}{dt} \quad (4.1)$$

$$\Delta I_L = \frac{V_L}{L} \times \Delta T \quad (4.2)$$

The inductor ripple current during on-state period is given by:

$$\Delta I_{L+} = \frac{V_L - (V_{DS} + I_L \times R_L)}{L} \times T_{ON} \quad (4.3)$$

According to Figure 4.3, when boost converter is in off-state, the voltage across the inductor is equal to $(V_{OUT} + V_D + I_L \times R_L) - V_{IN}$, where V_D is diode forward voltage and V_{OUT} is the output voltage. Since the input voltage is constant, the inductor current decreases linearly which can be expressed below:

$$\Delta I_{L-} = \frac{V_{OUT} + V_D + I_L \times R_L}{L} \times T_{OFF} \quad (4.4)$$

In the steady state conditions, the increase in current in the on state should be equal to the decrease in current in the off state. Therefore, the output voltage V_{OUT} of the boost converter can be obtained from the following conversion relationship:

$$V_{OUT} = (V_{IN} - I_L \times R_L) \times \left(1 + \frac{T_{ON}}{T_{OFF}}\right) - V_D - V_{DS} \times \left(\frac{T_{ON}}{T_{OFF}}\right) \quad (4.5)$$

It is known that $T_S = T_{ON} + T_{OFF}$, $D = T_{ON}/T_S$, the steady-state equation for V_{OUT} is:

$$V_{OUT} = \frac{V_{IN} - I_L \times R_L}{1 - D} - V_D - V_{DS} \times \frac{D}{1 - D} \quad (4.6)$$

Assuming that V_{DS} , V_D and R_L are small enough to ignore, which are equal to zero. The output voltage can be simplified as:

$$V_{OUT} = \frac{V_{IN}}{1 - D} \quad (4.7)$$

The above equation shows that the output voltage of the boost converter V_{OUT} can be adjusted by changing the duty cycle D . For an ideal boost converter, when the duty cycle is zero, the input and output voltages of the boost converter are equal, $V_{IN} = V_{OUT}$. When the duty cycle is infinitely close to 1 it results in an infinitely output voltage V_{OUT} . Figure 4.4 illustrates the relationship between the input and output voltages for different duty cycles, where $V_{OUT} \geq V_{IN}$.

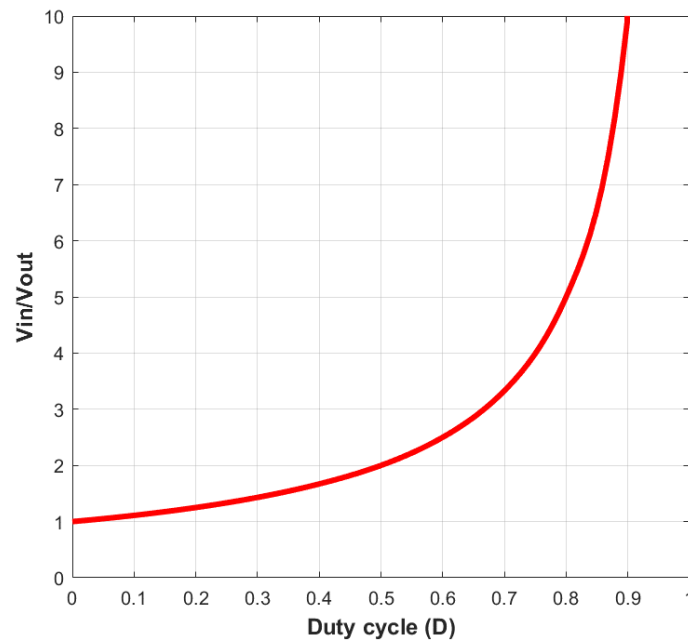


Figure 4.4 Relationship between input and output voltages of an ideal boost converter at different duty cycles

In addition, the input current (inductor current) for an ideal boost converter can be obtained:

$$I_{IN} = \frac{V_{IN}}{R_L(1-D)^2} = \frac{I_{OUT}}{1-D} \quad (4.8)$$

In order to prevent instability in the control loop and to ensure the proper operation of the boost converter, the duty cycle limitations of the practical application need to be taken into account. Compared to the ideal boost converter without power loss, the actual converter produces a lower output voltage at the same duty cycle due to the voltage drop across the inductor and MOSFET. For a non-ideal boost converter, the estimated duty ratio (D) can be expressed as [79]:

$$D = 1 - \frac{V_{IN} \times \eta}{V_{OUT}} \quad (4.9)$$

Where η is the efficiency of the regulator. In practice the relationship between boost converter and duty cycle is shown in Figure 4.5

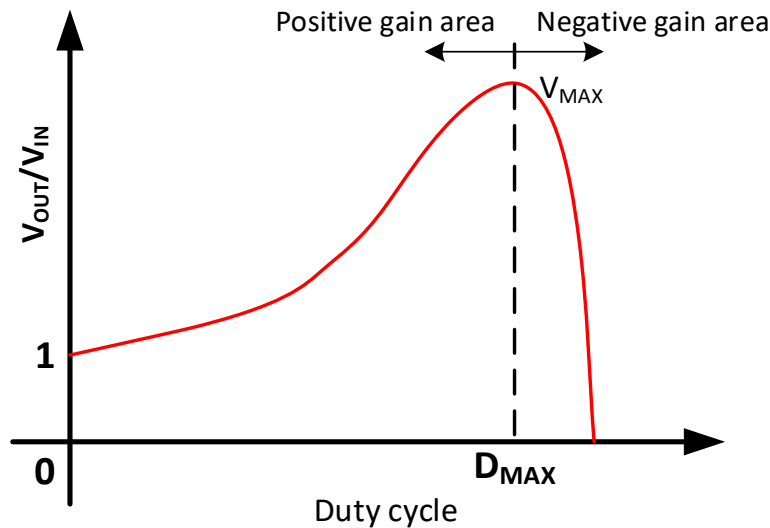


Figure 4.5 Relationship between V_{out}/V_{in} and duty cycle for a non-ideal boost converter

For a non-ideal boost converter, R_{LOAD} is not infinite and the V_{OUT}/V_{IN} conversion characteristic includes three regions [80]. When controller duty cycle D is smaller than critical duty cycle

$D_{CRITICAL}$, where $D_{CRITICAL}$ is the duty cycle at the maximum voltage output from the boost converter, there is positive gain and the characteristics of the output and input are close to the ideal relationship equation. When controller duty cycle D is equal to critical duty cycle $D_{CRITICAL}$, the boost converter provides a maximum output voltage of V_{MAX} . When controller duty cycle D is bigger than critical duty cycle $D_{CRITICAL}$, the boost converter will operate in the negative gain region, with the output voltage decreasing as the duty cycle increases. The approximate duty cycle range of a boost converter can be calculated by the following equation[81].

$$D_{MIN} \cong \frac{V_{OUT} + V_D - V_{IN-MAX}}{V_{OUT} + V_D} \quad (4.10)$$

$$D_{NOM} \cong \frac{V_{OUT} + V_D - V_{IN-NOM}}{V_{OUT} + V_D} \quad (4.11)$$

$$D_{MAX} \cong \frac{V_{OUT} + V_D - V_{IN-MIN}}{V_{OUT} + V_D} \quad (4.12)$$

Where V_{IN-MAX} is the maximum input voltage range with the value of 44.2V to 88.4V which is the open circuit voltage of single panel and two series-connected PV panels. The value of V_{OUT} is 50V to 100V. V_D is the forward voltage of the output diode, usually set to 0.5V. Therefore, a duty cycle operating range of 10% to 90% in which many boost controllers operates properly is appropriate based on the above formula and parameters settings.

4.3 Simulation results of hybrid global search adaptive perturb and observe MPPT algorithm

For the demonstration of the proposed algorithm, two series-connected PV panels are presented in this section. The simulation equivalent circuit is shown in Figure 4.6.

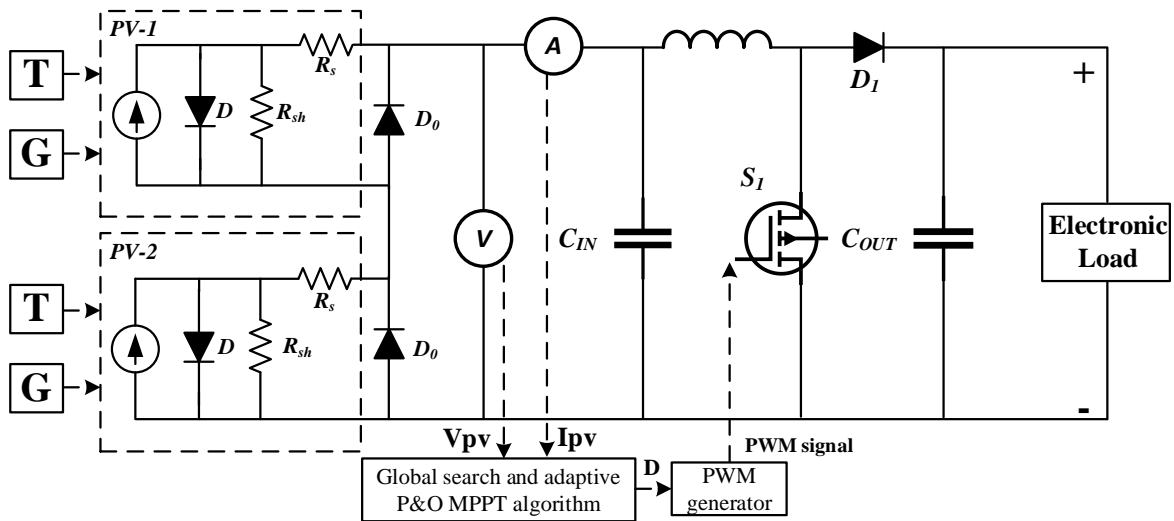


Figure 4.6 Equivalent circuit of simulation set up for global search adaptive P&O algorithm

According to the previous measured PV characteristics, the emulated PV system has similar characteristics to the actual I-V and P-V curves at $600\text{W}/\text{m}^2$ and $200\text{W}/\text{m}^2$. Figure 4.7 shows that the PV system is under two different partial shading cases.

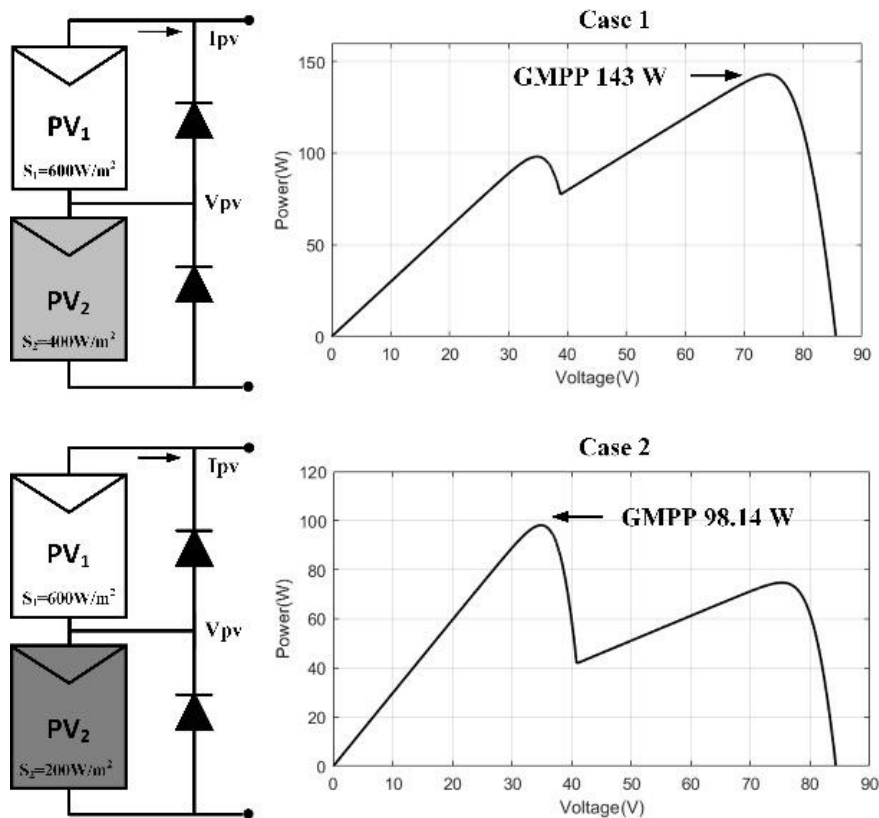


Figure 4.7 Case 1 and case 2 P-V curves from datasheet

It can be seen above that case 1 has a GMPP of 143W at 73.8V and GMPP for case 2 is 98.14W at 34.85V.

A conventional fixed step size (0.5V) P&O MPPT and the proposed adaptive P&O with global search method were simulated in MATLAB/Simulink. Both solar panels are initially not exposed to irradiation under the initialization conditions. After that, one of the simulated solar panels is under irradiation $600\text{W}/\text{m}^2$ while the other panel irradiation is $400\text{W}/\text{m}^2$. At 0.15s, the irradiation changes from $400\text{W}/\text{m}^2$ to $200\text{W}/\text{m}^2$ which results in a different GMPP. The sampling time of the P&O algorithm was set as 5ms corresponding to perturbation frequency 200Hz. Figure 4.8 shows the voltage waveforms under different irradiation. The proposed MPPT algorithm crossed the local maximum power point and eventually tracked the global MPP. The results also indicate that the proposed algorithm has faster dynamic response when the irradiation varies (0.05s and 0.1s). In addition, the steady-state oscillations around MPP shown in the zoom-in figures is reduced greatly with proposed adaptive P&O algorithm.

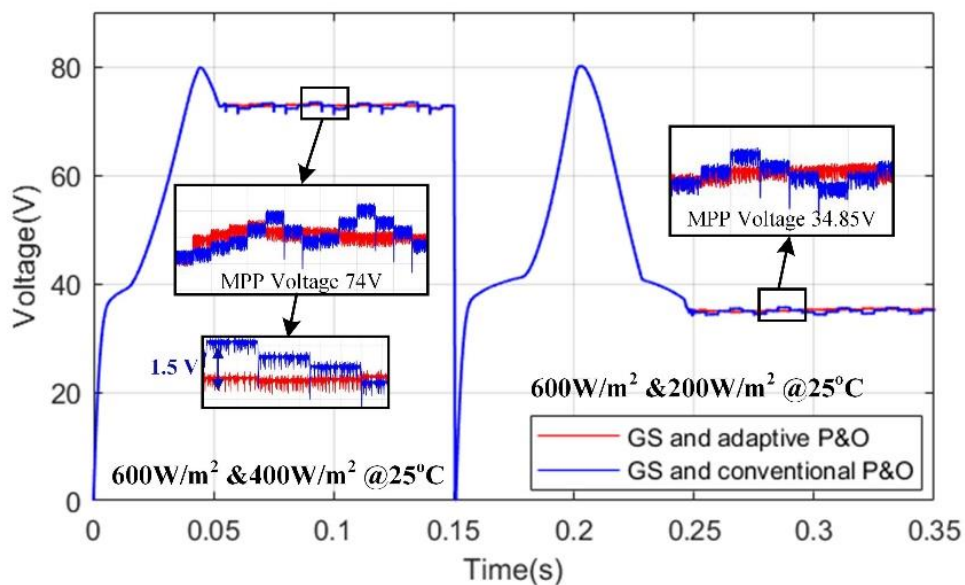


Figure 4.8 Voltage comparison of conventional P&O MPPT and the proposed adaptive variable step size P&O MPPT

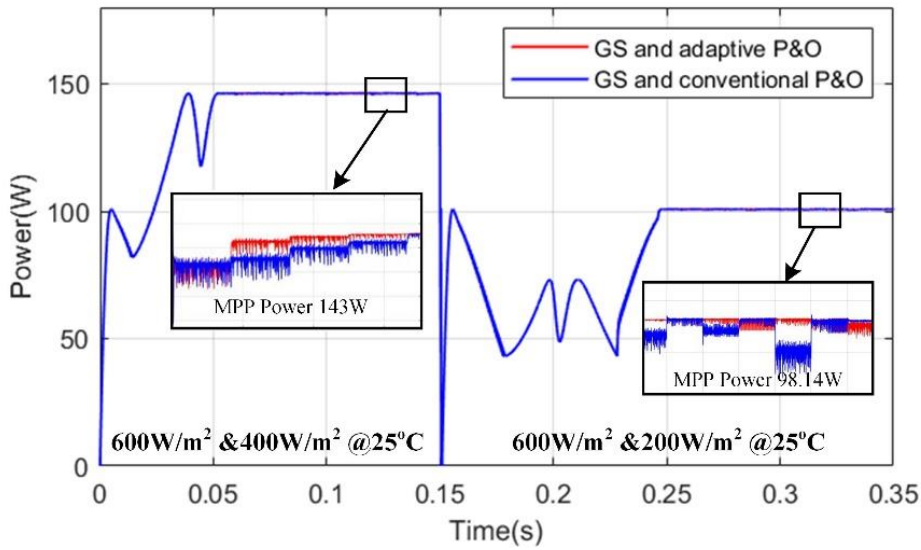


Figure 4.9 Power comparison of conventional P&O MPPT and the proposed adaptive variable step size P&O MPPT

Figure 4.9 shows the PV output power waveforms. The output power waveforms verify that the proposed adaptive P&O algorithm improves tracking speed and reduce the oscillation at the maximum power point. It is worth noting that the adaptive P&O algorithm has better steady-state performance in low irradiation condition.

4.4 Simulation results of FGT-fuzzy logic P&O algorithm

4.4.1 Simulation results of FGT algorithm

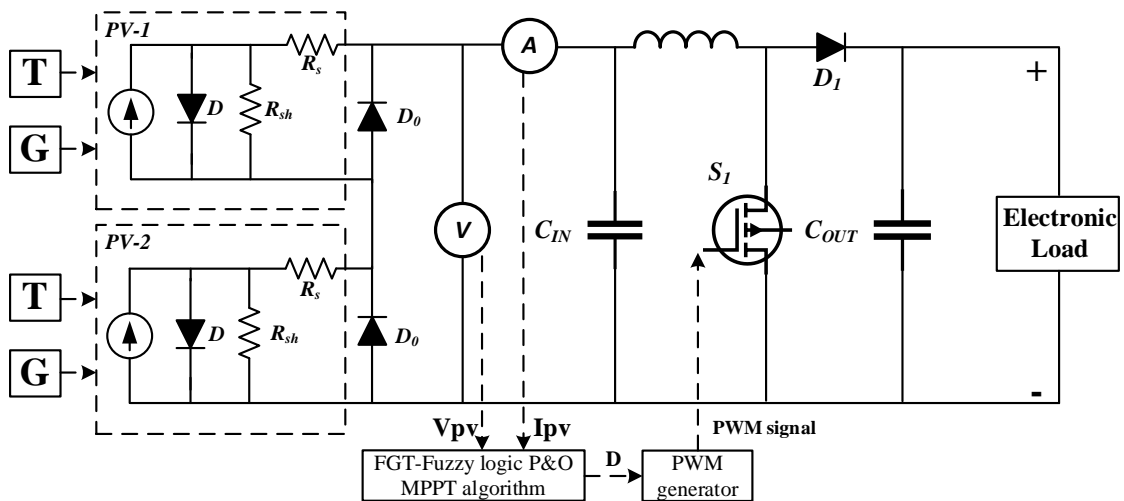
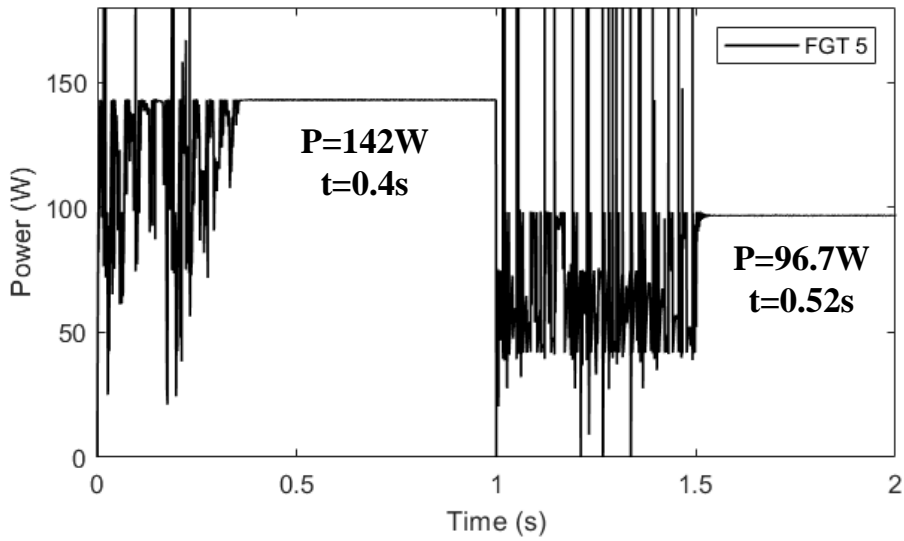
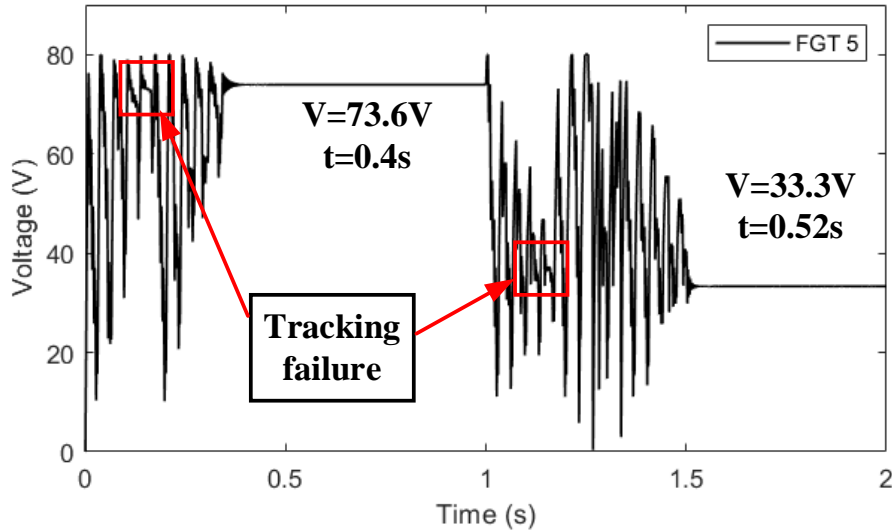


Figure 4.10 Equivalent circuit of simulation set up for FGT-fuzzy logic P&O algorithm

The simulation equivalent circuit of two series-connected PV system is shown in Figure 4.10. Two solar panels series-connected PV system is considered with pattern 1 and pattern 2 for simulation demonstration. In pattern 1, the global maximum power point voltage of the PV system is 74V, corresponding to a system maximum output power of 143W. In pattern 2, the global maximum power point voltage of the PV system is 34.85V while the maximum output power is 98.14W. Both solar panels are initially under zero irradiation at the beginning. Later, the PV system is under pattern 1 irradiation condition. At 1s, the irradiation changes from pattern 1 to pattern 2 which results in a different GMPP. In addition, the main drawback of FGT method is the conflict between tracking time and tracking accuracy. Hence, the setting of the number of iterations will affect the performance of FGT method. Furthermore, the power oscillations during tracking process cannot be ignored. Generally, the greater the number of iterations, the more accurate the tracked MPP is, but the longer the required computational time becomes. A smaller number of iterations allows the algorithm to converge quickly to the best position, but may result in inaccurate tracked MPP. The MPPT program was developed in MATLAB/Simulink. The sampling time of MPPT algorithm is equal to switching frequency. The computed results of output power and voltage with varying number of iterations are shown below.



(a)

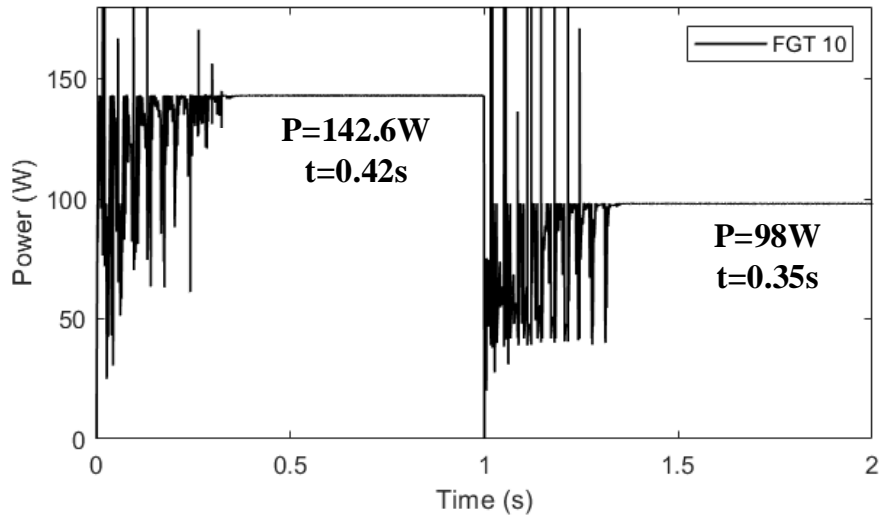


(b)

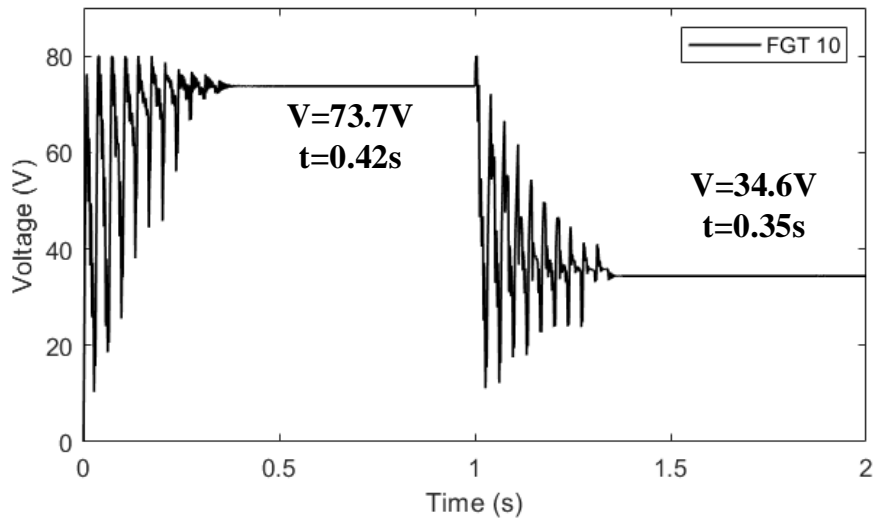
Figure 4.11 Simulation results for five times iterations of FGT MPPT algorithm

Figure 4.11 shows the simulation results of FGT MPPT algorithm with five iterations. The power curve show indicates large oscillation in the early stage of tracking, owing to particle exploration; however, as the tracking progresses, the turbulations considerably decreases. At 0.2 seconds, the FGT algorithm completed its iteration and output the global best position. However, the output did not satisfy the conditions for terminating the iteration, so the computing was restarted. In this way, the result of the FGT algorithm at 0.2 seconds can be seen as a tracking failure because the PV system is not operating at the maximum power point. At 0.4 seconds, the restarted FGT algorithm tracked the PV system MPP, at which point the

output voltage was 73.6V and the output power was 142W. The same tracking failure also occurs under pattern 2. The restarted FGT algorithm tracked the MPP after 0.52 seconds, the PV system had an output voltage of 33.3V and an output power of 96.7W.



(a)



(b)

Figure 4.12 Simulation results for ten times iterations of FGT MPPT algorithm

Figure 4.12 shows the simulation results of FGT MPPT algorithm with ten iterations. At 0.42 seconds, the PV system is operating at maximum power point. The output voltage of PV system V_{pv} is 73.7V while the output power of the PV system P_{pv} is 142.6W. At 1 second, the irradiation conditions change from pattern 1 to pattern 2. The FGT algorithm detects a large

power fluctuation and therefore restarts the computing in the range of possible voltage V_{pv} . After 0.35 seconds, the maximum power point of the PV system in pattern 2 is tracked by the FGT algorithm. At this point the output voltage of the PV system is 34.6V and the output power is 98W. It is worth to mention that when the iteration termination condition of FGT algorithm is set to ten times, no tracking failure occurs during the global tracking process. For the same irradiation variation conditions, ten iterations of FGT method has a better transient response compared to five iterations FGT method, with an average improvement of 30%. In addition, the PV system output is closer to the maximum power output of the system under ideal conditions, which means that the MPPT is more efficient when the termination condition of the FGT algorithm is set to ten times.

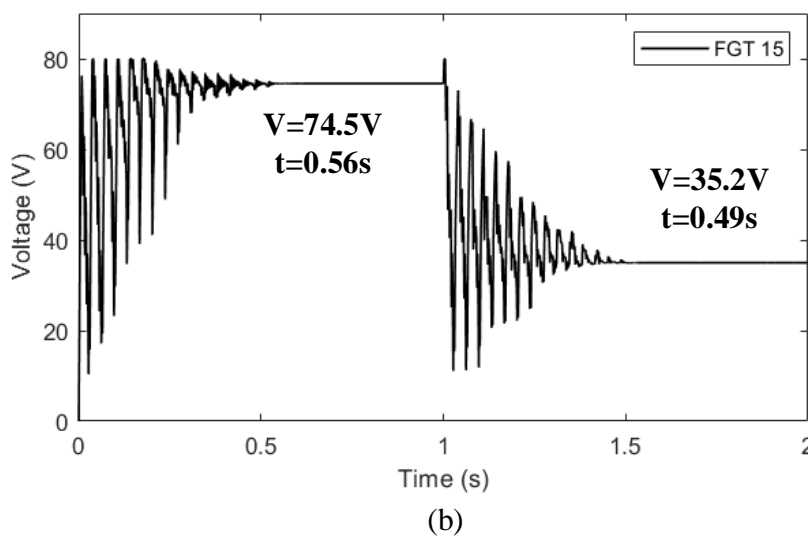
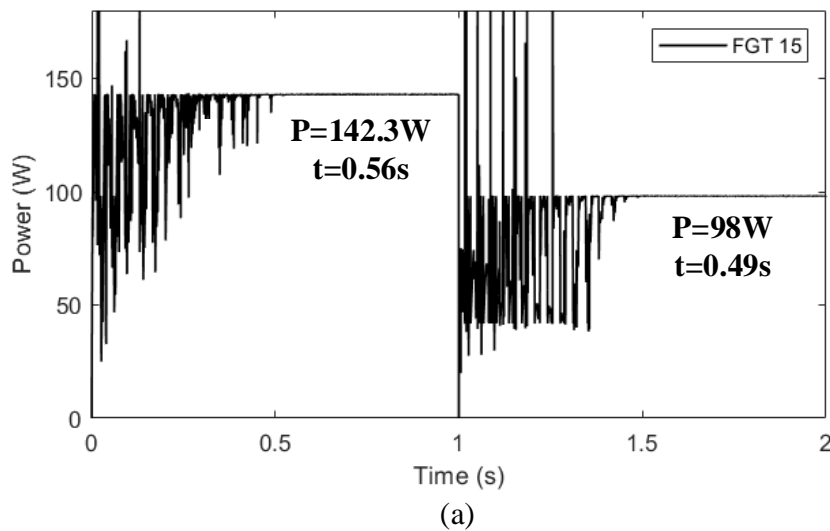


Figure 4.13 Simulation results for fifteen iterations of FGT MPPT algorithm

Figure 4.13 shows the simulation results of FGT MPPT algorithm with fifteen iterations. The optimization time for the FGT algorithm was 0.56 seconds under pattern 1 and the output power of the PV system P_{pv} is 142.3W. At 1 second, the irradiation conditions change from pattern 1 to pattern 2. The proposed FGT method yielded 98 W and required 0.49 seconds to settle to a new MPP. In terms of convergence speed, the fifteen times iteration method is slower than the previous FGT algorithm, as the method requires a more comprehensive search to be completed to set a new MPP.

Table 4.1 Performance comparison of different iteration setting

<i>Iteration</i>	<i>Irradiation</i>	<i>Power (W)</i>	<i>Tracking time (s)</i>	<i>Efficiency (%)</i>
5	Pattern 1	142 W	0.4 s	99.3%
	Pattern 2	96.7 W	0.52 s	98.5%
10	Pattern 1	142.6 W	0.42 s	99.7%
	Pattern 2	98 W	0.35 s	99.8%
15	Pattern 1	142.3 W	0.56 s	99.5%
	Pattern 2	98 W	0.49 s	99.8%

The comparison of different termination conditions for FGT MPPT algorithm is summarized in Table 4.1. The setting of the number of iterations directly affects the performance of the MPPT algorithm and thus the efficiency of the PV system power generation. Therefore, it is important to set the proper number of iterations for a given PV system. In general, for simple PV systems, such as single solar panels or systems under uniform irradiation, a smaller number of iterations can be sufficient. However, for complex PV systems, such as multiple solar panels or under PSC, more iterations are required to ensure that the PV system works on MPP. For the proposed PV emulator system, the number of iterations is set to 5, 10, 15 and the performance is evaluated. As can be seen from the Table 4.1, the setting of the number of iterative termination conditions significantly affects the performance of the MPPT. The setting of fewer iterations allows the FGT algorithm to quickly track to near the PV system maximum power point, but does not guarantee that the system is operating at the accurate MPP at the end of the iteration. Furthermore, with a small number of iterations, over-spreading of particles in the

FGT algorithm may cause the FGT algorithm to restart, resulting in increased search time due to tracking failure. On the contrary, a larger number of iterations ensures that the particles in the FGT algorithm converge, thus avoiding tracking failures. As the number of iterations is not infinite, the MPPT efficiency of 10-iteration (99.7%~99.88%) and 15-iteration setting (99.5%~99.8%) is significantly higher than the efficiency of 5-iteration setting (98.5%~99.3%). It is worth noting that the FGT algorithm causes the PV system output voltage V_{pv} to fluctuate around the maximum power point late in the iteration until the end of the iteration. It can be seen from Table 4.1 that the 15-iteration setting has a longer fluctuation time than the 10-iteration setting, which also results in more power loss. It is clear that the benefits of more iterations are diminishing. While more iterations may improve the accuracy of the tracked MPP, they also entail a loss due to longer power oscillations. Therefore, a compromise must be made between tracking speed and tracking accuracy by setting an appropriate number of iterations. For the two series-connected panels experimental system presented in this thesis, the proposed MPPT method has the best comprehensive performance when the number of iterations is set to 10. In summary, a suitable number of iterations setting of the FGT algorithm can improve the transient response and reduce the steady-state power loss of the PV system.

For critical analysis and proper validation of the proposed algorithm, more complex partial shading conditions will be considered. The MPPT algorithm will be further validated in pattern 3 and 4, where the PV system consists of three solar panels connected in series. In pattern 3, two solar panels are under $400\text{W}/\text{m}^2$ irradiation while the third solar panel is under $600\text{W}/\text{m}^2$ irradiation. The maximum power point of the PV system occurs at 109.4V and the maximum output power of the system is 209W. For pattern 4, three solar panels are irradiated by $600\text{W}/\text{m}^2$, $400\text{W}/\text{m}^2$, $200\text{W}/\text{m}^2$, respectively. The P-V curve of a photovoltaic system has three peaks, with the global maximum power point at the second peak. The terminal voltage at this point is 73.26V, and the output power of the PV system is 141.5W. The P-V schematic of pattern 3 and pattern 4 is shown in the Figure 4.14.

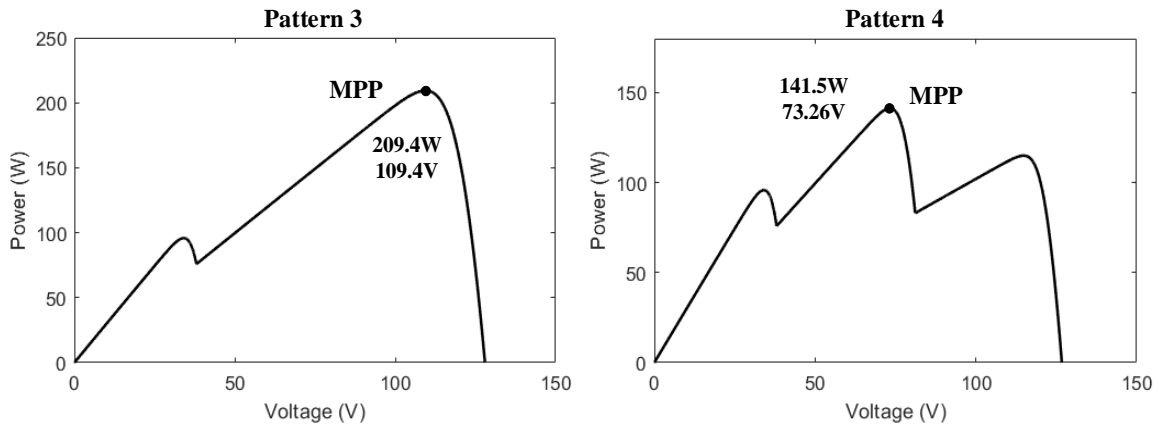


Figure 4.14 Schematic of patten 3 and pattern 4 irradiation conditions

The simulation results of proposed FGT MPPT algorithm under complex partial shading conditions are shown in Figure 4.15. The number of iterations is set to ten.

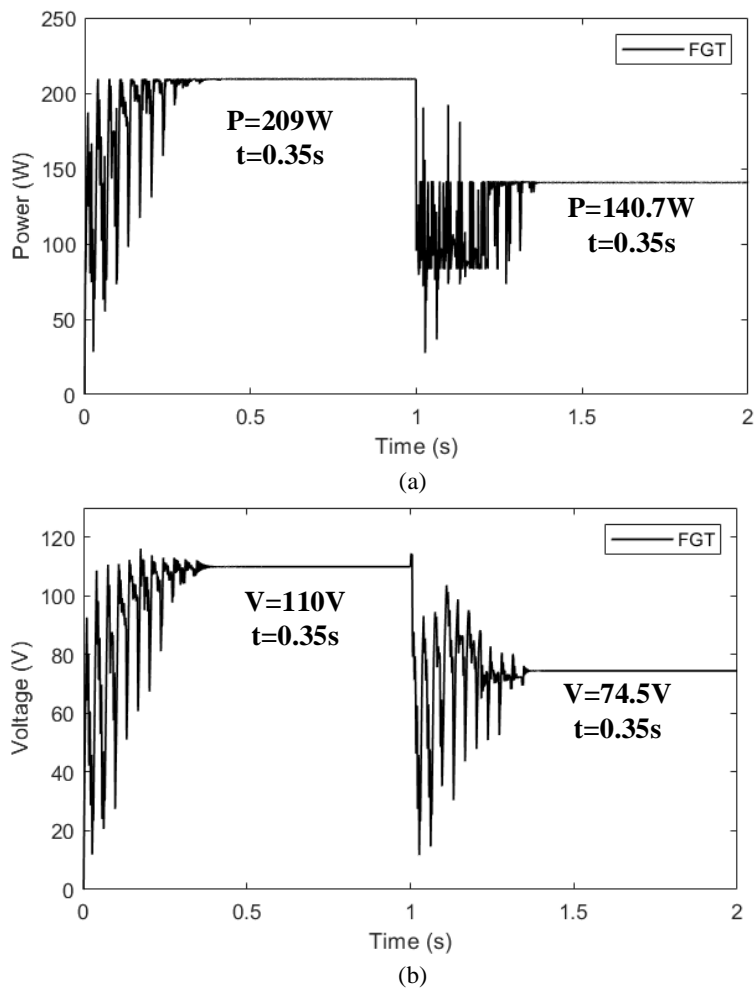


Figure 4.15 Simulation results of FGT MPPT algorithm under complex partial shading conditions

Figure 4.15 shows the behavior of the PV system when the irradiation levels were changed from pattern 3 to pattern 4. In pattern 3, the FGT algorithm takes 0.35 seconds to track down the global maximum power point. The changes in solar irradiation occurred at 1 second, after 0.35 seconds, the PV system operates at the maximum power point in pattern 4. The MPPT algorithm remains highly tracking efficient under complex irradiation conditions, 99.8% and 99.4%, respectively. The results of the simulation once again validate the global search capability of the FGT algorithm.

To further explore the effect of the algorithm particle count setting on the performance of the algorithm, additional experimental results are presented for comparison. There will always be a conflict between tracking accuracy and tracking time. The algorithm with fewer particles can complete iterations faster, but the accuracy of tracking global maximum power point may not be guaranteed. The algorithm with more particles can ensure that the PV system works on the maximum power point, but the tracking process can be more time consuming. As a comparison, the simulation results of the 5-particle and 9-particle FGT algorithms for pattern 1 and pattern 2 are shown in Figure 4.16 and Figure 4.17.

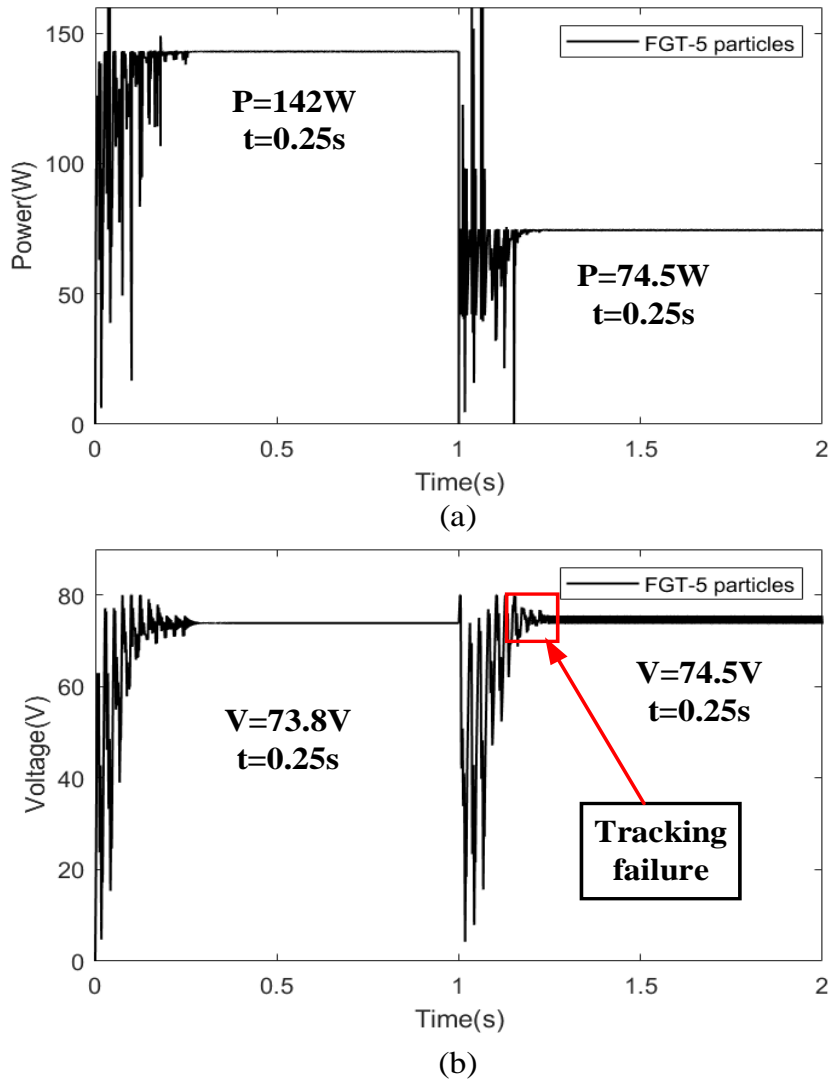


Figure 4.16 Simulation results of five-particle FGT MPPT algorithm

Figure 4.16 shows the simulation results of FGT MPPT algorithm with five particles. After 0.25 seconds, the PV system is operating at maximum power point, verifying that fewer particles can reduce tracking time. At 1 second, the irradiation conditions change from pattern 1 to pattern 2. The optimization time for the pattern 2 is 0.25 seconds and the output power of the PV system P_{pv} is 74.5W, which means that a tracking failure occurred in the PV system.

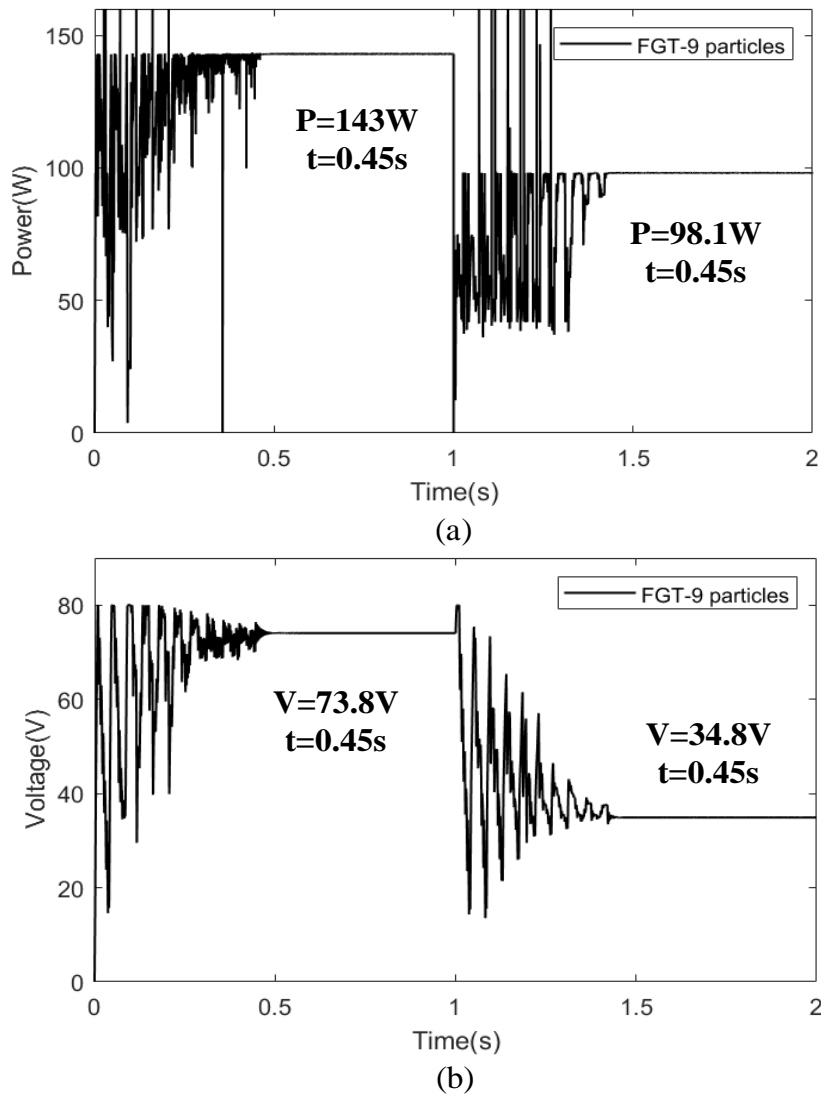


Figure 4.17 Simulation results of nine-particle FGT MPPT algorithm

As for the simulation results of nine-particle setting shown in Figure 4.17, the FGT algorithm accurately tracks the maximum power point under both pattern 1 and pattern 2. It is clear that the 9-particle FGT algorithm takes the longest time to track the MPP compared to the 5-particle and 7-particle FGT algorithms, taking 0.45 seconds. Besides, the PV system produces more power, 143W and 98.1W, respectively. Table 4.2 summarises the simulation results of the FGT algorithm for different settings of the number of search particles. Although increasing the number of particles ensures that the PV system tracks the maximum power point accurately, the power oscillations and energy losses associated with the tracking process must also be taken into account.

Table 4.2 Performance comparison of different particle setting

<i>Particles</i>	<i>Irradiation</i>	<i>Power (W)</i>	<i>Tracking time (s)</i>	<i>Efficiency (%)</i>
5	Pattern 1	142 W	0.25 s	99.3%
	Pattern 2	74.5 W	0.25 s	76%
7	Pattern 1	142.6 W	0.42 s	99.7%
	Pattern 2	98 W	0.35 s	99.8%
9	Pattern 1	143 W	0.45 s	99.9%
	Pattern 2	98.1 W	0.45 s	99.9%

The simulation results above show that the suggested fast global tracking method with good transient response and steady state performance is a promising way for tracking global maximum power point in partial shading PV system.

4.4.2 Simulation results of FGT-Fuzzy P&O algorithm

The simulation results of FGT assisted through fuzzy logic-based P&O under irradiation pattern 1 and pattern 2 is shown in Figure 4.18. According to the analysis in the previous section, the number of iterations is set to ten.

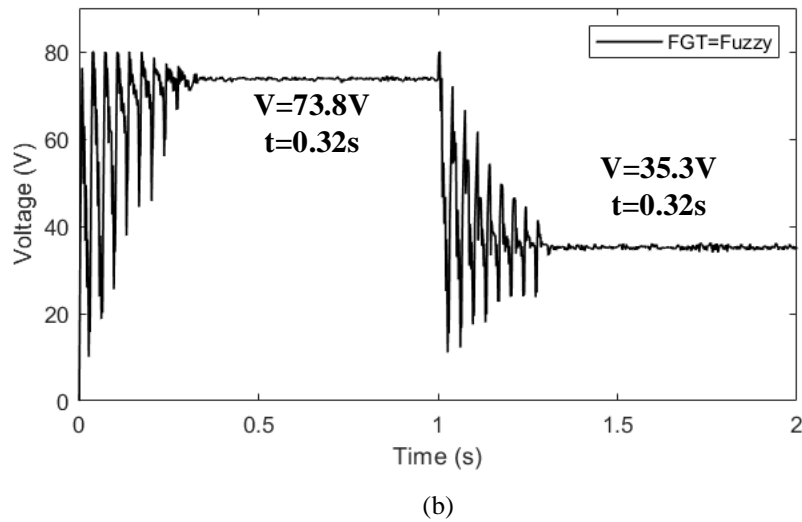
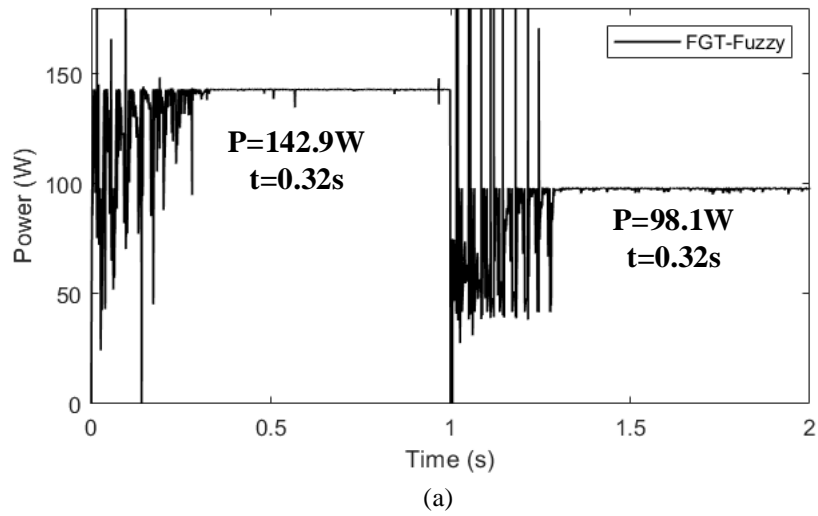


Figure 4.18 Simulation results for FGT-fuzzy logic-based P&O (a) output power and (b) output voltage under pattern 1 and pattern 2

Both solar panels are initially under zero irradiation. Later, one of the solar panels is under irradiation 600W/m^2 while the other panel is under 400W/m^2 . At 1s, the irradiation changes from 400W/m^2 to 200W/m^2 which results in a different GMPP. After ten iterations of the FGT algorithm, the fuzzy logic P&O algorithm intervened and accurately tracked the maximum power point. The results indicate that the proposed hybrid algorithm has faster dynamic response when the irradiation varies (0.32s).

Irradiation pattern 5 was added to the simulation to demonstrate the superiority of the FGT-fuzzy logic P&O algorithm. Irradiation conditions for pattern 5 are 600W/m^2 and 500W/m^2 ,

respectively, where the maximum power point voltage is 72.75V and the maximum output power is 176.9W. At 1s, the irradiation changes from pattern 5 to pattern 1 (600W/m^2 and 400W/m^2) which results in a new GMPP. The simulation results for FGT algorithm under pattern 5 and pattern 1 is shown in Figure 4.19.

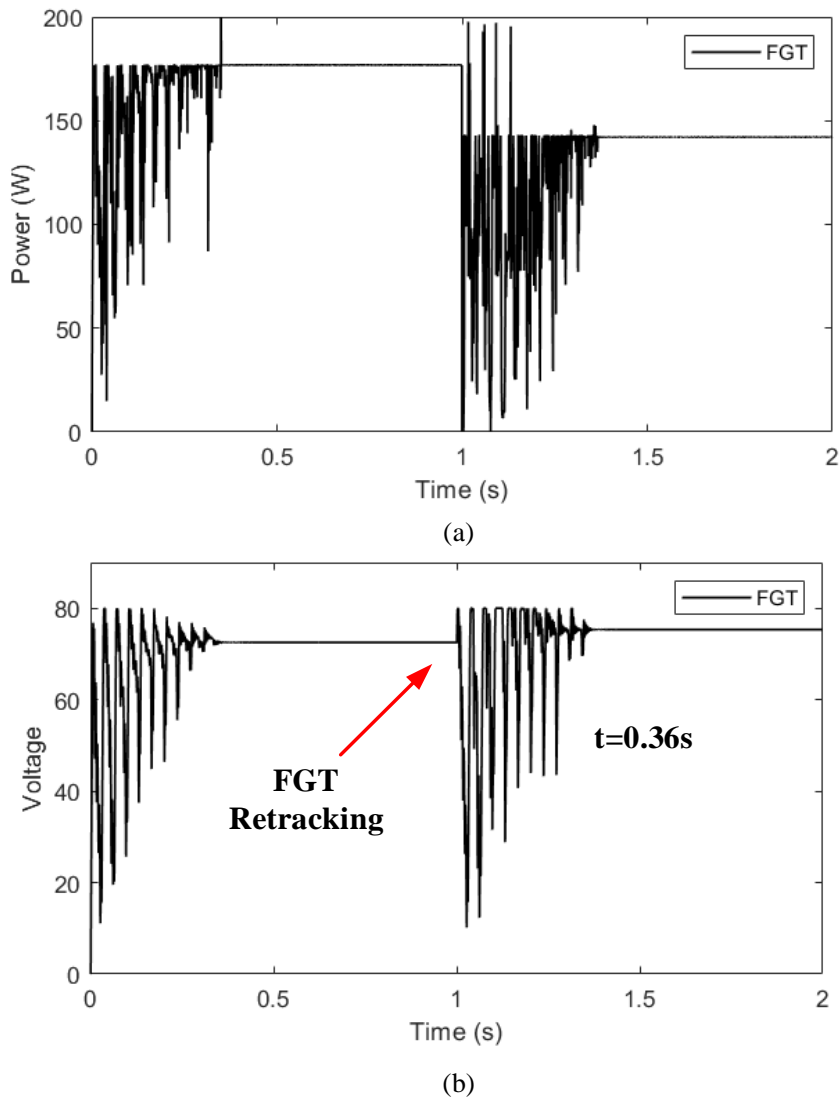


Figure 4.19 Simulation results for FGT-fuzzy logic-based P&O (a) output power and (b) output voltage under pattern 5 and pattern 1

As can be seen from Figure 4.19, the FGT algorithm accurately tracks the maximum power point in both pattern 5 and pattern 1. At one second, due to a small change in irradiation, the FGT algorithm restarts the global search and tracks a new maximum power point after 0.36

seconds. However, while the FGT algorithm ensures the PV system to maintain maximum power output, it can cause large power losses during the global search process. Under irradiation pattern 5 and pattern 1, the two different maximum power point voltages are very close (72.75V for pattern 5 and 74V for pattern 1), even though the PV system has different maximum power points. The fuzzy-P&O algorithm can track new maximum power points on a small scale while avoiding re-searching. Therefore, the intervention of fuzzy logic-P&O can effectively reduce the output power loss of the PV system under small changes in irradiation. The simulation results for FGT-fuzzy P&O is shown in Figure 4.20.

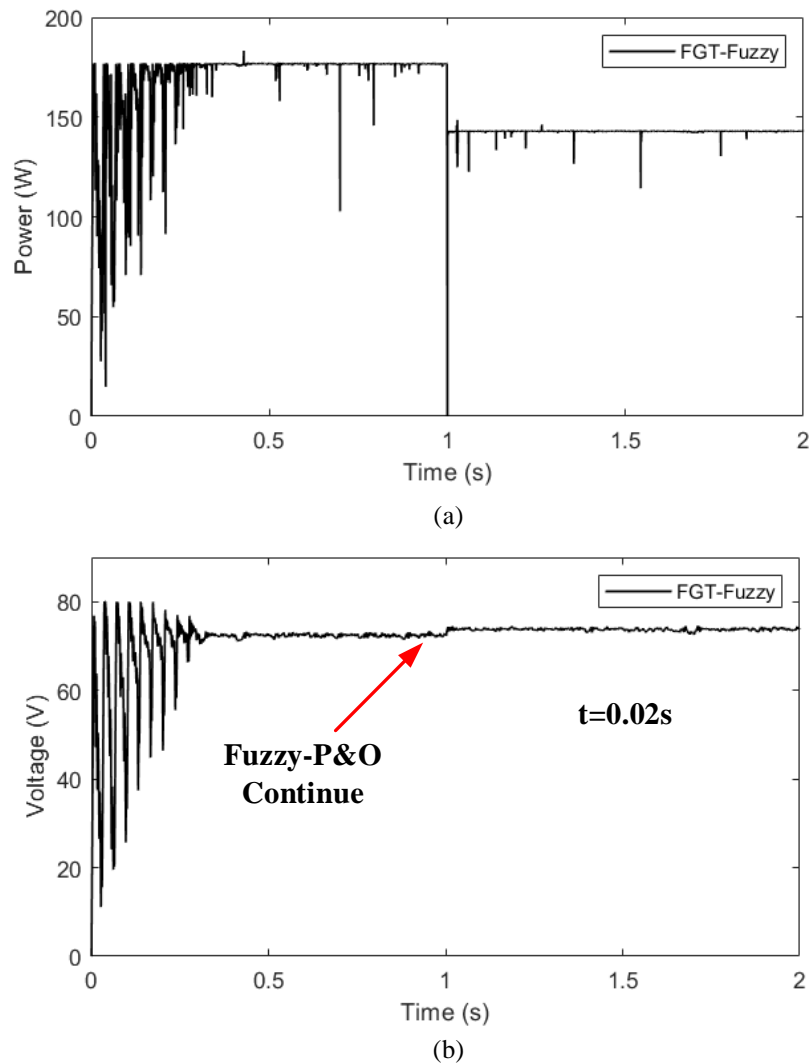


Figure 4.20 Simulation results for FGT-fuzzy logic-based P&O (a) output power and (b) output voltage under pattern 5 and pattern 1

After ten iterations of the FGT algorithm, the fuzzy logic P&O algorithm intervened and accurately tracked the maximum power point under pattern 5. At 1 second, the irradiation changes from pattern 5 to pattern 1. As this was a small magnitude irradiation change, the FGT-fuzzy P&O algorithm did not restart the global search and instead the Fuzzy-P&O continued to track the new maximum power point. After 0.02 seconds, the new maximum power point under pattern 1 was tracked. Compared to the FGT algorithm, the FGT-fuzzy P&O algorithm takes less time to track to the new maximum power point, significantly reducing the power loss during the tracking process. In summary, FGT-fuzzy P&O algorithm is superior to the single FGT algorithm for different irradiation conditions.

The particle swarm optimization MPPT algorithm is used as a comparison [71], and the results are given in Figure 4.21. The PSO parameters set up are shown in Table 4.3. Simulation results reveal that the PSO algorithm takes longer to track the MPP and the continuous oscillations of the output power is greater than proposed MPPT algorithm.

Table 4.3 Parameter of PSO algorithm

<i>Parameter</i>	<i>Values</i>
<i>Number of particles</i>	4
<i>w</i>	0.4
<i>C1</i>	1.2
<i>C2</i>	2
<i>Switching frequency</i>	20kHz

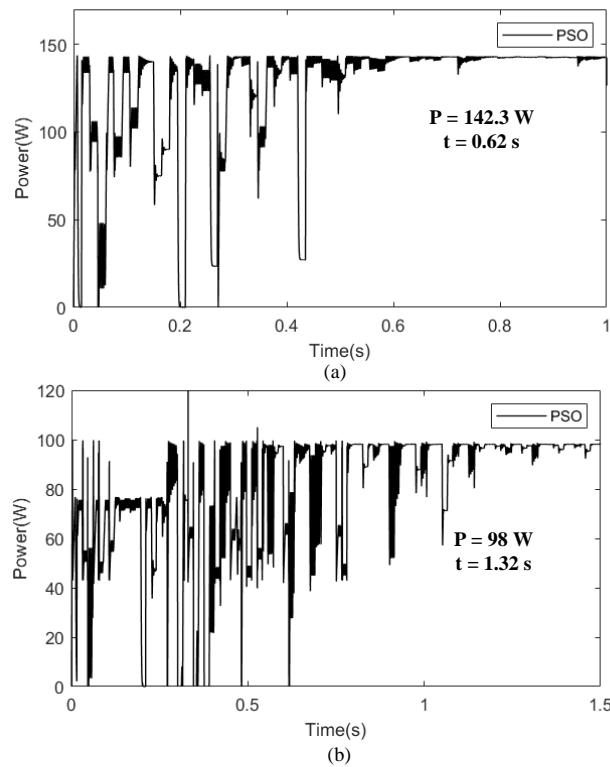


Figure 4.21 Simulation results of output power for PSO algorithm (a) pattern 1 and (b) pattern 2

The summarized simulation results of FGT, FGT-Fuzzy P&O and PSO techniques analysis are tabulated in Table 4.4. Tracking speed and efficiency are defined to evaluate the performance of MPPT techniques. Tracking speed is more important for MPPT techniques because the lesser the tracking time to track GMPP, the more energy can be extracted from the solar system. The comparison reveals that the FGT-Fuzzy P&O method is a promising way to track GMPP under partial shading conditions.

Table 4.4 Performance comparison of different MPPT methods

<i>Method</i>	<i>Irradiation</i>	<i>Power (W)</i>	<i>Tracking time (s)</i>	<i>Efficiency (%)</i>
FGT	Pattern 1	142.6 W	0.42 s	99.7%
	Pattern 2	98 W	0.35 s	99.8%
FGT- Fuzzy P&O	Pattern 1	142.9 W	0.32 s	99.7%
	Pattern 2	98.1 W	0.32 s	99.9%
PSO	Pattern 1	142.3 W	0.62 s	99.5%
	Pattern 2	98 W	1.32 s	99.8%

The results indicate that the FGT and hybrid FGT-Fuzzy logic P&O MPPT algorithm can accurately track to the global maximum power point of the PV system under complex irradiation conditions. Under pattern 1 and pattern 2, all three methods have similar MPPT efficiency (99.5%~99.8%). Another important reference for evaluating MPPT performance is the tracking time. Faster tracking times can effectively reduce the power generation loss of a PV system. As can be seen from Table 4.4, the proposed FGT-Fuzzy P&O has a faster dynamic response when the irradiation varies (0.32s). The oscillations during tracking in the early global search stage are greatly reduced using the proposed FGT method. When the operating voltage of the PV system is near the MPP voltage, the MPPT algorithm switches to a local search. This not only ensures tracking accuracy but also reduces the power oscillations in the steady state. The local search also avoids the problem of algorithm restarts due to small power variations, which greatly improves the power generation of the PV system.

4.5 Summary

This chapter shows the simulation results of two cascading strategies MPPT methods. The proposed global search adaptive P&O method is able to track down the global maximum power point of the PV system in the case of partial shading conditions. The P&O method with adaptive perturbation step-size in the local search stage overcomes the conflict between tracking speed and steady-state power oscillations of conventional P&O methods. In addition, the simulation results of the FGT-fuzzy logic P&O method are also presented. By comparing the simulation results for different particle numbers and iteration settings, the optimum number of particles and iterations for the proposed PV emulator is determined. It is worth mentioning that the fuzzy logic P&O in this hybrid method intervenes during the local search stage, optimizing the method for power loss due to small irradiation variations.

Chapter 5. Experimental verification of the proposed MPPT methods

5.1 Introduction

The experimental results of the proposed MPPT method are presented in this chapter. The MPPT methods were validated under two different irradiation conditions. The proposed PV emulator in this thesis will replace the actual solar panels. The MATLAB/simulink-based design of the MPPT methods are imported into the dSPACE system, which generates a control signal and then controls the power output of the PV emulator via a DC-DC converter. The block diagram of emulated PV system setup under partial shading condition is shown in Figure 5.1. The overall experiment system consists of two emulated solar panels connected in series, DC-DC boost converter, electronic load and dSPACE real-time interface system (processor board RTI1007, DS2004 A/D board, CP4002 digital I/O board). The dSPACE system is connected to the computer's dSPACE ControlDesk 5.5 via the LAN network port.

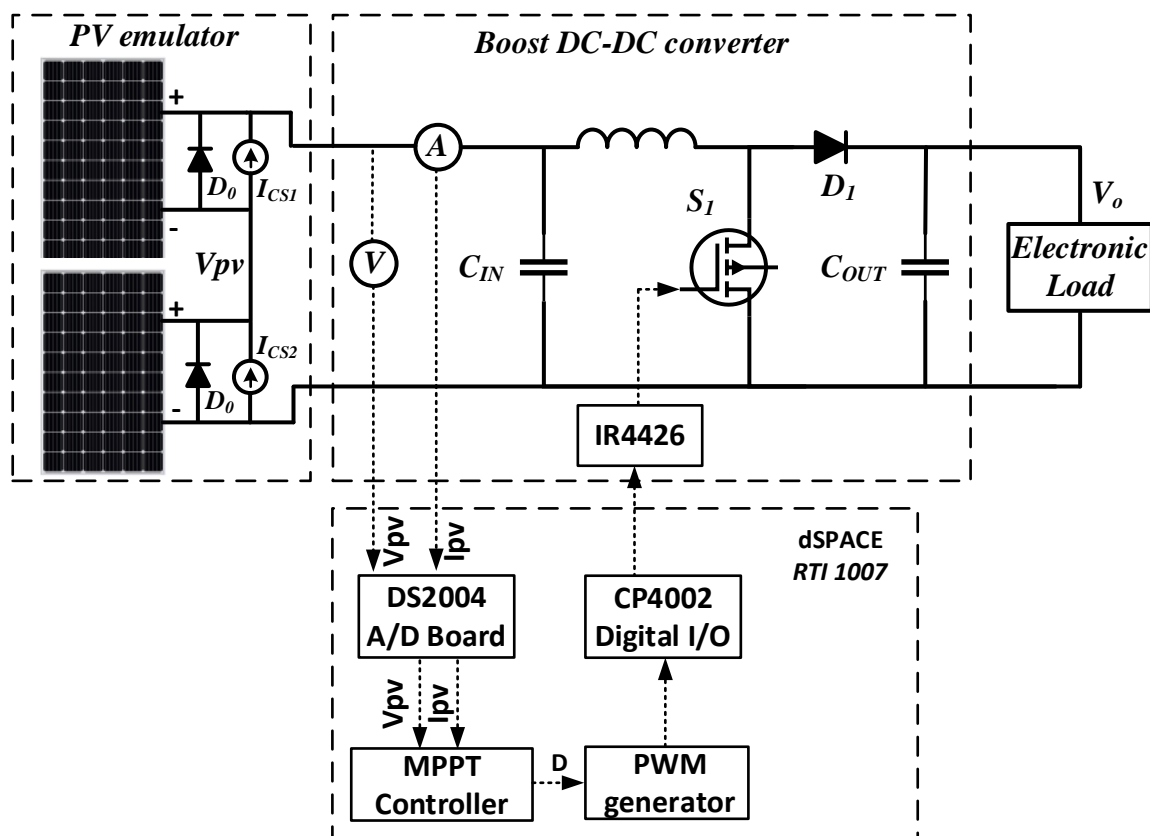


Figure 5.1 The block diagram of experiment PV system set up

The current and voltage measurement circuit integrated in the boost DC-DC converter circuit

will input the measured analogue signals I_{pv} and V_{pv} to the DS2004 A/D Board and convert these signals into digital signals. The MPPT method is pre-compiled into a C language-based program in Simulink and imported into dSPACE controldesk. Based on the digital signals provided by the DS2004 A/D board, the MPPT controller generates the corresponding duty cycle D and converts it into a PWM signal via the PWM generator. These PWM control signals will be fed into the CP4002 digital I/O interface. The CP4002 Digital I/O reconverts the digital signal into an analogue signal for the control of the boost converter. It is worth noting that the control signal generated by dSPACE cannot be used directly for the MOSFET IRF4321 used in this experiment. therefore, the analogue signal from dSPACE will be fed into the driver IR4426 before controlling the power switch IRF4321.

5.2 dSPACE system

dSPACE is widely used for planning, designing, execution of hardware and software. The dSPACE controller is extensively employed for regulating power electronics converters and electric vehicles [82]. In this thesis, dSPACE system was used to generate PWM signal in power electronics converters to regulate terminal voltage of the PV emulator. Pulse generation for DC-DC converters is done using dSPACE RTI blocksets and Simulink blocks. The brief block diagram of interface dSPACE system with a boost converter is shown in Figure 5.2.

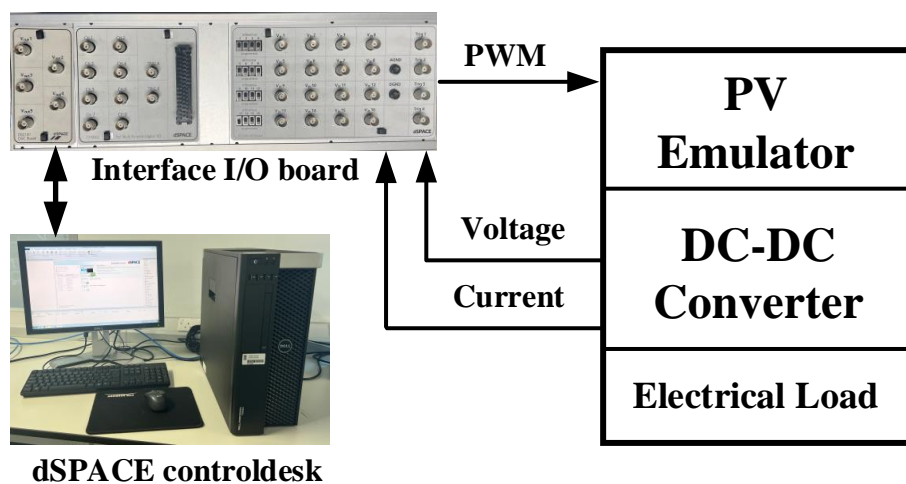


Figure 5.2 Brief block diagram of dSPACE implement

5.2.1 Composition of dSPACE system

The dSPACE controldesk 5.5 is a software tool which is interfaced with MATLAB and RTI library. The RTI library is a software package that is added to the MATLAB library to create a MATLAB simulink model and generate control signals for the dSPACE RTI1007 controller. In addition, the MATLAB Simulink program receive feedback from the sensor signals via dSPACE RTI1007 in a similar manner and both control signals or feedback signals can be controlled and monitored via controldesk 5.5.

dSPACE RTI1007 controller is a bridge between hardware and software and is used to transfer and interface control signals and feedback signals. It is connected with desktop and experimental circuits which is controlled by controldesk 5.5. The components of dSPACE RTI system are shown in Figure 5.3 consist of DS2004 A/D, CP4002 Digital I/O boards and a license key.



RTI 1007 controller



Licence key



DS2004 A/D Board



CP4002 Digital I/O

Figure 5.3 dSPACE accessories

5.3 Boost DC-DC converter components selection

Unlike a simulation environment, when an actual experimental circuit is to be implemented, not only the parameters of the design have to be considered, but also the packaging of the components, their size, commercial value, etc. The output diode conducts when the power switch is switched off and provides a path for the inductor current. The best choice of boost converter for experimental circuits with low voltage outputs is usually a Schottky diode. The choice of diode needs to take into account the breakdown voltage, current rating, forward voltage drops, and the package to suit the circuit. It is important to note that the diode breakdown voltage must be greater than the maximum output voltage and the current rating should be at least twice the output current of the maximum power stage [77]. The role of the output capacitor in a boost converter is energy storage. In essence, the function of the output capacitor is to maintain a constant voltage in the circuit. In addition, output capacitors are applied to limit the output voltage ripple to a defined range. The equivalent series resistance (ESR), equivalent series inductance (ESL) and capacitor (C) form the capacitive impedance, while the series impedance of the capacitor and the output current determine the output voltage ripple. During the on-state stage, the output capacitor supplies all the output current of the load, assuming that all the ripple in the output voltage of the circuit is caused by the capacitor. For a boost converter operating in continuous mode, the following equation can be consulted to determine the choice of output capacitor [79]:

$$C_{out} = \frac{I_{out_max} \times D_{max}}{f_s \times \Delta V_{out}} \quad (5.1)$$

where I_{out_max} represents the maximum output current, D_{max} is the maximum duty cycle for boost converter, f_s is switching frequency and ΔV_{out} is output voltage ripple. The function of the input inductor is to reduce the negative effects caused by current input ripple in the PV panel. When determining the type of this component, size, cost and capacitor losses are taken into account. The function of the boost converter inductor is to store energy, to maintain a constant current during operation and to limit the variation in current. Inductance value is often chosen according to the peak-to-peak ripple current that flows through it. In addition, the peak

current through which the inductor can pass and the maximum operating frequency must also be taken into account. It is important to ensure that the inductor will not overheat or saturate when operating within the rated current range [79]. The function of a power switch is to control the flow of energy from the input to the output. The switch must respond quickly, conducting the current in the inductor when switched on and blocking the full output voltage when switched off. In addition, excessive power loss during switching transitions must also be avoided. Both IGBT and MOSFET power devices can be used in boost converters, but given the performance and cost, MOSFETs are the best choice. N-channel MOSFETs are commonly used in boost converters because driving the gate is simpler than the gate drive required by p-channel MOSFETs [79]. In summary, the components of the boost converter were selected as shown in Table 5.1.

Table 5.1 List of boost converter components

<i>Component</i>	<i>Brand</i>	<i>Characteristic</i>	<i>Reference number</i>
Diode (D)	INFINEON	600 V, 12 A, 19 nC	IDH12SG60CXKSA2
Inductor (L)	MURATA	100 μ H, \pm 10%, 0.033 ohm	1410460C
Capacitor (C_{in})	RUBYCON	220 μ F, 400 V, \pm 20%	400VXG220MEFCSN
Capacitor (C_{out})	RUBYCON	440 μ F, 400 V, \pm 20%	100VXG470MEFCSN
Power switch (S)	INFINEON	150 V, 85 A, 0.012 ohm	IRFS4321TRLPBF

5.4 Experimental system setup

Figure 5.4 shows the test bench of the experiment. Each of the two SUNTECH STP175S-24/Ac solar panel is connected in parallel with TENMA72-2940 Power Supply set in constant current mode. The terminal voltage of the emulated PV panels is regulated by boost converter.

The proposed MPPT algorithm was achieved using MATLAB/Simulink 2015a and programmed into the dSPACE system. DS2004 A/D board is used to measure the voltage and current from the boost converter measured circuit which are the feedback signals to the MPPT algorithm.

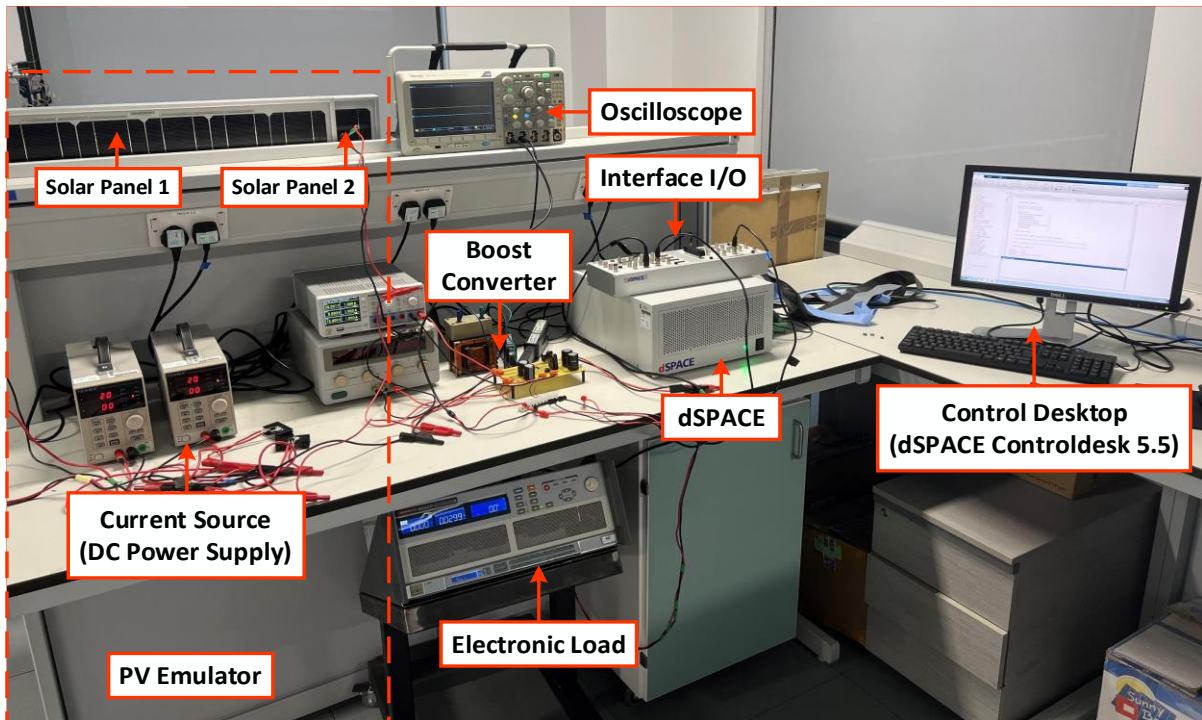


Figure 5.4 Experimental system set up

5.5 Experiment results of proposed hybrid global search adaptive perturb and observe MPPT algorithm

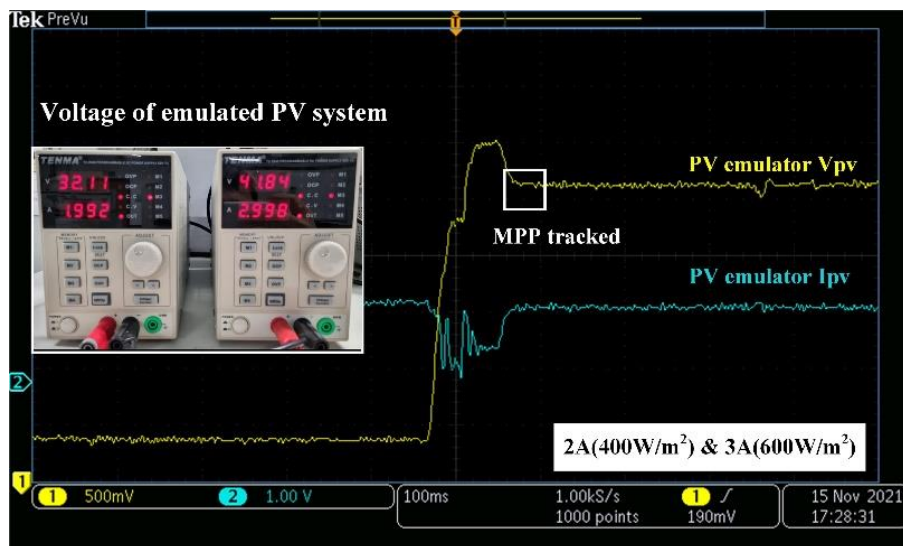
In the simulation and experiment system, the proposed emulated PV system was connected to a boost DC-DC converter. The terminal voltage of the emulated PV panels is regulated by boost converter with following specifications shown in Table 5.2.

Table 5.2 Boost DC-DC converter parameters

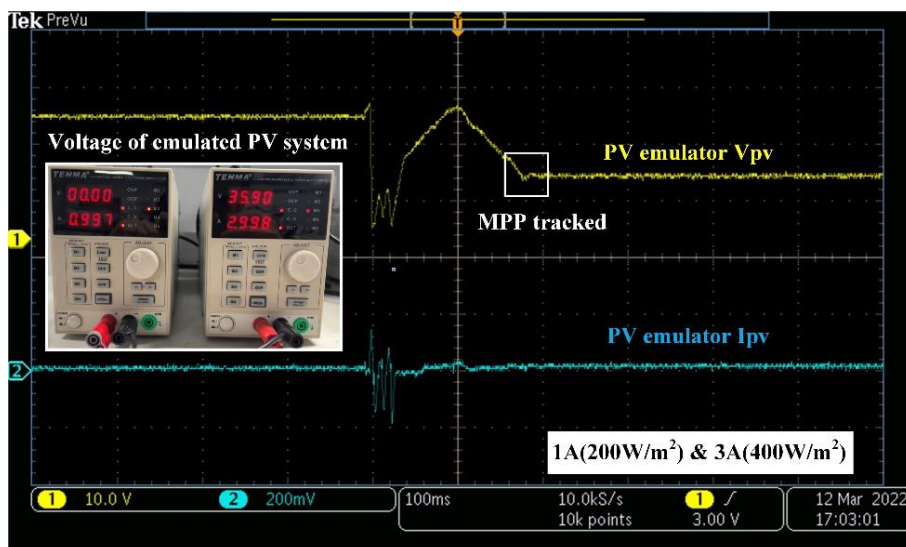
<i>Parameter</i>	<i>Value</i>
<i>Inductor L</i>	100 μ H
<i>Input capacitor C1</i>	220 μ F
<i>Output capacitor C2</i>	440 μ F
<i>Switching frequency</i>	20kHz

The control signal duty cycle D generated by the algorithm is output via the CP4002 digital I/O board. It is worth to mention that the measured currents and voltages are scaled due to the input voltage limit of the dSPACE analogue to digital A/D board channels is between -10V and +10V.

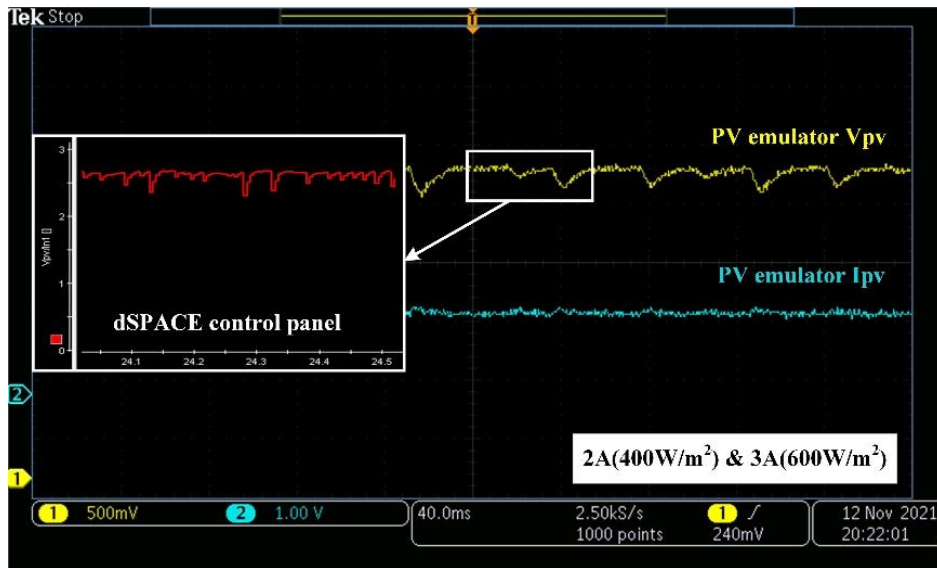
Hence, the measured voltage V_{pv} and current I_{pv} are scaled down by the circuit and multiplied by 28 and 2.6 respectively to obtain the actual values. The experiment results of emulated PV system under different irradiation with conventional and proposed MPPT algorithm are shown in Figure 5.5. For case 1, the PV system initially operating under $200W/m^2$ and $400W/m^2$ irradiation condition. After a period of time, the irradiation condition changes to $400W/m^2$ and $600W/m^2$ irradiation. For case 2, the PV system works under $400W/m^2$ and $600W/m^2$ irradiation and then suddenly changes to $200W/m^2$ and $400W/m^2$ irradiation. As can be seen from the external current source display, the output voltages of the PV emulator in cases 1 (73.95V) and case 2 (35.9V) are very close to the output voltages in the simulation results 73.8V and 34.85V.



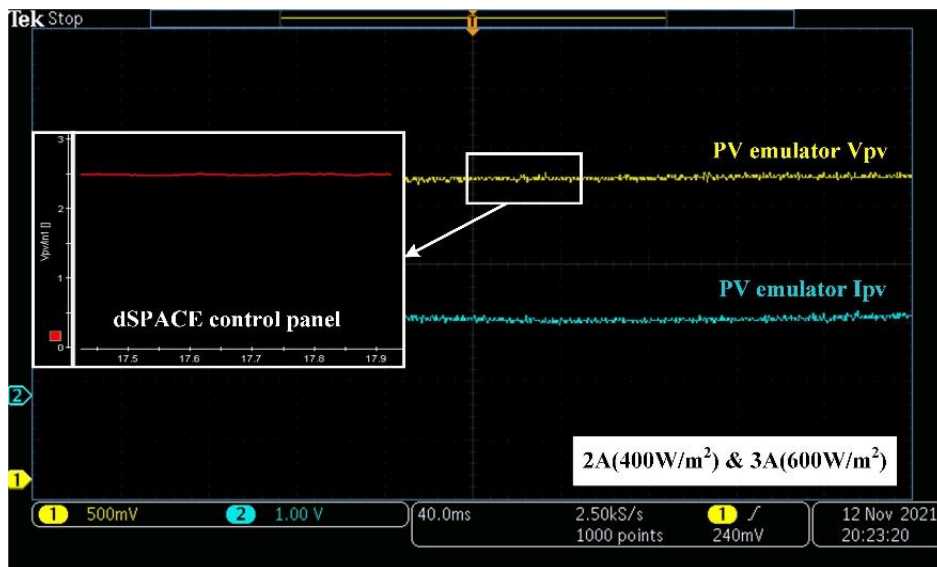
(a) transient response of PV systems under case 1 irradiation



(b) transient response of PV systems under case 2 irradiation



(c) steady-state with conventional P&O algorithm



(d) steady-state with adaptive P&O

Figure 5.5 Conventional and proposed MPPT PV voltage and current measured results for partial shading under case 1 and case 2 irradiation

The measured values in Figure 5.5 represent transient and steady-state responses in terms of constant current under case 1 and case 2. The maximum power point of the emulated PV system under testing irradiation was around 73.8V and 34.85V which can be seen in Figure 5.5(a) and (b). Figure 5.5(c) and (d) show that the adaptive P&O algorithm has less power oscillation around the voltage of MPP as it is expected. Since the partial shading is simulated by manually adjusting the external current source, sudden small irradiation changes are hard to be simulated.

In addition, the scale down factor of boost converter measurement circuit is too large and is affected by harmonics. As a result, it is difficult to see the difference in transient response of small magnitude irradiation changes between the conventional and proposed MPPT algorithm. This would be optimized in future experiment. Experimental results are in accordance with the simulation results and show that the proposed emulated PV system was effectively for the investigation of partial shading condition. Besides, the proposed MPPT algorithm has better tracking performance and smaller power oscillations around MPP than conventional P&O MPPT algorithm.

5.6 Experiment results of proposed hybrid FGT MPPT algorithm assisted through fuzzy logic based variable step-size perturb and observe method

The test bench of the experiment can be seen in Figure 5.1. An emulated PV system is employed to emulate the behavior of the PV cells. The output voltage of the emulated PV panels is controlled by a boost converter which is shown in Table 5.3.

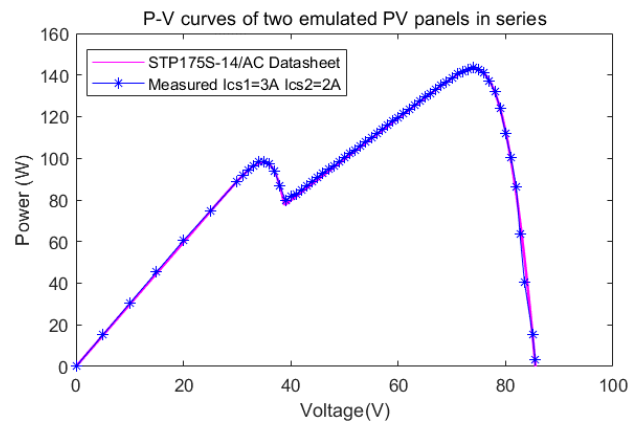
Table 5.3 Boost DC-DC converter parameters

<i>Parameter</i>	<i>Value</i>
<i>Inductor L</i>	2 mH
<i>Input capacitor C1</i>	220 μ F
<i>Output capacitor C2</i>	440 μ F
<i>Switching frequency</i>	20k Hz

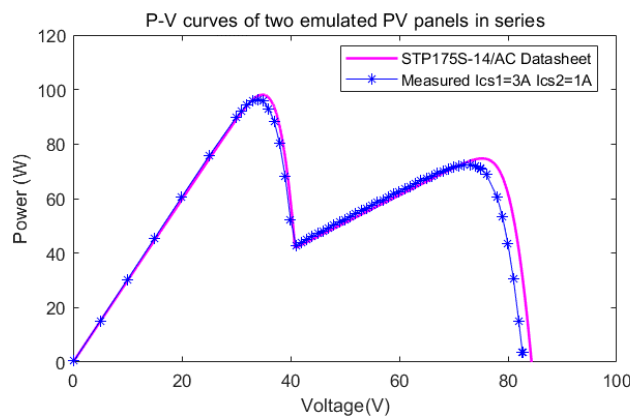
Due to the input voltage signals of dSPACE analogue to digital (A/D) board is in the range of -10V to +10V, the measured voltage V_{pv} and current I_{pv} from the measured circuit (Tektronix A622) are scaled down by 20 and 10, respectively. The PWM signal for controlling boost converter was generated from Modular Hardware (DS4002).

Figure 5.6 shows the measured and datasheet given P-V characteristics of the emulated PV

system under different irradiation. The different partial shading solar irradiance level was emulated by setting both injection external current source current as 1A/3A and 2A/3A, respectively (corresponding to the actual P-V curves under 200W/m^2 , 600W/m^2 and 400W/m^2 , 600W/m^2 solar irradiance). It is important to mention that different currents were injected into the Unilluminated emulation PV system to produce a suitable P-V characteristic curve. When partial shadowing occurs, the photocurrent of shaded PV cells decreases, while the photocurrent of unshaded PV cells remains larger. In this situation, the shaded cells will work in reverse bias and consume power due to reverse voltage polarity, resulting in a hot spot and the possibility of cell failure. An anti-parallel bypass diode is commonly attached to the PV panel to restrict the reverse voltage and prevent power loss in the shaded panel [70].



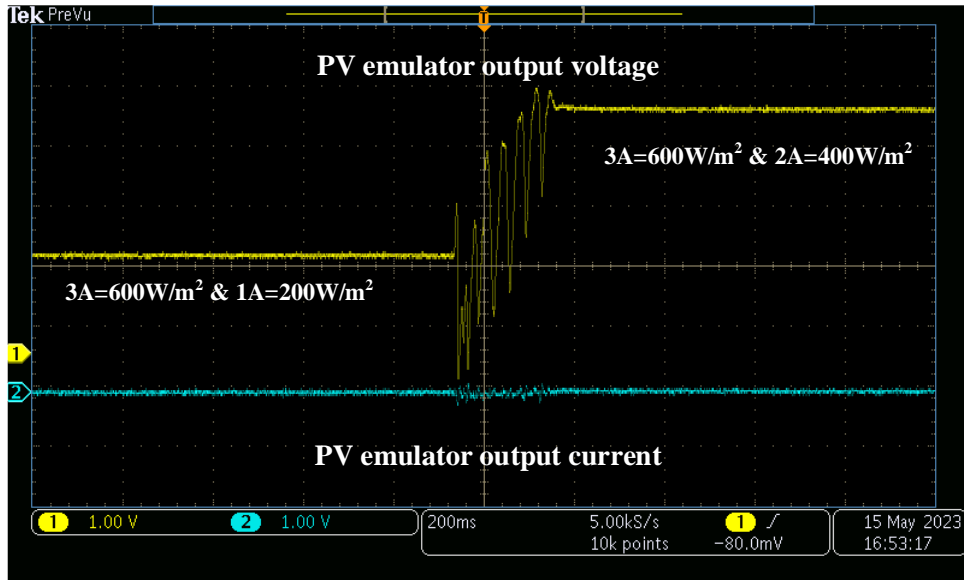
(a)



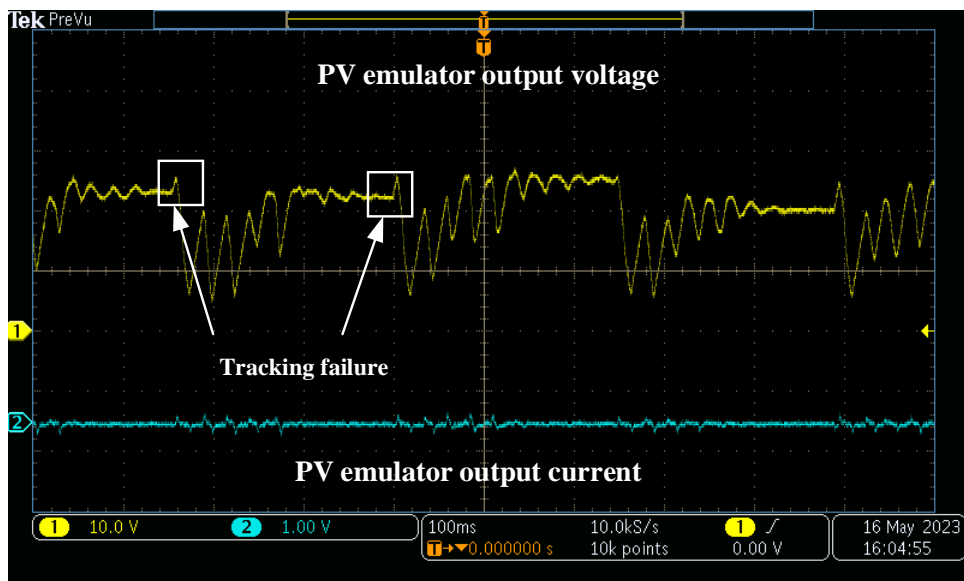
(b)

Figure 5.6 Measured and datasheet given P-V characteristics of the emulated PV arrays under pattern 1 and pattern 2

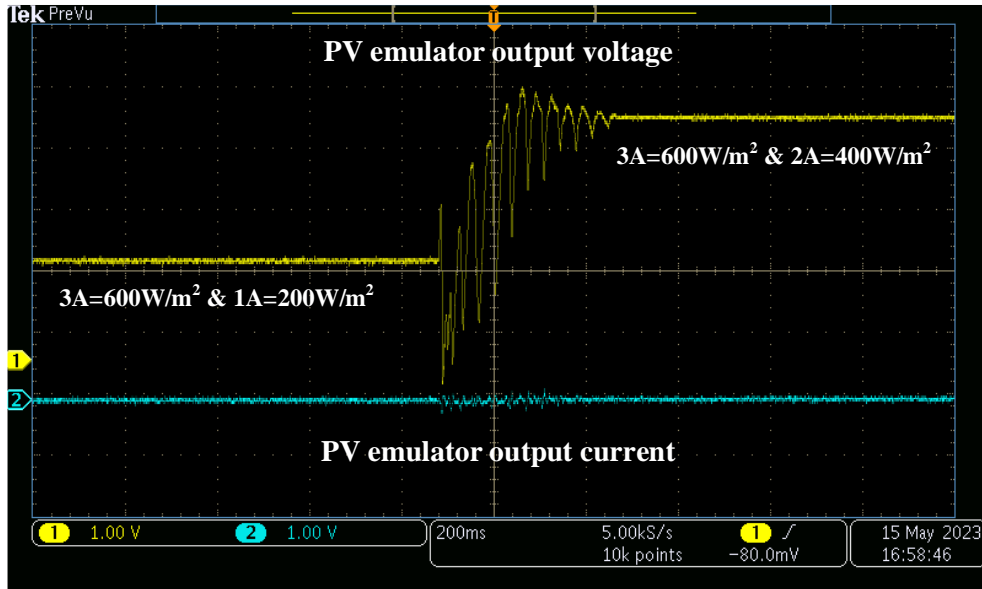
The experimental results of the proposed FGT method with different number of iterations are shown in Figure 5.7. The experimental conditions were set to mutate the irradiation from pattern 2 to pattern 1.



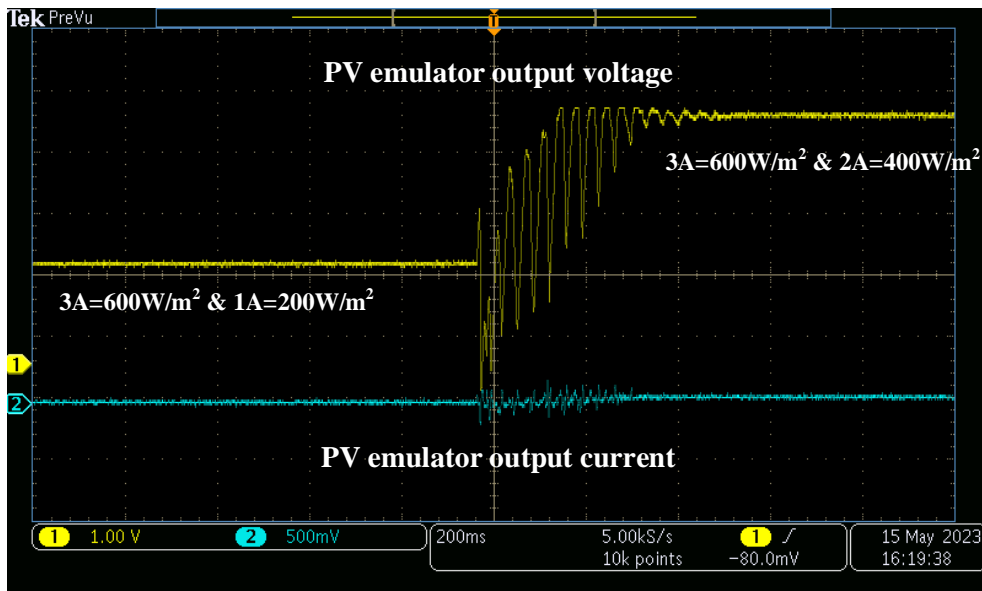
(a) 5 iterations



(b) 5 iterations (tracking failure)



(c) 10 iterations



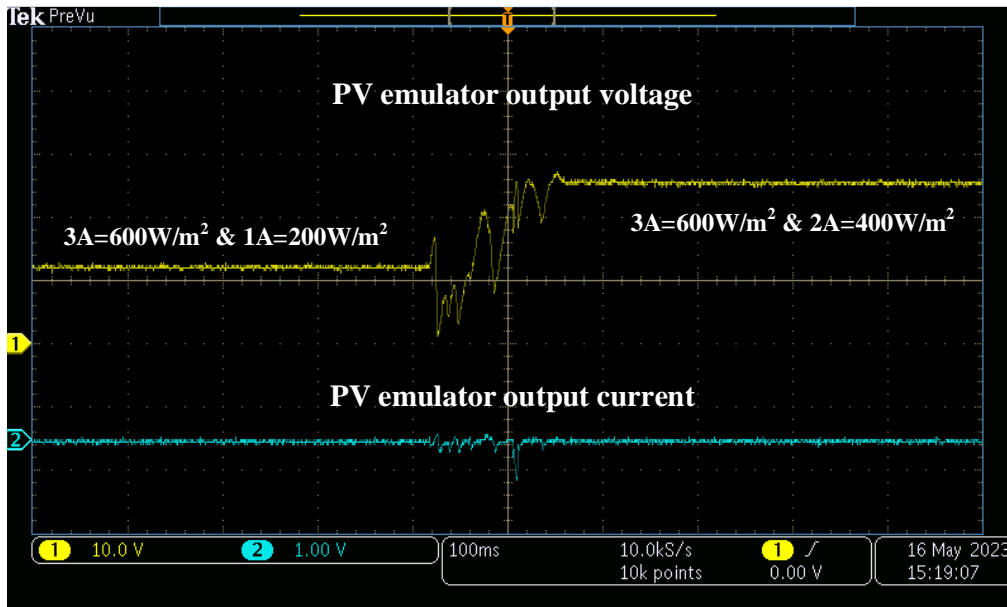
(d) 15 iterations

Figure 5.7 Experimental results of the proposed FGT method with different iteration settings for varying irradiation from pattern 2 to pattern 1

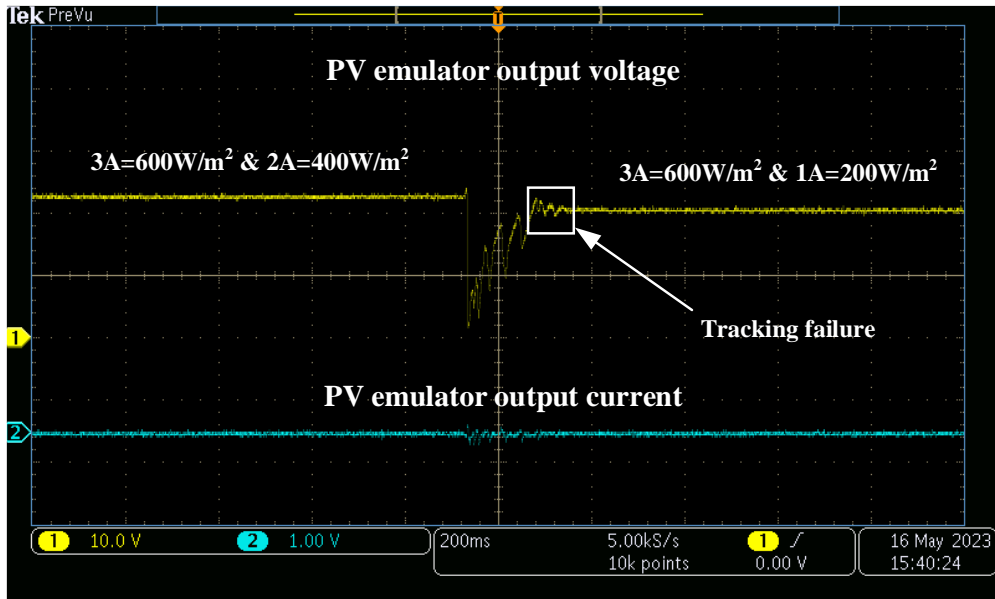
The experimental results are accordance with simulation results. Comparing (a)(c)(d) of Figure 5.7, it can be seen that the different settings of the number of iterations have a significant impact on the performance of the FGT method. A higher number of iterations may improve the accuracy of MPP tracking, but it will increase the tracking time. In addition, comparing Figure 5.7 (a)(b) shows that the FGT method has the potential for tracking failure when the number

of iterations is set to 5, with constant restarting of the global search leading to power loss. This is mainly because the FGT method is unable to determine the position of the current optimal particle due to the low number of iterations. Therefore, setting a small number of iterations should be avoided when considering the performance of the FGT method.

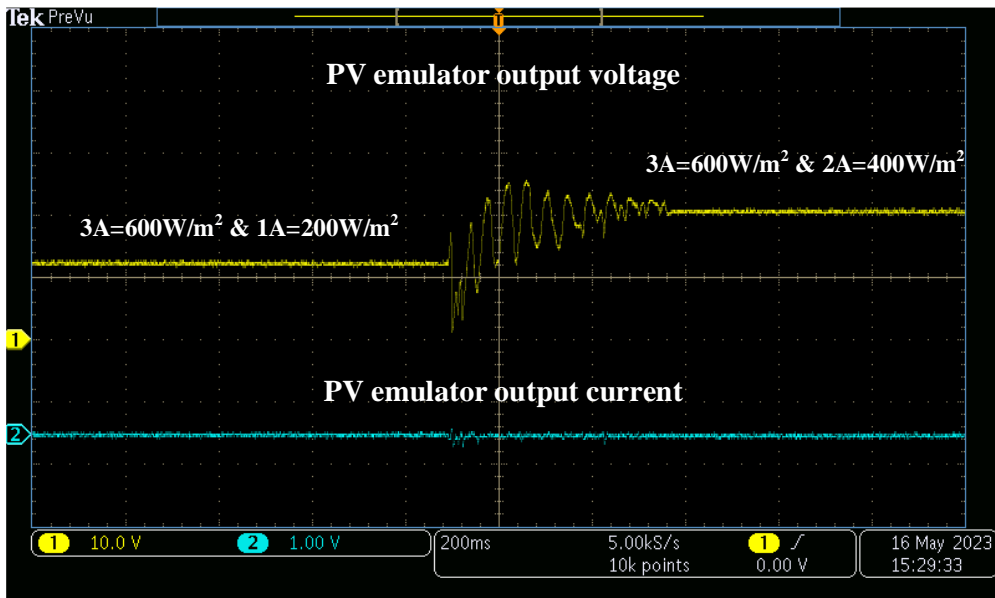
The experimental results of the FGT method with different particle number settings are given in Figure 5.8. All experimental results are based on 10 iterations setting. The experimental conditions were set to mutate the irradiation from pattern 2 to pattern 1 for Figure 5.8 (a)(c). The experimental condition in Figure 5.8 (b) is the change of irradiation from pattern 1 to pattern 2.



(a) 5 particles



(b) 5 particles (tracking failure)



(c) 9 particles

Figure 5.8 Experimental results of the FGT method with different particle number settings

The experimental results are accordance with simulation results. Comparing Figure 5.8 (a)(c) and Figure 5.7 (c), it can be seen that the increase in the number of particles may facilitates the search accuracy of the FGT method, but increases the tracking time. Furthermore, it is clear from Figure 5.8(b) that the tracking failure of the 5-particle FGT method occurs when the irradiation conditions change from pattern 1 to pattern 2. The output voltage and current of the PV emulator shows only small variations, which indicates that the PV system is not operating

at the maximum power point. This is mainly because a smaller number of particles may lead to MPP misclassification by the FGT method. Therefore, the effect of the number of particles on the performance of the FGT should be taken into account when setting the parameters.

The proposed FGT-Fuzzy P&O MPPT method experimental test result for pattern 1 and pattern 2 is given in Figure 5.9 and 5.10. The measure values in Figure 5.9 and Figure 5.10 represent both transient and steady-state responses in terms of PV emulator output voltage and current. Note that the the experimental results are based on 10 iterations and a 7-particle setup.

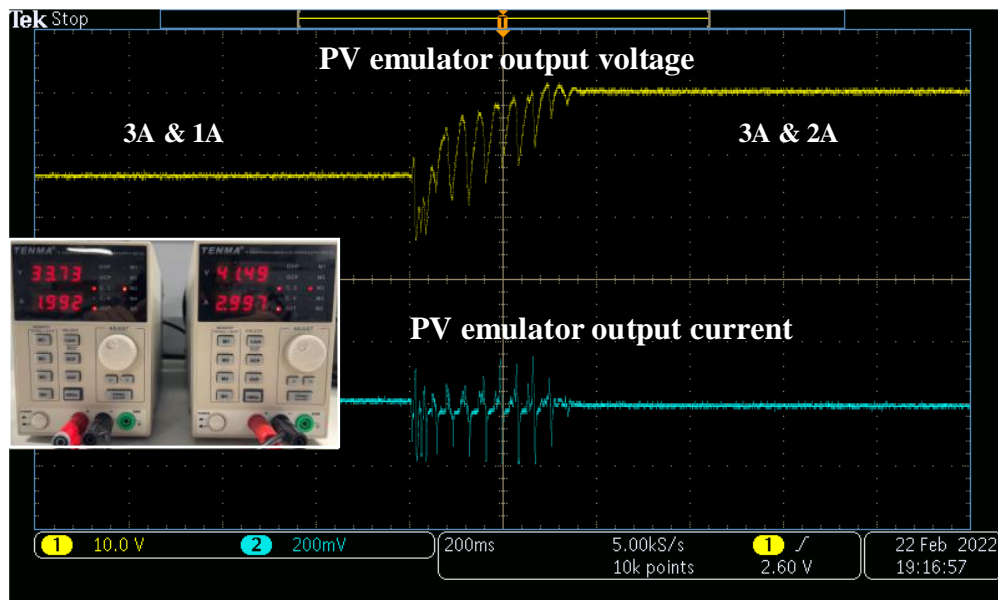


Figure 5.9 Experiment results of FGT-Fuzzy P&O method for varying irradiation from pattern 2 to pattern 1

As can be seen in Figure 5.9, PV system initially operating in pattern 2 irradiation condition ($600\text{W}/\text{m}^2$ and $200\text{W}/\text{m}^2$ irradiation). Later, the irradiation condition changes from pattern 2 to pattern 1 ($600\text{W}/\text{m}^2$ and $400\text{W}/\text{m}^2$ irradiation) and the new MPP is tracked by the proposed MPPT algorithm.

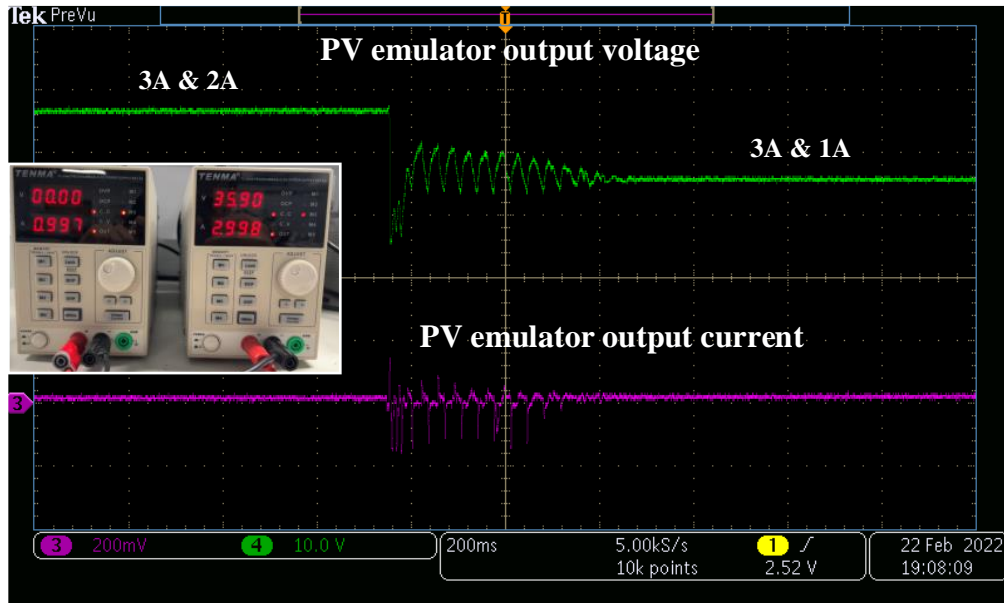


Figure 5.10 Experiment results of FGT-Fuzzy P&O method for varying irradiation from pattern 1 to pattern 2

The experimental test results for varying irradiation from pattern 1 to pattern 2 is shown in Figure 5.10. Initially, the emulated PV system operates at the MPP of pattern 1 (75.22V). As the irradiation drops to 600W/m^2 and 200W/m^2 (corresponding to emulated PV system with constant injection currents of 3A and 1A), a new MPP (35.9V) is tracked by the proposed algorithm. The results again show that the proposed indoor unilluminated PV emulator is very reliable and can be applied to power electronics experiments.

5.7 Summary

The validity of the two proposed MPPT methods has again been verified in this chapter. The experimental results again show that the proposed indoor unilluminated PV emulator is very reliable and can be applied to power electronics experiments and the results of the proposed MPPT methods are in accordance with the simulation outcomes. Both experimental results reveal that the proposed MPPT strategies can track to the global maximum power point under partial shading conditions. In addition, the optimized MPPT methods not only improve tracking speed, but also reduces steady-state oscillations around the maximum power point.

Chapter 6. Conclusions

This thesis has presented an innovative PV emulator and a state of-the-art learning-based real-time hybrid global search adaptive perturb and observe (P&O) maximum power point tracking (MPPT) technique and a hybrid fast global tracking MPPT algorithm assisted through a fuzzy logic based variable step-size P&O.

The main goal of the constructed emulator is to overcome obstacles such as the necessity for a large area, significant installation costs, and lack of control over environmental conditions by merging unilluminated solar panels with an external current supply. The proposed PV emulator consists only of photovoltaic panels and some basic laboratory equipment which is easy to set up in the laboratory. The experimental results show that the proposed PV emulator performs admirably in indoor unilluminated environments and successfully mimics the electrical characteristics curve of real solar panels under both uniform irradiation and partial shading conditions. It is worth noting that for the PV emulator, an external current source replaces the actual current generated to simulate power generation, which causes the PV emulator to experience voltage shifts. When the operating voltage of the PV system exceeds its MPP voltage, the output voltage of the PV emulator starts to shift. Under standard testing conditions ($1000\text{W}/\text{m}^2$ and 25°C), the voltage shift is the greatest when the PV system is operating at the open circuit voltage V_{oc} , which is approximately 4.8%. Therefore, the MPPT method should be tested with the PV emulator under low irradiation conditions. In addition, in the parallel-connected PV emulator, blocking diodes are usually connected in series with each solar panel in order to prevent reverse currents from flowing into the solar panels. In experiments it has been found that the application of different blocking diodes leads to a bias in the PV system branch currents. Therefore, to ensure proper operation of the PV system, blocking diodes of the same size should be used. Moreover, the PV emulator is applied to power electronics experiments on photovoltaic systems. This thesis verifies two different MPPT algorithms with the emulated system and demonstrates the feasibility of the PV emulator. Test results show the proposed emulator has excellent dynamic characteristics and is an ideal tool for testing various MPPT algorithms. It is a low-cost solution for researchers and university students.

This thesis presents two hybrid MPPT algorithms. The proposed MPPT algorithms overcome the shortcomings of conventional MPPT methods, such as poor transient response, high continuous steady-state oscillation, and inefficient tracking performance of maximum power point voltage in the presence of partial shading. The proposed global search adaptive P&O method is a cascading strategy that searches globally in the early stages of tracking on the operating voltage range where the maximum power point is likely to occur in the PV system. After the global search, the algorithm moves to the P&O method for local optimization. Simulation results show that the proposed global search adaptive P&O MPPT method provides a fast response for tracking the maximum power point under PSCs with more than 99% energy extracting efficiency with reduced steady-state oscillation. Compared to the conventional P&O method, adaptive P&O based on power-voltage characteristics can effectively reduce the power loss during local search. Compared to traditional P&O methods, adaptive P&O based on power-voltage characteristics can effectively reduce power losses during local search, and MPPT efficiency is increased to 99.3%. The proposed Fast Global Tracking (FGT)-Fuzzy logic P&O method is another MPPT method with superior performance. This cascading method continuously speeds up the search in the early global search stage, thus increasing the efficiency of the tracking. When the algorithm moves to the local search stage, the intervention of the fuzzy logic controller provides a variable perturbation step for the P&O method, thus resolving the conflict between tracking speed and power loss of the traditional P&O method. Compared to the PSO method, the proposed method improves the average tracking speed by 70% while maintaining a high MPPT efficiency (99.7%~99.9%).

Verification and validation of the proposed control scheme have been carried out with the implementation of MATLAB/Simulink/Stateflow on the dSPACE real-time interface (RTI) 1007 processor board and DS2004 A/D and CP4002 Digital I/O boards. The experimental results show that the proposed PV simulator is a reliable device for indoor PV experiments and can be used to test the MPPT algorithm. In addition, the experimental results indicate the feasibility and superiority of the two proposed MPPT methods, which can be applied to PV systems.

Chapter 7. Future work

Overall, the proposed PV emulator achieves promising results under indoor unilluminated conditions and can effectively simulate the electrical characteristics curve of actual solar panels under uniform outdoor irradiation and partial shading conditions. However, the proposed PV emulator relies on the application of actual solar panels and external current sources. Therefore, the electrical characteristic curves of the PV emulator may not be simulated under more complex irradiation conditions, such as a P-V curve with two local maximum power points and one global maximum power point. One way to address this shortcoming is to add solar panels and external current sources to simulate more complex PV arrays. This would increase the complexity and installation cost of the PV emulator. Furthermore, in order to simplify the proposed PV emulator, only the effects of irradiation are considered when conducting the tests, ignoring the effects of temperature on the electrical characteristics of the PV array. In practice, the injection of solar panel current leads to an increase in solar panel surface temperature, which results in a shift in the P-V characteristic curve. In addition, since the partial shading is simulated by manually adjusting the external current source, sudden changes in solar irradiance are hard to be simulated. As a result, it is difficult to see the transient differences in subsequent tests of the MPPT algorithm. In order to be applied to more complex PV systems, more research on PV simulators will be conducted to improve performance and to be able to simulate accurate electrical characteristics under more complex environmental conditions. Besides, the proposed FGT algorithm is proved to be a promising MPPT algorithm that can track the global maximum power point of a PV system under partial shading conditions. It is worth mentioning that the number of search particles and the number of iterations set can significantly affect the performance of the MPPT algorithm. Fewer search particles and iterations can evidently reduce the search time, but may lead to algorithmic search failures. Conversely, more search particles and iterations will ensure that the system works at the maximum power point, but may result in more power loss. In future work, a generic FGT algorithm with dynamic and adaptive particle number and iteration number settings will be developed based on the proposed algorithm to achieve better performance in different PV systems. The dSPACE system used in this thesis is a control system for developing and testing electronics. It provides a real-time

environment for testing and verifying control algorithms and software. The application of the dSPACE system therefore brings great convenience to the testing of MPPT algorithms. However, in practical industrial applications, in view of the cost and size of the dSPACE systems, microcontrollers are often used to substitute dSPACE systems. The MC56F8245 is a controller chip often used in solar inverters and can be used as a replacement for the dSPACE system. The proposed MPPT methods are implemented into a single chip microprocessor MC56F8245 for the control of the PV systems. The experimental topology is shown in Figure 7.1. In future work, microcontroller-based experimental systems will be investigated.

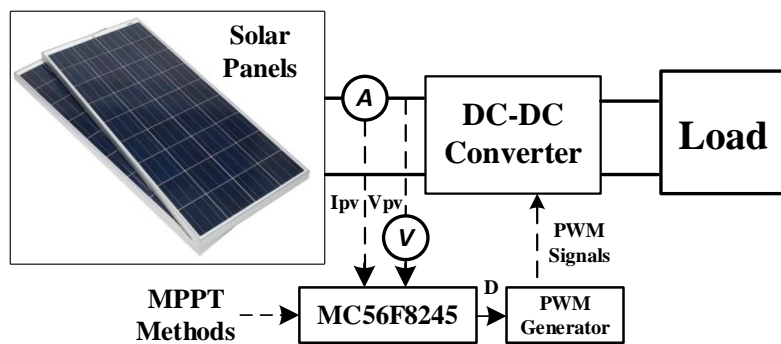


Figure 7.1 Microcontroller-based experimental system topology

REFERENCES

- [1] J. Andújar, F. Segura, and T. Domínguez, "Study of a renewable energy sources-based smart grid. requirements, targets and solutions," in *2016 3rd Conference on Power Engineering and Renewable Energy (ICPERE)*, 2016: IEEE, pp. 45-50.
- [2] O. Edenhofer *et al.*, *Renewable energy sources and climate change mitigation: Special report of the intergovernmental panel on climate change*. Cambridge University Press, 2011.
- [3] T. Guozden, J. P. Carbajal, E. Bianchi, and A. Solarte, "Optimized balance between electricity load and wind-solar energy production," *Frontiers in Energy Research*, vol. 8, p. 16, 2020.
- [4] R. Wolniak and B. Skotnicka-Zasadzień, "Development of Photovoltaic Energy in EU Countries as an Alternative to Fossil Fuels," *Energies*, vol. 15, no. 2, p. 662, 2022.
- [5] Y. Wang, C. Yanarates, and Z. Zhou, "External Current Source–Based Unilluminated PV Partial Shading Emulation System Verified Through the Hybrid Global Search Adaptive Perturb and Observe MPPT Algorithm," *Frontiers in Energy Research*, vol. 10, p. 1, 2022.
- [6] R. Ayop and C. W. Tan, "A comprehensive review on photovoltaic emulator," *Renewable and Sustainable Energy Reviews*, vol. 80, pp. 430-452, 2017.
- [7] A. S. Al-Ezzi and M. N. M. Ansari, "Photovoltaic Solar Cells: A Review," *Applied System Innovation*, vol. 5, no. 4, p. 67, 2022.
- [8] D. Sharma, R. Mehra, and B. Raj, "Comparative analysis of photovoltaic technologies for high efficiency solar cell design," *Superlattices and Microstructures*, vol. 153, p. 106861, 2021.
- [9] R. P. Smith, A. A.-C. Hwang, T. Beetz, and E. Helgren, "Introduction to semiconductor processing: Fabrication and characterization of pn junction silicon solar cells," *American Journal of Physics*, vol. 86, no. 10, pp. 740-746, 2018.
- [10] E. Radziemska, "Thermal performance of Si and GaAs based solar cells and modules: a review," *Progress in Energy and Combustion Science*, vol. 29, no. 5, pp. 407-424, 2003.
- [11] A. R. Jordehi, "Parameter estimation of solar photovoltaic (PV) cells: A review," *Renewable and Sustainable Energy Reviews*, vol. 61, pp. 354-371, 2016.
- [12] T. Ahmad, S. Sobhan, and M. F. Nayan, "Comparative analysis between single diode and double diode model of PV cell: concentrate different parameters effect on its efficiency," *Journal of Power and Energy Engineering*, vol. 4, no. 3, pp. 31-46, 2016.
- [13] H.-L. Tsai, C.-S. Tu, and Y.-J. Su, "Development of generalized photovoltaic model using MATLAB/SIMULINK," in *Proceedings of the world congress on Engineering and computer science*, 2008, vol. 2008: San Francisco, USA, pp. 1-6.
- [14] P. Dubey and V. Paranjape, "Open-circuit voltage of a Schottky-barrier solar cell," *Journal of Applied Physics*, vol. 48, no. 1, pp. 324-328, 1977.
- [15] Z. He *et al.*, "Simultaneous enhancement of open-circuit voltage, short-circuit current density, and fill factor in polymer solar cells," *Advanced materials*, vol. 23, no. 40, pp.

- 4636-4643, 2011.
- [16] Z. Cheng, H. Zhou, and H. Yang, "Research on MPPT control of PV system based on PSO algorithm," in *2010 Chinese Control and Decision Conference*, 2010: IEEE, pp. 887-892.
- [17] S. Mohanty, B. Subudhi, and P. K. Ray, "A new MPPT design using grey wolf optimization technique for photovoltaic system under partial shading conditions," *IEEE Transactions on Sustainable Energy*, vol. 7, no. 1, pp. 181-188, 2015.
- [18] J. P. Ram, H. Manghani, D. S. Pillai, T. S. Babu, M. Miyatake, and N. Rajasekar, "Analysis on solar PV emulators: A review," *Renewable and Sustainable Energy Reviews*, vol. 81, pp. 149-160, 2018.
- [19] I. Moussa, A. Khedher, and A. Bouallegue, "Design of a low-cost PV emulator applied for PVECS," *Electronics*, vol. 8, no. 2, p. 232, 2019.
- [20] G. Vachtsevanos and K. Kalaitzakis, "A hybrid photovoltaic simulator for utility interactive studies," *IEEE Transactions on Energy Conversion*, no. 2, pp. 227-231, 1987.
- [21] K. Nishioka, N. Sakitani, Y. Uraoka, and T. Fuyuki, "Analysis of multicrystalline silicon solar cells by modified 3-diode equivalent circuit model taking leakage current through periphery into consideration," *Solar energy materials and solar cells*, vol. 91, no. 13, pp. 1222-1227, 2007.
- [22] T. S. Babu, J. P. Ram, K. Sangeetha, A. Laudani, and N. Rajasekar, "Parameter extraction of two diode solar PV model using Fireworks algorithm," *Solar energy*, vol. 140, pp. 265-276, 2016.
- [23] H. Nagayoshi, S. Orio, Y. Kono, and H. Nakajima, "Novel PV array/module IV curve simulator circuit," in *Conference Record of the Twenty-Ninth IEEE Photovoltaic Specialists Conference, 2002.*, 2002: IEEE, pp. 1535-1538.
- [24] D. Schofield, M. Foster, and D. Stone, "Low-cost solar emulator for evaluation of maximum power point tracking methods," *Electronics Letters*, vol. 47, no. 3, pp. 208-209, 2011.
- [25] J. P. Ram, N. Rajasekar, and M. Miyatake, "Design and overview of maximum power point tracking techniques in wind and solar photovoltaic systems: A review," *Renewable and Sustainable Energy Reviews*, vol. 73, pp. 1138-1159, 2017.
- [26] H. Can, "Model of a photovoltaic panel emulator in MATLAB-Simulink," *Turkish journal of electrical engineering and computer sciences*, vol. 21, no. 2, pp. 300-308, 2013.
- [27] Z. Zhou, P. Holland, and P. Iqic, "MPPT algorithm test on a photovoltaic emulating system constructed by a DC power supply and an indoor solar panel," *Energy Conversion and Management*, vol. 85, pp. 460-469, 2014.
- [28] A. F. Ebrahim, S. Ahmed, S. Elmasry, and O. A. Mohammed, "Implementation of a PV emulator using programmable DC power supply," in *SoutheastCon 2015*, 2015: IEEE, pp. 1-7.
- [29] ETSYSTEM. <https://www.et-system.de/en/> (accessed 2022).
- [30] Magna-Power. <https://magna-power.com/> (accessed 2022).
- [31] AmetekProgrammablePower. <https://www.programmablepower.com/> (accessed 2022).
- [32] M. Shahabuddin, A. Riyaz, M. Asim, M. M. Shadab, A. Sarwar, and A. Anees, "Performance based analysis of solar PV emulators: a review," in *2018 International*

- Conference on Computational and Characterization Techniques in Engineering & Sciences (CCTES)*, 2018: IEEE, pp. 94-99.
- [33] I. R. Balasubramanian, S. Ilango Ganesan, and N. Chilakapati, "Impact of partial shading on the output power of PV systems under partial shading conditions," *IET power Electronics*, vol. 7, no. 3, pp. 657-666, 2014.
- [34] H. Patel and V. Agarwal, "MATLAB-based modeling to study the effects of partial shading on PV array characteristics," *IEEE transactions on energy conversion*, vol. 23, no. 1, pp. 302-310, 2008.
- [35] P. Manganiello, M. Balato, and M. Vitelli, "A survey on mismatching and aging of PV modules: The closed loop," *IEEE Transactions on Industrial Electronics*, vol. 62, no. 11, pp. 7276-7286, 2015.
- [36] S. Daliento, F. Di Napoli, P. Guerriero, and V. d'Alessandro, "A modified bypass circuit for improved hot spot reliability of solar panels subject to partial shading," *Solar Energy*, vol. 134, pp. 211-218, 2016.
- [37] R. Moretón, E. Lorenzo, and L. Narvarte, "Experimental observations on hot-spots and derived acceptance/rejection criteria," *Solar energy*, vol. 118, pp. 28-40, 2015.
- [38] A. Dhass, E. Natarajan, and L. Ponnusamy, "Influence of shunt resistance on the performance of solar photovoltaic cell," in *2012 International conference on emerging trends in electrical engineering and energy management (ICETEEEM)*, 2012: IEEE, pp. 382-386.
- [39] P. Guerriero, F. Di Napoli, V. d'Alessandro, and S. Daliento, "Accurate maximum power tracking in photovoltaic systems affected by partial shading," *International Journal of Photoenergy*, vol. 2015, 2015.
- [40] M. A. G. De Brito, L. Galotto, L. P. Sampaio, G. d. A. e Melo, and C. A. Canesin, "Evaluation of the main MPPT techniques for photovoltaic applications," *IEEE transactions on industrial electronics*, vol. 60, no. 3, pp. 1156-1167, 2012.
- [41] A. Ali *et al.*, "Investigation of MPPT techniques under uniform and non-uniform solar irradiation condition—a retrospection," *IEEE Access*, vol. 8, pp. 127368-127392, 2020.
- [42] Ö. Çelik and A. Teke, "A Hybrid MPPT method for grid connected photovoltaic systems under rapidly changing atmospheric conditions," *Electric Power Systems Research*, vol. 152, pp. 194-210, 2017.
- [43] N. Karami, N. Moubayed, and R. Outbib, "General review and classification of different MPPT Techniques," *Renewable and Sustainable Energy Reviews*, vol. 68, pp. 1-18, 2017.
- [44] B. Bendib, H. Belmili, and F. Krim, "A survey of the most used MPPT methods: Conventional and advanced algorithms applied for photovoltaic systems," *Renewable and Sustainable Energy Reviews*, vol. 45, pp. 637-648, 2015.
- [45] M. Killi and S. Samanta, "Modified perturb and observe MPPT algorithm for drift avoidance in photovoltaic systems," *IEEE transactions on Industrial Electronics*, vol. 62, no. 9, pp. 5549-5559, 2015.
- [46] R. B. Bollipo, S. Mikkili, and P. K. Bonthagorla, "Critical review on PV MPPT techniques: classical, intelligent and optimisation," *IET Renewable Power Generation*, vol. 14, no. 9, pp. 1433-1452, 2020.
- [47] S. Motahhir, A. El Hammoumi, and A. El Ghzizal, "The most used MPPT algorithms:

- Review and the suitable low-cost embedded board for each algorithm," *Journal of cleaner production*, vol. 246, p. 118983, 2020.
- [48] G. Yüsek and A. N. Mete, "A hybrid variable step size MPPT method based on P&O and INC methods," in *2017 10th International Conference on Electrical and Electronics Engineering (ELECO)*, 2017: IEEE, pp. 949-953.
- [49] U. Yilmaz, A. Kircay, and S. Borekci, "PV system fuzzy logic MPPT method and PI control as a charge controller," *Renewable and Sustainable Energy Reviews*, vol. 81, pp. 994-1001, 2018.
- [50] A. M. Noman, K. E. Addoweesh, and H. M. Mashaly, "A fuzzy logic control method for MPPT of PV systems," in *IECON 2012-38th Annual Conference on IEEE Industrial Electronics Society*, 2012: IEEE, pp. 874-880.
- [51] J.-K. Shiau, Y.-C. Wei, and B.-C. Chen, "A study on the fuzzy-logic-based solar power MPPT algorithms using different fuzzy input variables," *Algorithms*, vol. 8, no. 2, pp. 100-127, 2015.
- [52] K. Ishaque, Z. Salam, M. Amjad, and S. Mekhilef, "An improved particle swarm optimization (PSO)-based MPPT for PV with reduced steady-state oscillation," *IEEE transactions on Power Electronics*, vol. 27, no. 8, pp. 3627-3638, 2012.
- [53] R. B. Koad and A. F. Zobaa, "Comparison between the conventional methods and PSO based MPPT algorithm for photovoltaic systems," 2014.
- [54] N. A. Kamarzaman and C. W. Tan, "A comprehensive review of maximum power point tracking algorithms for photovoltaic systems," *Renewable and Sustainable Energy Reviews*, vol. 37, pp. 585-598, 2014.
- [55] L. L. Jiang, R. Srivatsan, and D. L. Maskell, "Computational intelligence techniques for maximum power point tracking in PV systems: A review," *Renewable and Sustainable Energy Reviews*, vol. 85, pp. 14-45, 2018.
- [56] F. Zhao, Z. Yao, J. Luan, and X. Song, "A novel fused optimization algorithm of genetic algorithm and ant colony optimization," *Mathematical Problems in Engineering*, vol. 2016, 2016.
- [57] K. Sundareswaran, V. Vigneshkumar, P. Sankar, S. P. Simon, P. S. R. Nayak, and S. Palani, "Development of an improved P&O algorithm assisted through a colony of foraging ants for MPPT in PV system," *IEEE transactions on industrial informatics*, vol. 12, no. 1, pp. 187-200, 2015.
- [58] K.-H. Chao and M. N. Rizal, "A hybrid MPPT controller based on the genetic algorithm and ant colony optimization for photovoltaic systems under partially shaded conditions," *Energies*, vol. 14, no. 10, p. 2902, 2021.
- [59] S. Titri, C. Larbes, K. Y. Toumi, and K. Benatchba, "A new MPPT controller based on the Ant colony optimization algorithm for Photovoltaic systems under partial shading conditions," *Applied Soft Computing*, vol. 58, pp. 465-479, 2017.
- [60] D. Kumar and K. Chatterjee, "A review of conventional and advanced MPPT algorithms for wind energy systems," *Renewable and sustainable energy reviews*, vol. 55, pp. 957-970, 2016.
- [61] M. Joisher, D. Singh, S. Taheri, D. R. Espinoza-Trejo, E. Pouresmaeil, and H. Taheri, "A hybrid evolutionary-based MPPT for photovoltaic systems under partial shading conditions," *IEEE Access*, vol. 8, pp. 38481-38492, 2020.

- [62] J. Macaulay and Z. Zhou, "A fuzzy logical-based variable step size P&O MPPT algorithm for photovoltaic system," *Energies*, vol. 11, no. 6, p. 1340, 2018.
- [63] M. N. Ali, K. Mahmoud, M. Lehtonen, and M. M. Darwish, "An efficient fuzzy-logic based variable-step incremental conductance MPPT method for grid-connected PV systems," *Ieee Access*, vol. 9, pp. 26420-26430, 2021.
- [64] C. Manickam, G. R. Raman, G. P. Raman, S. I. Ganesan, and C. Nagamani, "A hybrid algorithm for tracking of GMPP based on P&O and PSO with reduced power oscillation in string inverters," *IEEE Transactions on Industrial Electronics*, vol. 63, no. 10, pp. 6097-6106, 2016.
- [65] R. B. Bollipo, S. Mikkili, and P. K. Bonthagorla, "Hybrid, optimal, intelligent and classical PV MPPT techniques: A review," *CSEE Journal of Power and Energy Systems*, vol. 7, no. 1, pp. 9-33, 2020.
- [66] Z. Zhou and J. Macaulay, "An emulated pv source based on an unilluminated solar panel and dc power supply," *Energies*, vol. 10, no. 12, p. 2075, 2017.
- [67] H. Zheng, S. Li, R. Chaloo, and J. Proano, "Shading and bypass diode impacts to energy extraction of PV arrays under different converter configurations," *Renewable Energy*, vol. 68, pp. 58-66, 2014.
- [68] M. G. Villalva, J. R. Gazoli, and E. Ruppert Filho, "Comprehensive approach to modeling and simulation of photovoltaic arrays," *IEEE Transactions on power electronics*, vol. 24, no. 5, pp. 1198-1208, 2009.
- [69] J. Macaulay, C. W. Lin, and Z. Zhou, "An emulated PV source based on an Indoor Solar Panel with external excitement current and voltage compensation," in *2018 International Symposium on Power Electronics, Electrical Drives, Automation and Motion (SPEEDAM)*, 2018: IEEE, pp. 859-864.
- [70] A. Bidram, A. Davoudi, and R. S. Balog, "Control and circuit techniques to mitigate partial shading effects in photovoltaic arrays," *IEEE Journal of Photovoltaics*, vol. 2, no. 4, pp. 532-546, 2012.
- [71] K. Ishaque and Z. Salam, "A deterministic particle swarm optimization maximum power point tracker for photovoltaic system under partial shading condition," *IEEE transactions on industrial electronics*, vol. 60, no. 8, pp. 3195-3206, 2012.
- [72] infineon. "IDH08S120." <https://datasheetspdf.com/parts/IDH08S120.pdf?id=701880> (accessed).
- [73] infineon."IDT12S60C."
<http://pdf3.datasheet.su/Infineon%20Technologies/IDH12S60C.pdf> (accessed).
- [74] A. M. Furtado, F. Bradaschia, M. C. Cavalcanti, and L. R. Limongi, "A reduced voltage range global maximum power point tracking algorithm for photovoltaic systems under partial shading conditions," *IEEE Transactions on Industrial Electronics*, vol. 65, no. 4, pp. 3252-3262, 2017.
- [75] M. Boztepe, F. Guinjoan, G. Velasco-Quesada, S. Silvestre, A. Chouder, and E. Karatepe, "Global MPPT scheme for photovoltaic string inverters based on restricted voltage window search algorithm," *IEEE transactions on Industrial Electronics*, vol. 61, no. 7, pp. 3302-3312, 2013.
- [76] M. Kermadi, Z. Salam, J. Ahmed, and E. M. Berkouk, "A high-performance global maximum power point tracker of PV system for rapidly changing partial shading

- conditions," *IEEE Transactions on Industrial Electronics*, vol. 68, no. 3, pp. 2236-2245, 2020.
- [77] B. Hasaneen and A. A. E. Mohammed, "Design and simulation of DC/DC boost converter," in *2008 12th International Middle-East Power System Conference*, 2008: IEEE, pp. 335-340.
- [78] N. Mohan, T. M. Undeland, and W. Robbins, "DC-DC switch-mode converters," *Power electronics: converters, applications, and design*, vol. 3, pp. 161-184, 2002.
- [79] T. Instruments, "Understanding Boost Power Stage in Switchmode Power Supplies," *Texas Instruments*, Mar, 1999.
- [80] V. Michal, "Dynamic duty-cycle limitation of the boost DC/DC converter allowing maximal output power operations," in *2016 International Conference on Applied Electronics (AE)*, 2016: IEEE, pp. 177-182.
- [81] C. Yanarates, Y. Wang, and Z. Zhou, "Unity proportional gain resonant and gain scheduled proportional (PR-P) controller-based variable perturbation size real-time adaptive perturb and observe (P&O) MPPT algorithm for PV systems," *IEEE Access*, vol. 9, pp. 138468-138482, 2021.
- [82] S. Banerjee, A. Ghosh, and S. Padmanaban, "Modeling and analysis of complex dynamics for dSPACE controlled closed-loop DC-DC boost converter," *International Transactions on Electrical Energy Systems*, vol. 29, no. 4, p. e2813, 2019.

APPENDIX A. DATASHEET FOR POWER MOSFET IRFS4321



PD - 97105C

IRFS4321PbF IRFSL4321PbF

HEXFET® Power MOSFET

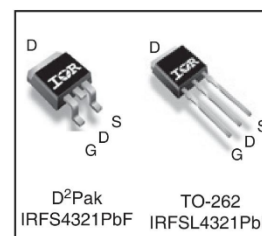
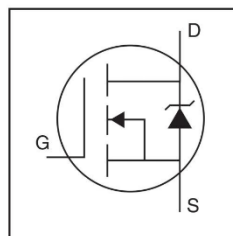
Applications

- Motion Control Applications
- High Efficiency Synchronous Rectification in SMPS
- Uninterruptible Power Supply
- Hard Switched and High Frequency Circuits

Benefits

- Low $R_{DS(on)}$ Reduces Losses
- Low Gate Charge Improves the Switching Performance
- Improved Diode Recovery Improves Switching & EMI Performance
- 30V Gate Voltage Rating Improves Robustness
- Fully Characterized Avalanche SOA

V_{DSS}	150V
$R_{DS(on)}$ typ.	12mΩ
	15mΩ
I_D	85A ①



G	D	S
Gate	Drain	Source

Absolute Maximum Ratings

Symbol	Parameter	Max.	Units
I_D @ $T_C = 25^\circ\text{C}$	Continuous Drain Current, $V_{GS} @ 10\text{V}$	85 ①	A
I_D @ $T_C = 100^\circ\text{C}$	Continuous Drain Current, $V_{GS} @ 10\text{V}$	60	A
I_{DM}	Pulsed Drain Current ②	330	A
P_D @ $T_C = 25^\circ\text{C}$	Maximum Power Dissipation	350	W
	Linear Derating Factor	2.3	W/ $^\circ\text{C}$
V_{GS}	Gate-to-Source Voltage	± 30	V
E_{AS} (Thermally limited)	Single Pulse Avalanche Energy ③	120	mJ
T_J	Operating Junction and	-55 to + 175	$^\circ\text{C}$
T_{STG}	Storage Temperature Range		
	Soldering Temperature, for 10 seconds (1.6mm from case)	300	

Thermal Resistance

	Parameter	Typ.	Max.	Units
$R_{\theta JC}$	Junction-to-Case ⑤	—	0.43*	$^\circ\text{C}/\text{W}$
$R_{\theta JA}$	Junction-to-Ambient ⑥	—	40	

* $R_{\theta JC}$ (end of life) for D²Pak and TO-262 = 0.65 $^\circ\text{C}/\text{W}$. This is the maximum measured value after 1000 temperature cycles from -55 to 150 $^\circ\text{C}$ and is accounted for by the physical wearout of the die attach medium.

Notes ① through ⑤ are on page 2

www.irf.com

1
12/9/10

APPENDIX B. DATASHEET FOR DIODE IDH12S60C



IDH12S60C

2nd Generation thinQ!™ SiC Schottky Diode

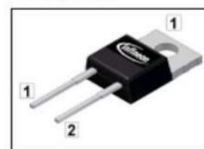
Features

- Revolutionary semiconductor material - Silicon Carbide
- Switching behavior benchmark
- No reverse recovery/ No forward recovery
- No temperature influence on the switching behavior
- High surge current capability
- Pb-free lead plating; RoHS compliant
- Qualified according to JEDEC¹⁾ for target applications
- Breakdown voltage tested at 5mA²⁾

Product Summary

V_{DC}	600	V
Q_c	30	nC
I_F	12	A

PG-T0220-2



thinQ! 2G Diode specially designed for fast switching applications like:

- CCM PFC
- Motor Drives

Type	Package	Marking	Pin 1	Pin 2
IDH12S60C	PG-T0220-2	D12S60C	C	A

Maximum ratings, at $T_j=25\text{ °C}$, unless otherwise specified

Parameter	Symbol	Conditions	Value	Unit
Continuous forward current	I_F	$T_C < 140\text{ °C}$	12	A
RMS forward current	$I_{F,RMS}$	$f = 50\text{ Hz}$	18	
Surge non-repetitive forward current, sine halfwave	$I_{F,SM}$	$T_C = 25\text{ °C}$, $t_p = 10\text{ ms}$	98	
Repetitive peak forward current	$I_{F,RM}$	$T_j = 150\text{ °C}$, $T_C = 100\text{ °C}$, $D = 0.1$	49	
Non-repetitive peak forward current	$I_{F,max}$	$T_C = 25\text{ °C}$, $t_p = 10\text{ μs}$	410	
i^2t value	$\int i^2 dt$	$T_C = 25\text{ °C}$, $t_p = 10\text{ ms}$	48	A ² s
Repetitive peak reverse voltage	V_{RRM}		600	V
Diode dv/dt ruggedness	dv/dt	$V_R = 0 \dots 480\text{V}$	50	V/ns
Power dissipation	P_{tot}	$T_C = 25\text{ °C}$	115	W
Operating and storage temperature	T_j , T_{stg}		-55 ... 175	°C
Mounting torque		M3 and M3.5 screws	60	Mcm
Soldering temperature, wavesoldering only allowed at leads	T_{sold}	1.6mm (0.063 in.) from case for 10s	260	°C

APPENDIX C. DATASHEET FOR DIODE IDH08S120



IDH08S120

thinQ!™ SiC Schottky Diode

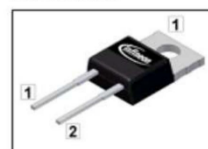
Features

- Revolutionary semiconductor material - Silicon Carbide
- Switching behavior benchmark
- No reverse recovery / No forward recovery
- Temperature independent switching behavior
- High surge current capability
- Pb-free lead plating; RoHS compliant
- Qualified according to JEDEC¹⁾ for target applications
- Optimized for high temperature operation
- Lowest Figure of Merit Q_C/I_F

Product Summary

V_{DC}	1200	V
Q_C	27	nC
$I_F; T_C < 130\text{ °C}$	7.5	A

PG-TO220-2



thinQ!™ Diode designed for fast switching applications like:

- SMPS e.g.; CCM PFC
- Motor Drives; Solar Applications; UPS

Type	Package	Marking	Pin 1	Pin 2
IDH08S120	PG-TO220-2	D08S120	C	A

Maximum ratings

Parameter	Symbol	Conditions	Value	Unit
Continuous forward current	I_F	$T_C < 130\text{ °C}$	7.5	A
Surge non-repetitive forward current, sine halfwave	$I_{F,SM}$	$T_C = 25\text{ °C}, t_p = 10\text{ ms}$	39	
		$T_C = 150\text{ °C}, t_p = 10\text{ ms}$	33	
Non-repetitive peak forward current	$I_{F,max}$	$T_C = 25\text{ °C}, t_p = 10\text{ }\mu\text{s}$	160	
i^2t value	$\int i^2 dt$	$T_C = 25\text{ °C}, t_p = 10\text{ ms}$	7	A^2s
		$T_C = 150\text{ °C}, t_p = 10\text{ ms}$	5	
Repetitive peak reverse voltage	V_{RRM}	$T_J = 25\text{ °C}$	1200	V
Diode dv/dt ruggedness	dv/dt	$V_R = 0 \dots 960\text{ V}$	50	V/ns
Power dissipation	P_{tot}	$T_C = 25\text{ °C}$	100	W
Operating and storage temperature	T_J, T_{slg}		-55 ... 175	°C
Soldering temperature, wavesoldering only allowed at leads	T_{sold}	1.6mm (0.063 in.) from case for 10s	260	
Mounting torque		M3 and M3.5 screws	60	Mcm

APPENDIX D. DATASHEET FOR DIODE IDH12SG60CXKSA2



IDH12SG60C

3rd Generation thinQ!TM SiC Schottky Diode

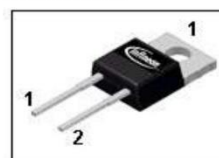
Features

- Revolutionary semiconductor material - Silicon Carbide
- Switching behavior benchmark
- No reverse recovery / No forward recovery
- Temperature independent switching behavior
- High surge current capability
- Pb-free lead plating; RoHS compliant
- Qualified according to JEDEC¹⁾ for target applications
- Breakdown voltage tested at 20mA²⁾
- Optimized for high temperature operation
- Lowest Figure of Merit Q_C/I_F

Product Summary

V_{DC}	600	V
Q_C	19	nC
$I_F; T_C < 130\text{ °C}$	12	A

PG-TO220-2



thinQ! 3G Diode designed for fast switching applications like:

- SMPS e.g.; CCM PFC
- Motor Drives; Solar Applications; UPS



Type	Package	Marking	Pin 1	Pin 2
IDH12SG60C	PG-TO220-2	D12G60C	C	A

Maximum ratings

Parameter	Symbol	Conditions	Value	Unit
Continuous forward current	I_F	$T_C < 130\text{ °C}$	12	A
Surge non-repetitive forward current, sine halfwave	$I_{F,SM}$	$T_C = 25\text{ °C}, t_p = 10\text{ ms}$	59	
		$T_C = 150\text{ °C}, t_p = 10\text{ ms}$	51	
Non-repetitive peak forward current	$I_{F,max}$	$T_C = 25\text{ °C}, t_p = 10\text{ }\mu\text{s}$	430	
i^2t value	$\int i^2 dt$	$T_C = 25\text{ °C}, t_p = 10\text{ ms}$	17	A ² s
		$T_C = 150\text{ °C}, t_p = 10\text{ ms}$	12	
Repetitive peak reverse voltage	V_{RRM}	$T_j = 25\text{ °C}$	600	V
Diode dv/dt ruggedness	dv/dt	$V_R = 0 \dots 480\text{ V}$	50	V/ns
Power dissipation	P_{tot}	$T_C = 25\text{ °C}$	125	W
Operating and storage temperature	T_j, T_{stg}		-55 ... 175	°C
Soldering temperature, wavesoldering only allowed at leads	T_{sold}	1.6mm (0.063 in.) from case for 10s	260	
Mounting torque		M3 and M3.5 screws	60	Ncm

APPENDIX E. DATASHEET FOR DRIVER IR4426

International
IR Rectifier

Data Sheet No. PD60177 Rev. E

IR4426/IR4427/IR4428(S) & (PbF)

DUAL LOW SIDE DRIVER

Features

- Gate drive supply range from 6 to 20V
- CMOS Schmitt-triggered inputs
- Matched propagation delay for both channels
- Outputs out of phase with inputs (IR4426)
- Outputs in phase with inputs (IR4427)
- OutputA out of phase with inputA and OutputB in phase with inputB (IR4428)
- Also available LEAD-FREE

Descriptions

The IR4426/IR4427/IR4428 (S) is a low voltage, high speed power MOSFET and IGBT driver. Proprietary latch immune CMOS technologies enable ruggedized monolithic construction. Logic inputs are compatible with standard CMOS or LSTTL outputs. The output drivers feature a high pulse current buffer stage designed for minimum driver cross-conduction. Propagation delays between two channels are matched.

Product Summary

$I_{O+/-}$	1.5A / 1.5A
V_{OUT}	6V - 20V
$t_{on/off}$ (typ.)	85 & 65 ns

Packages

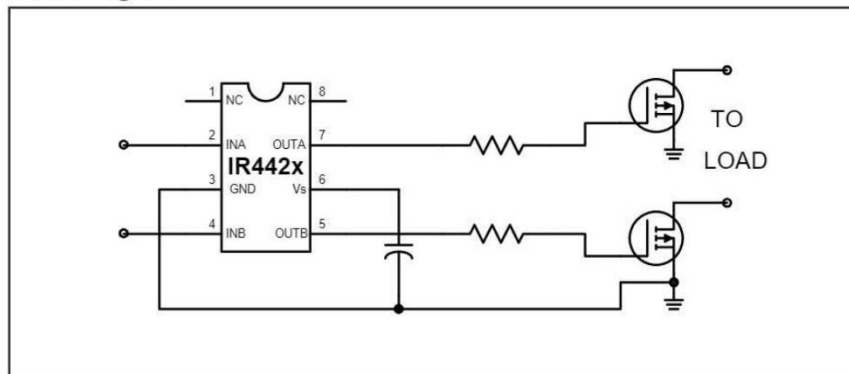


8 Lead PDIP



8 Lead SOIC

Block Diagram



www.irf.com

1

IR4426/IR4427/IR4428(S) & (PbF)

ADVANCE INFORMATION

International
IR Rectifier

Absolute Maximum Ratings

Absolute maximum ratings indicate sustained limits beyond which damage to the device may occur. All voltage parameters are absolute voltages referenced to GND. The thermal resistance and power dissipation ratings are measured under board mounted and still air conditions.

Symbol	Definition	Min.	Max.	Units	
V _S	Fixed supply voltage	-0.3	25	V	
V _O	Output voltage	-0.3	V _S + 0.3		
V _{IN}	Logic input voltage	-0.3	V _S + 0.3		
P _D	Package power dissipation @ T _A ≤ +25°C	(8 Lead PDIP)	—	1.0	W
		(8 lead SOIC)	—	0.625	
R _{thJA}	Thermal resistance, junction to ambient	(8 lead PDIP)	—	125	°C/W
		(8 lead SOIC)	—	200	
T _J	Junction temperature	—	150	°C	
T _S	Storage temperature	-55	150		
T _L	Lead temperature (soldering, 10 seconds)	—	300		

Recommended Operating Conditions

The input/output logic timing diagram is shown in figure 1. For proper operation the device should be used within the recommended conditions. All voltage parameters are absolute voltages referenced to GND.

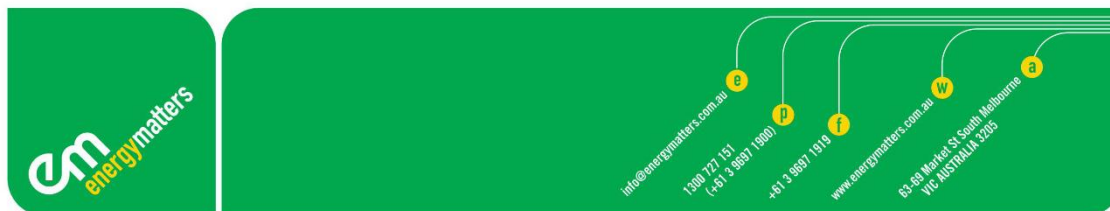
Symbol	Definition	Min.	Max.	Units
V _S	Fixed supply voltage	6	20	V
V _O	Output voltage	0	V _S	
V _{IN}	Logic input voltage	0	V _S	
T _A	Ambient temperature	-40	125	°C

DC Electrical Characteristics

V_{BIAS} (V_S) = 15V, T_A = 25°C unless otherwise specified. The V_{IN} and I_{IN} parameters are referenced to GND and are applicable to input leads: INA and INB. The V_O and I_O parameters are referenced to GND and are applicable to the output leads: OUTA and OUTB.

Symbol	Definition	Min.	Typ.	Max.	Units	Test Conditions
V _{IH}	Logic "0" input voltage (OUTA=LO, OUTB=LO) (IR4426)	2.7	—	—	V	
	Logic "1" input voltage (OUTA=HI, OUTB=HI) (IR4427)					
	Logic "0" input voltage (OUTA=LO), Logic "1" input voltage (OUTB=HI) (IR4428)					

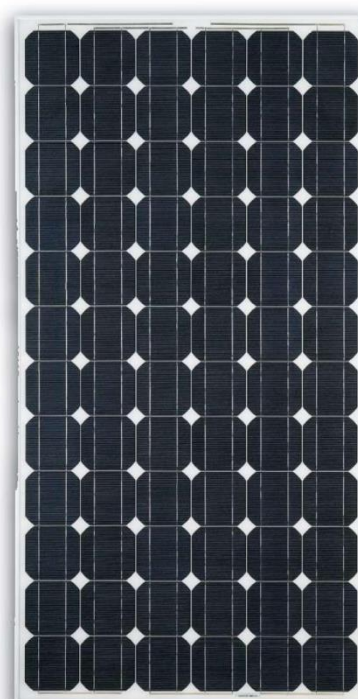
APPENDIX F. DATASHHET SOLAR PANEL SUNTECH STP175S-24/Ac



SUNTECH 175 WATT STP175S-24/Ac

High Efficiency, High Quality PV Module

Suntech's STPAc is designed and built to deliver highest efficiency and reliable power for on-grid residential and commercial systems worldwide. Relying on Suntech's well-known stringent manufacturing standards and latest PV technology, the module provides the highest possible energy output per Watt with total module efficiency of 14.1%. Superior conversion rate and exceptional low-light performance enable it to deal with the most challenging conditions of military, utility, residential and commercial installations. The module is the perfect choice for those who demand outstanding performance and exceptional uniform appearance.



FEATURES AND BENEFITS

- » High efficiency
- » Nominal 24 V DC for standard output
- » Outstanding low-light performance
- » High transparent low-iron, tempered glass
- » Unique techniques give the panel following features: esthetic appearance, with stands high wind-pressure and snow load, and easy installation
- » Unique technology ensure that problems of water freezing and warping do not occur
- » Design to meet unique demand of customer
- » 25 year module output warranty

ELECTRICAL CHARACTERISTICS

Model	STP175S-24/Ac	STP170S-24/Ac
Open-circuit voltage (Voc)	44.7V	44.4V
Optimum operating voltage (Vmp)	35.8V	35.6V
Short-circuit current (Isc)	5.23A	5.15A
Optimum operating current (Imp)	4.9A	4.8A
Maximum power at STC (Pmax)	175Wp	170Wp
Operating temperature	-40 to +85	-40 to +85
Maximum system voltage	1000V DC	1000V DC

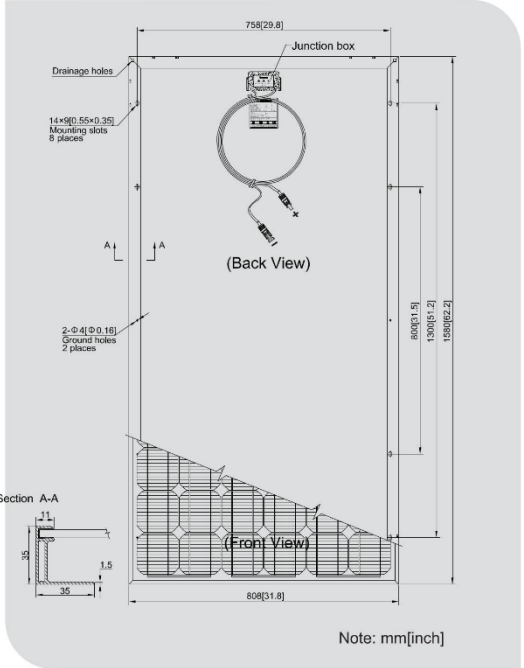
STC: Irradiance 1000W/m² Module temperature 25 AM=1.5



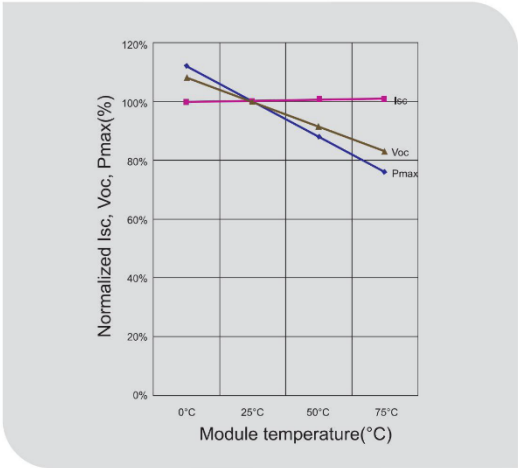
For further information: www.energymatters.com.au

Module Diagram

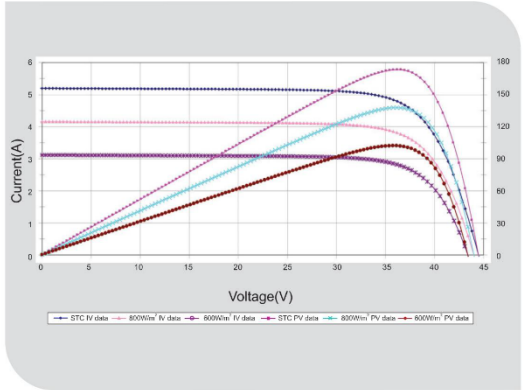
SPECIFICATIONS	
Cell	Monocrystalline silicon solar cells
No. of cells and connections	72(6x12)
Dimension of module	1580mm×808mm×35mm
Weight	15.5kg
TEMPERATURE COEFFICIENTS	
NOCT	48°C±2°C
Short-circuit current temperature coefficient	0.017 %/K
Peak power temperature coefficient	-0.34 %/K
Power tolerance	-0.48 %/K
NOCT: Nominal Operating Cell Temperature (data refer to STP165S)	
OUTPUT	
Cable	LAPP(4.0mm ²)
Asymmetrical Lengths	1200mm(-) and 800mm(+)
Connection	MC Plug Type IV



Normalized Isc, Voc, Pmax VS. Module Temperature Characteristics



Characteristics Module IV Graph 175W



For further information: www.energymatters.com.au

APPENDIX G. TEST DATA FOR CONSTRUCTED PV EMULATOR

5A 3A in series connected				5A injection			3A injection		
Vpvset	Vpvactual	Ipv	Ppv	Vpvactual	Ipv	Ppv	Vpvactual	Ipv	Ppv
90	89.3	0.0413	3.6881	44.91	4.997	1.8548	43.25	2.998	1.7862
89	87.7	0.0413	3.6220	44.87	4.997	1.8531	43.21	2.998	1.7846
88	87.6	0.0413	3.6179	44.82	4.997	1.8511	43.18	2.998	1.7833
87	87	0.2708	23.5596	44.58	4.997	12.0723	42.84	2.998	11.6011
86	86	0.6397	55.0142	44.16	4.997	28.2492	42.28	2.998	27.0465
85	84.99	0.9931	84.4036	43.76	4.997	43.4581	41.66	2.998	41.3725
84	83.99	1.319	110.7828	43.36	4.997	57.1918	41.08	2.998	54.1845
83	83	1.6166	134.1778	43	4.997	69.5138	40.45	2.998	65.3915
82	81.99	1.889	154.8791	42.67	4.997	80.6036	39.82	2.998	75.2200
81	81	2.1288	172.4328	42.34	4.997	90.1334	39.13	2.998	83.2999
80	79.99	2.3416	187.3046	42.06	4.997	98.4877	38.41	2.998	89.9409
79	79	2.5138	198.5902	41.81	4.997	105.1020	37.66	2.998	94.6697
78	78	2.6543	207.0354	41.62	4.997	110.4720	36.87	2.998	97.8640
77	77	2.7657	212.9589	41.45	4.997	114.6383	36.02	2.998	99.6205
76	76	2.8495	216.5620	41.35	4.997	117.8268	35.14	2.998	100.1314
75	75	2.9087	218.1525	41.26	4.997	120.0130	34.25	2.998	99.6230
74	73.99	2.9515	218.3815	41.21	4.997	121.6313	33.3	2.998	98.2850
73	72.99	2.9799	217.5029	41.17	4.997	122.6825	32.33	2.998	96.3402
72	71.99	2.9997	215.9484	41.15	4.997	123.4377	31.35	2.998	94.0406
71	70.99	3.0132	213.9071	41.15	4.997	123.9932	30.35	2.998	91.4506
70	70	3.0226	211.5820	41.15	4.997	124.3800	29.34	2.998	88.6831
69	68.99	3.0296	209.0121	41.15	4.997	124.6680	28.33	2.998	85.8286
68	68	3.0351	206.3868	41.15	4.997	124.8944	27.32	2.998	82.9189
67	66.99	3.039	203.5826	41.15	4.997	125.0549	26.32	2.998	79.9865
66	65.99	3.0416	200.7152	41.17	4.997	125.2227	25.34	2.998	77.0741
65	64.99	3.044	197.8296	41.17	4.997	125.3215	24.32	2.998	74.0301
64	63.99	3.0461	194.9199	41.19	4.997	125.4689	23.32	2.998	71.0351
63	62.99	3.0477	191.9746	41.21	4.997	125.5957	22.3	2.998	67.9637
62	61.99	3.0488	188.9951	41.21	4.997	125.6410	21.3	2.998	64.9394
61	60.99	3.0502	186.0317	41.22	4.997	125.7292	20.28	2.998	61.8581
60	59.99	3.0511	183.0355	41.22	4.997	125.7663	19.27	3.001	58.7947
59	58.995	3.0516	180.0291	41.24	4.997	125.8480	18.03	3.001	55.0203
58	57.995	3.0523	177.0181	41.24	4.997	125.8769	17.01	3.001	51.9196
57	56.996	3.0528	173.9974	41.27	4.997	125.9891	16	3.001	48.8448
56	55.994	3.0533	170.9665	41.27	4.997	126.0097	15	3.001	45.7995
55	54.995	3.0534	167.9217	41.29	4.997	126.0749	13.98	3.001	42.6865
54	53.995	3.0538	164.8899	41.31	4.997	126.1525	12.97	3.001	39.6078
53	52.995	3.0536	161.8255	41.33	4.997	126.2053	11.96	3.001	36.5211
52	51.995	3.0544	158.8135	41.33	4.997	126.2384	10.94	3.001	33.4151
51	50.996	3.0538	155.7316	41.34	4.997	126.2441	9.94	3.001	30.3548
50	49.996	3.0539	152.6828	41.36	4.997	126.3093	8.92	3.001	27.2408
49	48.996	3.0538	149.6240	41.38	4.997	126.3662	7.92	3.001	24.1861
48	47.995	3.0535	146.5527	41.38	4.997	126.3538	6.9	3.001	21.0692
47	46.996	3.0531	143.4835	41.4	4.997	126.3983	5.9	3.001	18.0133
46	45.996	3.0526	140.4074	41.4	4.997	126.3776	4.88	3.001	14.8967
45	44.997	3.0521	137.3353	41.4	4.997	126.3569	3.88	3.001	11.8421
44	43.998	3.0515	134.2599	41.41	4.997	126.3626	2.88	3.001	8.7883
43	42.997	3.0509	131.1795	41.43	4.997	126.3988	1.86	3.001	5.6747
42	41.997	3.0508	128.1244	41.43	4.997	126.3946	0.86	3.001	2.6237
41	40.996	3.0508	125.0706	41.45	4.997	126.4557	0	3.001	0.0000
40	39.997	3.0501	121.9948	41.45	4.997	126.4266	0	3.001	0.0000
39	38.996	3.495	136.2910	40.61	4.997	141.9320	0	3.001	0.0000
38	37.999	3.9172	148.8497	39.68	4.997	155.4345	0	3.001	0.0000
37	36.998	4.2415	156.9270	38.72	4.997	164.2309	0	3.001	0.0000
36	35.997	4.486	161.4825	37.76	4.997	169.3914	0	3.001	0.0000
35	34.997	4.666	163.2960	36.81	4.997	171.7555	0	3.001	0.0000
34	33.997	4.8348	164.3687	35.85	4.997	173.3276	0	3.001	0.0000
33	32.997	4.9033	161.7942	34.82	4.997	170.7329	0	3.001	0.0000
32	31.997	4.948	158.3212	33.83	4.997	167.3908	0	3.001	0.0000
31	30.997	4.9777	154.2938	32.84	4.997	163.4677	0	3.001	0.0000
30	29.997	4.987	149.5950	31.83	4.997	158.7362	0	3.001	0.0000
25	24.997	5.0284	125.6949	26.84	4.997	134.9623	0	3.001	0.0000
20	19.997	5.0361	100.7069	21.85	4.997	110.0388	0	3.001	0.0000
15	14.997	5.0388	75.5669	16.86	4.997	84.9542	0	3.001	0.0000
10	9.996	5.0399	50.3788	11.85	4.997	59.7228	0	3.001	0.0000
5	4.996	5.0402	25.1808	6.86	4.997	34.5758	0	3.001	0.0000
0	0.253	5.0349	1.2738	2.13	4.997	10.7243	0	3.001	0.0000

3A 1A in series connected											
Vpvset	Vpvactual	Ipv	Ppv		Vpvactual	Ipv	Ppv		Vpvactual	Ipv	Ppv
85	82.72	0.0418	3.4577		43.19	2.99	1.8053		39.47	0.993	1.6498
84	82.71	0.0419	3.4655		43.19	2.99	1.8097		39.56	0.993	1.6576
83	82.66	0.0419	3.4635		43.15	2.99	1.8080		39.56	0.993	1.6576
82	81.99	0.1825	14.9632		42.94	2.99	7.8366		39.13	0.993	7.1412
81	81	0.3779	30.6099		42.65	2.99	16.1174		38.43	0.993	14.5227
80	79.99	0.5425	43.3946		42.41	2.99	23.0074		37.68	0.993	20.4414
79	79	0.6738	53.2302		42.2	2.99	28.4344		36.88	0.993	24.8497
78	78	0.7756	60.4968		42.04	2.99	32.6062		36.06	0.993	27.9681
77	76	0.9076	68.9776		41.83	2.99	37.9649		34.25	0.993	31.0853
76	74.99	0.9465	70.9780		41.76	2.99	39.5258		33.32	0.993	31.5374
75	74.99	0.9473	71.0380		41.74	2.99	39.5403		33.32	0.993	31.5640
74	73.99	0.9735	72.0293		41.73	2.99	40.6242		32.37	0.993	31.5122
73	72.99	0.9924	72.4353		41.67	2.99	41.3533		31.42	0.993	31.1812
72	71.99	1.0053	72.3715		41.66	2.99	41.8808		30.43	0.993	30.5913
71	70.99	1.0145	72.0194		41.64	2.99	42.2438		29.45	0.993	29.8770
70	69.99	1.0211	71.4668		41.62	2.99	42.4982		28.47	0.993	29.0707
69	68.99	1.0261	70.7906		41.62	2.99	42.7063		27.48	0.993	28.1972
68	68	1.0298	70.0264		41.62	2.99	42.8603		26.48	0.993	27.2691
67	66.99	1.0329	69.1940		41.62	2.99	42.9893		25.48	0.993	26.3183
66	65.99	1.0352	68.3128		41.61	2.99	43.0747		24.48	0.993	25.3417
65	64.99	1.037	67.3946		41.61	2.99	43.1496		23.5	0.993	24.3695
64	63.98	1.039	66.4752		41.61	2.99	43.2328		22.49	0.995	23.3671
63	62.99	1.0404	65.5348		41.61	2.99	43.2910		21.49	0.995	22.3582
62	61.99	1.0412	64.5440		41.61	2.99	43.3243		20.5	0.995	21.3446
61	60.99	1.0425	63.5821		41.61	2.99	43.3784		19.5	0.995	20.3288
60	59.99	1.043	62.5696		41.61	2.99	43.3992		18.52	0.995	19.3164
59	58.996	1.0439	61.5859		41.61	2.99	43.4367		17.5	0.995	18.2683
58	57.995	1.0446	60.5816		41.61	2.99	43.4658		16.5	0.995	17.2359
57	56.995	1.0451	59.5655		41.61	2.99	43.4866		15.5	0.995	16.1991
56	55.994	1.0457	58.5529		41.61	2.99	43.5116		14.49	0.995	15.1522
55	54.995	1.0461	57.5303		41.61	2.99	43.5282		13.49	0.995	14.1119
54	53.994	1.0465	56.5047		41.61	2.99	43.5449		12.49	0.995	13.0708
53	52.995	1.0468	55.4752		41.61	2.99	43.5573		11.5	0.995	12.0382
52	51.995	1.0471	54.4440		41.61	2.99	43.5698		10.5	0.995	10.9946
51	50.996	1.0472	53.4030		41.61	2.99	43.5740		9.5	0.995	9.9484
50	49.995	1.0474	52.3648		41.61	2.99	43.5823		8.5	0.995	8.9029
49	48.996	1.0474	51.3184		41.61	2.99	43.5823		7.5	0.995	7.8555
48	47.995	1.0475	50.2748		41.61	2.99	43.5865		6.5	0.995	6.8088
47	46.996	1.0475	49.2283		41.61	2.99	43.5865		5.5	0.995	5.7613
46	45.996	1.0473	48.1716		41.61	2.99	43.5782		4.49	0.995	4.7024
45	44.997	1.0467	47.0984		41.62	2.99	43.5637		3.49	0.995	3.6530
44	43.997	1.0468	46.0561		41.62	2.99	43.5678		2.49	0.995	2.6065
43	42.996	1.0465	44.9953		41.61	2.99	43.5449		1.49	0.995	1.5593
42	41.996	1.0462	43.9362		41.62	2.99	43.5428		0.49	0.995	0.5126
41	40.996	1.0456	42.8654		41.62	2.99	43.5179		0	0.995	0.0000
40	39.996	1.3087	52.3428		41.15	2.99	53.8530		0	0.995	0.0000
39	38.997	1.752	68.3227		40.22	2.99	70.4654		0	0.995	0.0000
38	37.997	2.109	80.1357		39.29	2.99	82.8626		0	0.995	0.0000
37	36.997	2.3853	88.2489		38.34	2.99	91.4524		0	0.995	0.0000
36	35.996	2.5806	92.8913		37.38	2.99	96.4628		0	0.995	0.0000
35	34.996	2.7355	95.7316		36.41	2.99	99.5996		0	0.995	0.0000
34	33.996	2.8356	96.3991		35.43	2.99	100.4653		0	0.995	0.0000
33	32.996	2.9029	95.7841		34.39	2.99	99.8307		0	0.995	0.0000
32	31.997	2.946	94.2632		33.4	2.99	98.3964		0	0.995	0.0000
31	30.997	2.9746	92.2037		32.41	2.99	96.4068		0	0.995	0.0000
30	29.996	2.9933	89.7870		31.42	2.99	94.0495		0	0.995	0.0000
25	24.996	3.0252	75.6179		26.43	2.99	79.9560		0	0.995	0.0000
20	19.995	3.0316	60.6168		21.43	2.99	64.9672		0	0.995	0.0000
15	14.996	3.0336	45.4919		16.43	2.99	49.8420		0	0.995	0.0000
10	9.996	3.0347	30.3349		11.44	2.99	34.7170		0	0.995	0.0000
5	4.996	3.0349	15.1624		6.45	2.99	19.5751		0	0.995	0.0000
0	0.143	3.0289	0.4331		1.59	2.99	4.8160		0	0.995	0.0000

5A 3A in parallel connected (same diode)				5A injection			3A injection		
Vpvset	Vpvactual	Ipv	Ppv	Vpvactual	Ipv	Ppv	Vpvactual	Ipv	Ppv
46	45.995	0.0432	1.9870	46.51	0	0.0000	44.25	0	0.0000
45.5	45.496	0.2735	12.4432	46.21	0.217	10.0276	44.23	0	0.0000
45	44.997	0.6033	27.1467	45.8	0.548	25.0984	44.16	0	0.0000
44.5	44.496	0.955	42.4937	45.38	0.902	40.9328	44.13	0	0.0000
44	43.997	1.29	56.7561	44.93	1.242	55.8031	44.07	0	0.0000
43.5	43.496	1.6325	71.0072	44.47	1.581	70.3071	44.02	0	0.0000
43	42.996	2.1525	92.5489	44.02	1.902	83.7260	43.72	0.194	8.4817
42.5	42.496	2.7322	116.1076	43.57	2.22	96.7254	43.3	0.46	19.9180
42	41.997	3.306	138.8421	43.12	2.52	108.6624	42.86	0.736	31.5450
41.5	41.497	3.8542	159.9377	42.65	2.808	119.7612	42.42	1	42.4200
41	40.997	4.374	179.3209	42.2	3.079	129.9338	41.96	1.25	52.4500
40.5	40.497	4.8586	196.7587	41.73	3.331	139.0026	41.52	1.486	61.6987
40	39.997	5.3022	212.0721	41.26	3.564	147.0506	41.07	1.702	69.9011
39.5	39.497	5.7076	225.4331	40.81	3.778	154.1802	40.57	1.9	77.0830
39	38.996	6.071	236.7447	40.32	3.967	159.9494	40.12	2.072	83.1286
38.5	38.495	6.388	245.9061	39.85	4.134	164.7399	39.64	2.226	88.2386
38	37.997	6.664	253.2120	39.36	4.275	168.2640	39.17	2.358	92.3629
37.5	37.496	6.905	258.9099	38.88	4.402	171.1498	38.69	2.474	95.7191
37	36.997	7.107	262.9377	38.39	4.51	173.1389	38.2	2.57	98.1740
36.5	36.498	7.278	265.6324	37.9	4.603	174.4537	37.71	2.654	100.0823
36	35.996	7.443	267.9182	37.43	4.689	175.5093	37.22	2.73	101.6106
35.5	35.498	7.556	268.2229	36.93	4.748	175.3436	36.73	2.783	102.2196
35	34.998	7.648	267.6647	36.44	4.796	174.7662	36.23	2.826	102.3860
34.5	34.499	7.721	266.3668	35.94	4.834	173.7340	35.74	2.862	102.2879
34	33.998	7.779	264.4704	35.45	4.866	172.4997	35.23	2.89	101.8147
33.5	33.497	7.827	262.1810	34.91	4.891	170.7448	34.74	2.912	101.1629
33	32.997	7.864	259.4884	34.41	4.911	168.9875	34.23	2.929	100.2597
32.5	32.497	7.894	256.5313	33.92	4.927	167.1238	33.72	2.942	99.2042
32	31.998	7.919	253.3922	33.42	4.94	165.0948	33.25	2.954	98.2205
31.5	31.497	7.937	249.9917	32.93	4.951	163.0364	32.74	2.964	97.0414
31	30.998	7.953	246.5271	32.44	4.959	160.8700	32.24	2.972	95.8173
30.5	30.498	7.967	242.9776	31.92	4.967	158.5466	31.73	2.978	94.4919
30	29.998	7.977	239.2940	31.43	4.973	156.3014	31.24	2.982	93.1577
29.5	29.499	7.985	235.5495	30.93	4.977	153.9386	30.73	2.986	91.7598
29	28.998	7.992	231.7520	30.42	4.981	151.5220	30.24	2.988	90.3571
28.5	28.499	7.998	227.9350	29.94	4.985	149.2509	29.75	2.992	89.0120
28	27.997	8.003	224.0600	29.43	4.989	146.8263	29.24	2.994	87.5446
26	25.997	8.016	208.3920	27.43	4.997	137.0677	27.24	3	81.7200
24	23.998	8.024	192.5600	25.43	5.001	127.1754	25.25	3.001	75.7753
22	21.996	8.03	176.6279	23.43	5.005	117.2672	23.25	3.006	69.8895
20	19.996	8.033	160.6279	21.43	5.007	107.3000	21.25	3.008	63.9200
18	17.997	8.023	144.3899	19.45	5.009	97.4251	19.38	3.008	58.2950
16	15.998	8.037	128.5759	17.44	5.011	87.3918	17.25	3.008	51.8880
14	13.997	8.038	112.5079	15.45	5.011	77.4200	15.27	3.008	45.9322
12	11.997	8.039	96.4439	13.45	5.013	67.4249	13.26	3.01	39.9126
10	9.997	8.04	80.3759	11.45	5.013	57.3989	11.26	3.01	33.8926
8	7.998	8.04	64.3039	9.45	5.013	47.3729	9.27	3.01	27.9027
6	5.996	8.04	48.2078	7.45	5.013	37.3469	7.27	3.01	21.8827
4	3.998	8.04	32.1439	5.44	5.013	27.2707	5.27	3.01	15.8627
2	1.995	8.042	16.0438	3.46	5.014	17.3484	3.26	3.01	9.8126
0	0.394	8.036	3.1662	1.84	5.015	9.2276	1.66	3.01	4.9966

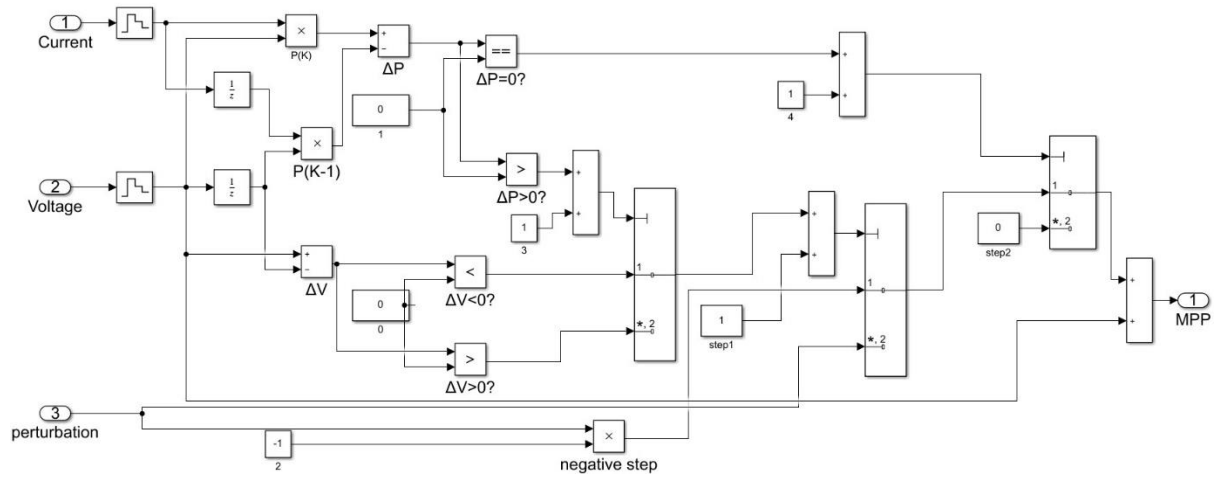
3A 1A in parallel connected (same diode)											
Vpvset	Vpvactual	Ipv	Ppv	Vpvactual	Ipv	Ppv	Vpvactual	Ipv	Ppv		
44	43.792	0.0419	1.8349	44.16	0	0.0000	40.49	0	0.0000		
43.5	43.496	0.0425	1.8486	43.95	0	0.0000	40.49	0	0.0000		
43	42.996	0.2331	10.0224	43.67	0.183	7.9916	40.49	0	0.0000		
42.5	42.497	0.5166	21.9540	43.26	0.469	20.2889	40.49	0	0.0000		
42	41.997	0.7988	33.5472	42.8	0.76	32.5280	40.49	0	0.0000		
41.5	41.498	1.068	44.3199	42.34	1.028	43.5255	40.47	0	0.0000		
41	40.998	1.3186	54.0600	41.88	1.276	53.4389	40.47	0	0.0000		
40.5	40.498	1.5576	63.0797	41.41	1.514	62.6947	40.47	0	0.0000		
40	39.996	1.7719	70.8689	40.94	1.727	70.7034	40.45	0	0.0000		
39.5	39.497	2.0774	82.0511	40.47	1.92	77.7024	40.14	0.111	4.4555		
39	38.998	2.3814	92.8698	40.01	2.091	83.6609	39.7	0.246	9.7662		
38.5	38.497	2.6548	102.2018	39.54	2.24	88.5696	39.22	0.372	14.5898		
38	37.998	2.8916	109.8750	39.05	2.369	92.5095	38.75	0.479	18.5613		
37.5	37.497	3.1035	116.3719	38.56	2.485	95.8216	38.23	0.576	22.0205		
37	36.999	3.2701	120.9904	38.07	2.578	98.1445	37.8	0.652	24.6456		
36.5	36.497	3.4115	124.5095	37.59	2.653	99.7263	37.32	0.716	26.7211		
36	35.997	3.5326	127.1630	37.08	2.719	100.8205	36.83	0.771	28.3959		
35.5	35.496	3.6264	128.7227	36.6	2.768	101.3088	36.34	0.814	29.5808		
35	34.996	3.7022	129.5622	36.11	2.81	101.4691	35.85	0.85	30.4725		
34.5	34.497	3.7635	129.8295	35.61	2.844	101.2748	35.34	0.878	31.0285		
34	33.997	3.8126	129.6170	35.1	2.87	100.7370	34.83	0.9	31.3470		
33.5	33.498	3.8523	129.0443	34.58	2.892	100.0054	34.34	0.918	31.5241		
33	32.998	3.8837	128.1543	34.08	2.91	99.1728	33.83	0.933	31.5634		
32.5	32.497	3.9106	127.0828	33.59	2.924	98.2172	33.35	0.946	31.5491		
32	31.998	3.9306	125.7713	33.08	2.935	97.0898	32.86	0.955	31.3813		
31.5	31.497	3.9464	124.2998	32.58	2.943	95.8829	32.35	0.962	31.1207		
31	30.998	3.9603	122.7614	32.09	2.951	94.6976	31.86	0.968	30.8405		
30.5	30.497	3.9712	121.1097	31.59	2.957	93.4116	31.37	0.973	30.5230		
30	29.996	3.9799	119.3811	31.01	2.961	91.8206	30.86	0.976	30.1194		
29.5	29.497	3.987	117.6045	30.6	2.967	90.7902	30.35	0.98	29.7430		
29	28.996	3.9935	115.7955	30.9	2.97	91.7730	29.87	0.982	29.3323		
28.5	28.497	3.9985	113.9453	29.59	2.973	87.9711	29.36	0.984	28.8902		
28	27.997	4.0027	112.0636	29.1	2.975	86.5725	28.85	0.987	28.4750		
26	25.997	4.015	104.3780	27.1	2.983	80.8393	26.87	0.992	26.6550		
24	23.998	4.0219	96.5176	25.1	2.991	75.0741	24.86	0.994	24.7108		
22	21.997	4.0267	88.5753	23.1	2.991	69.0921	22.86	0.996	22.7686		
20	19.997	4.03	80.5879	21.1	2.993	63.1523	20.87	0.998	20.8283		
18	17.998	4.0314	72.5571	19.1	2.995	57.2045	18.87	0.998	18.8323		
16	15.996	4.0334	64.5183	17.11	2.995	51.2445	16.87	0.998	16.8363		
14	13.998	4.0334	56.4595	15.11	2.997	45.2847	14.88	0.998	14.8502		
12	11.998	4.0353	48.4155	13.11	2.997	39.2907	12.88	1	12.8800		
10	9.997	4.0351	40.3389	11.11	2.998	33.3078	10.89	1	10.8900		
8	7.998	4.0355	32.2759	9.11	2.999	27.3209	8.89	1	8.8900		
6	5.999	4.0361	24.2126	7.11	2.999	21.3229	6.88	1	6.8800		
4	3.997	4.0373	16.1371	5.11	2.999	15.3249	4.88	1.001	4.8849		
2	1.995	4.0377	8.0552	3.11	2.999	9.3269	2.88	1.001	2.8829		
0	0.189	4.0309	0.7618	1.3	2.999	3.8987	1.07	1.001	1.0711		

5A 3A in parallel connected (different diode)				5A injection			3A injection		
Vpset	Vpvactual	Ipv	Ppv	Vpvactual	Ipv	Ppv	Vpvactual	Ipv	Ppv
46	44.75	0.0414	1.8527	45.53	0	0.0000	45.44	0	0.0000
45.5	44.701	0.0418	1.8685	45.41	0	0.0000	45.34	0	0.0000
45	44.65	0.0418	1.8664	45.38	0	0.0000	45.28	0	0.0000
44.5	44.498	0.0424	1.8867	45.33	0	0.0000	45.23	0	0.0000
44	44	0.04239	1.8652	45.07	0.067	3.0197	44.97	0.268	12.0520
43.5	43.499	1.0103	43.9470	44.65	0.342	15.2703	44.56	0.584	26.0230
43	42.999	1.6138	69.3918	44.23	0.685	30.2976	44.13	0.848	37.4222
42.5	42.498	2.202	93.5806	43.78	1.044	45.7063	43.7	1.094	47.8078
42	41.998	2.7823	116.8510	43.36	1.395	60.4872	43.26	1.324	57.2762
41.5	41.498	3.3395	138.5826	42.91	1.745	74.8780	42.82	1.54	65.9428
41	40.998	3.8685	158.6008	42.47	2.2075	93.7525	42.4	1.741	73.8184
40.5	40.499	4.3774	177.2803	42.02	2.386	100.2597	41.96	1.932	81.0667
40	39.998	4.8377	193.4983	41.58	2.692	111.9334	41.51	2.099	87.1295
39.5	39.497	5.2674	208.0465	41.14	2.968	122.1035	41.05	2.256	92.6088
39	38.999	5.6587	220.6836	40.68	3.218	130.9082	40.59	2.397	97.2942
38.5	38.498	6.0127	231.4769	40.21	3.452	138.8049	40.15	2.522	101.2583
38	38	6.342	240.9960	39.76	3.679	146.2770	39.7	2.629	104.3713
37.5	37.499	6.627	248.5059	39.29	3.87	152.0523	39.22	2.725	106.8745
37	36.998	6.864	253.9543	38.82	4.026	156.2893	38.75	2.808	108.8100
36.5	36.498	7.068	257.9679	38.34	4.158	159.4177	38.23	2.878	110.0259
36	35.999	7.239	260.5968	37.85	4.272	161.6952	37.38	2.98	111.3924
35.5	35.496	7.381	261.9960	37.4	4.366	163.2884	37.31	2.985	111.3704
35	34.999	7.499	262.4575	36.89	4.446	164.0129	36.83	3.025	111.4108
34.5	34.497	7.598	262.1082	36.42	4.51	164.2542	36.34	3.058	111.1277
34	33.998	7.682	261.1726	35.92	4.573	164.2622	35.83	3.081	110.3922
33.5	33.5	7.745	259.4575	35.43	4.618	163.6157	35.34	3.1	109.5540
33	32.998	7.797	257.2854	34.91	4.654	162.4711	34.83	3.116	108.5303
32.5	32.498	7.838	254.7193	34.41	4.684	161.1764	34.34	3.128	107.4155
32	31.996	7.872	251.8725	33.92	4.703	159.5258	33.84	3.138	106.1899
31.5	31.497	7.899	248.7948	33.42	4.727	157.9763	33.35	3.146	104.9191
31	30.998	7.92	245.5042	32.93	4.742	156.1541	32.86	3.152	103.5747
30.5	30.498	7.938	242.0931	32.42	4.756	154.1895	32.37	3.158	102.2245
30	29.998	7.952	238.5441	31.94	4.766	152.2260	31.86	3.161	100.7095
29.5	29.498	7.963	234.8926	31.41	4.776	150.0142	31.37	3.164	99.2547
29	28.998	7.971	231.1431	30.93	4.782	147.9073	30.87	3.167	97.7653
28.5	28.498	7.98	227.4140	30.44	4.79	145.8076	30.36	3.17	96.2412
28	28	7.987	223.6360	29.94	4.794	143.5324	29.87	3.17	94.6879
26	25.998	8.005	208.1140	27.94	4.806	134.2796	27.87	3.176	88.5151
24	23.996	8.015	192.3279	25.94	4.816	124.9270	25.88	3.178	82.2466
22	21.997	8.021	176.4379	23.94	4.822	115.4387	23.88	3.18	75.9384
20	19.998	8.026	160.5039	21.94	4.826	105.8824	21.88	3.182	69.6222
18	17.997	8.028	144.4799	19.94	4.827	96.2504	19.89	3.18	63.2502
16	15.998	8.03	128.4639	17.96	4.832	86.7827	17.89	3.178	56.8544
14	13.998	8.032	112.4319	15.96	4.836	77.1826	15.9	3.176	50.4984
12	11.9996	8.033	96.3928	13.96	4.836	67.5106	13.9	3.177	44.1603
10	9.999	8.034	80.3320	11.96	4.836	57.8386	11.9	3.177	37.8063
8	7.998	8.035	64.2639	9.96	4.84	48.2064	9.91	3.176	31.4742
6	5.996	8.035	48.1779	7.96	4.842	38.5423	7.9	3.176	25.0904
4	3.996	8.036	32.1119	5.96	4.842	28.8583	5.9	3.176	18.7384
2	1.996	8.036	16.0399	3.96	4.843	19.1783	3.91	3.176	12.4182
0	0.395	8.033	3.1730	2.34	4.844	11.3350	2.31	3.174	7.3319

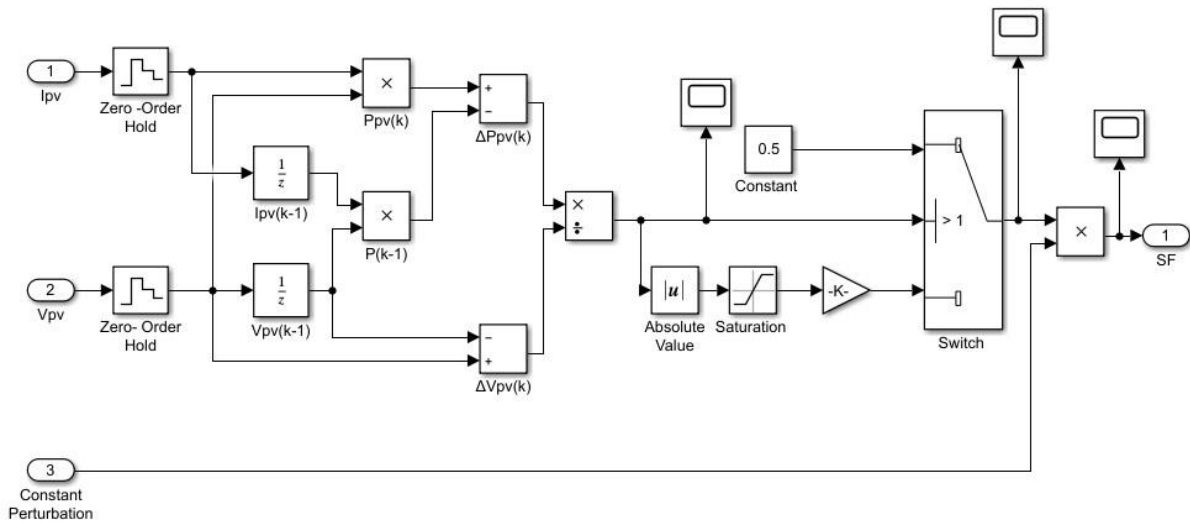
3A 1A in parallel connected (different diode)				3A injection			1A injection		
Vpvset	Vpvactual	Ipv	Ppv	Vpvactual	Ipv	Ppv	Vpvactual	Ipv	Ppv
44	42.5	0.0409	1.7383	43.26	0	0.0000	43.16	0	0.0000
43.5	42.482	0.041	1.7418	43.17	0	0.0000	43.09	0	0.0000
43	42.446	0.0411	1.7445	43.14	0	0.0000	43.05	0	0.0000
42.5	42.422	0.0411	1.7435	43.1	0	0.0000	43.02	0	0.0000
42	41.999	0.1913	8.0344	42.96	0.09	3.8664	42.86	0.119	5.1003
41.5	41.499	0.5053	20.9694	42.56	0.143	6.0861	42.47	0.403	17.1154
41	40.999	1.022	41.9010	42.13	0.354	14.9140	42.03	0.612	25.7224
40.5	40.499	1.421	57.5491	41.67	0.578	24.0853	41.58	0.788	32.7650
40	39.999	1.7854	71.4142	41.21	0.794	32.7207	41.14	0.94	38.6716
39.5	39.498	2.1157	83.5659	40.75	0.992	40.4240	40.66	1.071	43.5469
39	38.999	2.4106	94.0110	40.28	1.174	47.2887	40.21	1.188	47.7695
38.5	38.498	2.6711	102.8320	39.81	1.334	53.1065	39.73	1.29	51.2517
38	38	2.8968	110.0784	39.34	1.476	58.0658	39.26	1.375	53.9825
37.5	37.499	3.0911	115.9132	38.86	1.596	62.0206	38.78	1.448	56.1534
37	36.999	3.2556	120.4539	38.37	1.701	65.2674	38.29	1.508	57.7413
36.5	36.498	3.3924	123.8158	37.88	1.788	67.7294	37.82	1.558	58.9236
36	36	3.5073	126.2628	37.4	1.86	69.5640	37.32	1.602	59.7866
35.5	35.5	3.6018	127.8639	36.93	1.922	70.9795	36.85	1.635	60.2498
35	35	3.6784	128.7440	36.42	1.977	72.0023	36.34	1.663	60.4334
34.5	34.5	3.7407	129.0542	35.92	2.012	72.2710	35.85	1.683	60.3356
34	34	3.7915	128.9110	35.43	2.045	72.4544	35.36	1.702	60.1827
33.5	33.5	3.8319	128.3687	34.89	2.07	72.2223	34.83	1.715	59.7335
33	33	3.8654	127.5582	34.41	2.097	72.1578	34.34	1.725	59.2365
32.5	32.499	3.8917	126.4764	33.9	2.115	71.6985	33.84	1.733	58.6447
32	31.999	3.9129	125.2089	33.4	2.129	71.1086	33.35	1.741	58.0624
31.5	31.498	3.9304	123.7997	32.91	2.142	70.4932	32.84	1.747	57.3715
31	30.999	3.9445	122.2756	32.42	2.15	69.7030	32.35	1.751	56.6449
30.5	30.498	3.9564	120.6623	31.92	2.167	69.1706	31.84	1.753	55.8155
30	29.999	3.9656	118.9640	31.42	2.166	68.0557	31.35	1.758	55.1133
29.5	29.499	3.9748	117.2526	30.91	2.176	67.2602	30.86	1.757	54.2210
29	29	3.9812	115.4548	30.41	2.18	66.2938	30.35	1.759	53.3857
28.5	28.5	3.9871	113.6324	29.92	2.186	65.4051	29.87	1.759	52.5413
28	27.998	3.9907	111.7316	29.42	2.184	64.2533	29.36	1.765	51.8204
26	25.999	4.0045	104.1130	27.43	2.188	60.0168	27.36	1.774	48.5366
24	23.999	4.0121	96.2864	25.42	2.196	55.8223	25.36	1.773	44.9633
22	21.998	4.0174	88.3748	23.43	2.2	51.5460	23.35	1.775	41.4463
20	19.999	4.0208	80.4120	21.43	2.202	47.1889	21.37	1.777	37.9745
18	17.999	4.0231	72.4118	19.44	2.206	42.8846	19.36	1.777	34.4027
16	15.999	4.0256	64.4056	17.44	2.207	38.4901	17.38	1.778	30.9016
14	13.999	4.0261	56.3614	15.44	2.21	34.1224	15.37	1.777	27.3125
12	11.999	4.0273	48.3236	13.44	2.21	29.7024	13.37	1.777	23.7585
10	9.999	4.028	40.2760	11.44	2.212	25.3053	11.38	1.777	20.2223
8	7.998	4.0285	32.2199	9.44	2.212	20.8813	9.38	1.778	16.6776
6	5.998	4.029	24.1659	7.44	2.212	16.4573	7.38	1.778	13.1216
4	3.998	4.0301	16.1123	5.44	2.212	12.0333	5.37	1.779	9.5532
2	1.998	4.0302	8.0523	3.44	2.212	7.6093	3.37	1.779	5.9952
0	0.189	4.024	0.7605	1.63	2.212	3.6056	1.58	1.778	2.8092

APPENDIX H. SIMULINK BLOCK DIAGRAM OF ADAPTIVE P&O

Conventional P&O method

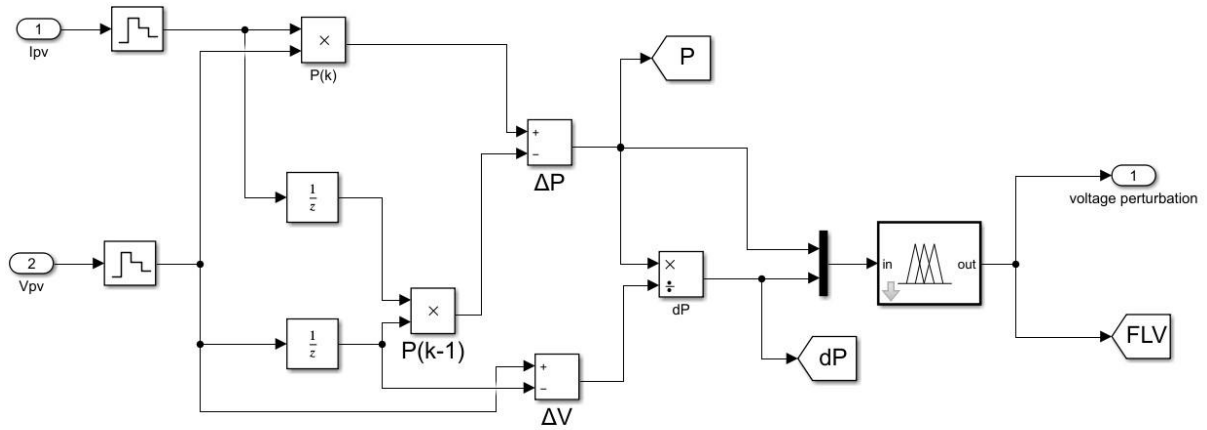


Adaptive perturbation step-size



APPENDIX I. SIMULINK BLOCK DIAGRAM OF FL CONTROLLER

Fuzzy logic controller for variable perturbation step-size



APPENDIX J. PROPOSED GLOBAL SEARCH METHOD

```
function [duty,Vref,flag] = GS(vpv,ipv)
Voc=88.4;
Vref=0.9*Voc;
duty_init=0.7;
duty_max=0.95;
duty_min=0.1;
deltaD=0.0003;
persistent Pmax Vmax duty_old Pold GS;

if isempty(Pmax) %Initialisation
    Pmax=0;
    Vmax=0;
    duty_old=duty_init;
    GS=0;
    Pold=0;
end
if GS==1
    Vref=Vmax;
end
if vpv<Vref %Perturb PV system operating voltage
    duty=duty_old-deltaD;
else
    duty=duty_old+deltaD;
end
if duty>duty_max
    duty=duty_max;
end
if duty<duty_min
    duty=duty_min;
end
ppv=vpv*ipv;
deltaP=abs(ppv-Pold);
if Pmax<ppv
    Pmax=ppv;
    Vmax=vpv;
end
if GS==0 & vpv>Vref
    GS=1;
end
duty_old=duty;
Pold=ppv;
```



```
if GS==1 & deltaP>0.15*Pold %Check if research conditions are met
    Vmax=0;
    scan=0;
    Pmax=0;
    duty_old=duty_init;
end
flag=GS;
end
```

APPENDIX K. PROPOSED FAST GLOBAL TRACKING METHOD

```
function [duty,iterations] = FGTMPPT(vpv,ipv)
persistent ppv p dc pbest delay iteration termination num Pold;
if isempty(num)
    num=7;
end
if isempty(ppv) %Initialisation
    p=zeros(1,num);
    pbest=0;
    delay=0;
    p=1;
    iteration=0;
    termination= ;
    Pold=0;
end

if isempty(dc)
    dc=linspace(0,0.8,num);
end

iterations=iteration;
if iterations<termination
if(delay>=1 && delay<100) %Delay
    duty=dc(p);
    delay=delay+1;
    return;
end

if(p>=1 && p<=num)
    ppv(p)=vpv*ipv;
end

p=p+1;
if(p<num+1)
    duty=dc(p);
    delay=1;
    return;
end
p=1;
delay=1;
iteration=iteration+1;
[m,i]=max(ppv);
```

```

Pold=m
pbest=dc(i);
dcupdate=UpdateDuty(dbest,dc,iteration,iter_max,num);
dc=dcupdate;
duty=dc(p);
return;
else
    P=vpv*ipv;
    deltaP=abs(P-Pold);
    if deltaP>0.1*Pold %Check if research conditions are met
        ppv=zeros(1,num);
        pbest=0;
        delay=0;
        p=0;
        iteration=0;
        dc=linspace(0,0.8,num);
    end
    duty=p_best;
end
end

function D1=UpdateDuty(pbest,d,iteration,termination,num) %Particles position update
D1=zeros(1,num);
a=sqrt(iteration/termination);
for kk=1:num
    pup=d(kk)+(pbest-d(kk))*a*rand();
    if pup>1
        pup=1;
    end
    if pup<0
        pup=0;
    end
    D1(kk)=pup;
end
end
end

```